Instituto Tecnológico y de Estudios Superiores de Monterrey

Campus Monterrey

School of Engineering and Sciences

Synthesis of a Finite-Time Convergence Controller for Trajectory Tracking of Unmanned Underwater Vehicles

A thesis presented by

Néstor Alejandro Narcizo-Nuci

Submitted to the
School of Engineering and Sciences
in partial fulfillment of the requirements for the degree of

Master of Science

in

Engineering Science

Monterrey, Nuevo León, June 2021

Dedication

I thank God for allowing me to reach one more goal in my life.

To my parents, Artemio and Verónica, who have always shown me their unconditional love and have helped me overcome every challenge in my life. Thank you for teaching me and leading me on a good path.

To my family and friends who have shown me their love and understanding and who have supported me in my projects.

This work is the result of each and every one of those who were there, offering their hand, their words and their understanding when I needed it.

I Can Do All Things Through Christ Who Strengthens Me.
Fil. 4.13

Doy gracias a Dios por permitirme alcanzar una meta más en mi vida.

A mis padres, Artemio y Verónica, quienes siempre me han mostrado su amor incondicional y me han ayudado a superar todos los obstáculos a los que me he enfrentado. Gracias por enseñarme y llevarme siempre por un buen camino.

A mi familia y amigos, que me han enseñado su amor, amistad y su comprensión y me han apoyado en mis proyectos.

Este trabajo es el resultado de todos y cada uno de los que estuvieron ahí, ofreciendo una mano, sus palabras y su comprensión cuando lo necesitaba.

Todo lo puedo en Cristo que me fortalece.
Fil. 4.13

Acknowledgements

Synthesis of a Finite-Time Convergence Controller for Trajectory Tracking of Unmanned Underwater Vehicles

by

Néstor Alejandro Narcizo-Nuci

Abstract

Unmanned underwater vehicles have gained importance, since they can perform tasks in underwater environments such as exploration and construction. Proper control of the vehicle trajectory is fundamental for successfully complete a task. When disturbances are frequent and the dynamics of the vehicle change, a fast response of the control scheme is required and the classical controllers do not adapt to overcome these conditions.

As the main contribution of this work, we propose the synthesis and implementation of a control scheme with finite-time convergence applied to the trajectory tracking including a time variable gain in the sliding surface of a 2nd Order Sliding Mode Control. In a firt part the parameterized trajectory considered five degrees of freedom: x,y,z,ϕ and ψ. In a second part an emulation of a simultaneous scheme between two vehicles is proposed, taking advantage of the finite-time convergence of the proposed controller.

The dynamic parameterization of the vehicle is based on BlueROV2 vehicle by BlueRobotics, which counts with four horizontal and vectored thrusters, and two vertical thrusters. A finite-time second order sliding-mode controller will be synthesize applying a variable gain on the sliding surface. This gain will be parametrized by a Time Base Generator.

The controller was tested to determine its performance, accuracy and prompt response for trajectory tracking in space and were compared against classical controllers: a Proportional-Integral-Derivative Controller, a Feedback Linearization controller and a Lyapunov function based controller. In the second part, the controller was compared with two state-of-the-art controllers, that also counts with finite-time convergence.

The proposed control schemes will be evaluated in a simulator constructed in a Matlab/Simulink environment with the actual parameters of the underwater vehicle, and where the parameters of the RMS values of the tracking error and the RMS values of the control signals are analyzed to evaluate the performance of the controllers.

The results of this work demonstrated that it is possible to synthesize the 2nd Order Sliding Mode Controller with finite-time convergence and apply it in the trajectory tracking of underwater vehicles, in trajectories that involved the five degrees of freedom and even in the presence of marine currents.

The results of these thesis are expected to be implemented in future work related with trajectory tracking and collaborative tasks with underwater vehicles.

List of Figures

viii

List of Tables

Contents

Chapter 1

Introduction

Unmanned underwater vehicles (UUVs) have gained importance due to their capability to perform tasks in marine environments, where humans cannot reach such as exploration, extraction of samples from seabed with scientific purposes, inspection and construction of gas and oil ducts, construction of damps and bridges, among others [10, 40]. Depending on their operation methods underwater vehicles can be classified in two categories: Autonomous Underwater Vehicles (AUV) and Remotely Operated Vehicles (ROV). The main difference is that AUVs are completely autonomous and sometimes are underactuated [21], which means, that they have a reduced number of actuators which cannot permit the displacement in the whole space. On the other hand, ROVs require an operator to be controlled and posses a tether cable to supply electricity and to transfer data between the human operator and the vehicle [38]. This condition makes ROVs a more complex model since it may suffer of uncertainties in the dynamic model.

Even when ROVs are human operated, its performance requires several techniques for helping the operator to assure a correct positioning and trajectory control of the vehicle [31]. This task becomes particularly hard due to underwater marine currents, the complexity of the environment and the variability of the tools used to perform their activities [72]. Further,the variability and uncertainty of the underwater vehicle behavior required strong and robust control strategies, since these conditions make the vehicle a complex non-linear system and thus a matter of study.

There exist three basic areas for control of underwater vehicles: Dynamic Positioning, Path Following and Trajectory Tracking. The concepts of path following and trajectory might be used as synonyms, since in both of them the vehicle must converge to and follow a desired path. However, path following does not involved any temporal specifications while trajectory tracking control requires the vehicle to track the path in a desired time [3]. On the other hand, in point stabilization or dynamic positioning, the vehicle is commanded to be steered to a desired position and orientation from an initial configuration [2].

The paradigm of the finite-time convergence in trajectory tracking guarantees that the vehicle will converge to a trajectory in a specific time. This behavior creates the possibility of uses this approach as a solution for tasks that requires more than one vehicle since the problem of localization and navigation must be addressed for establishing a collaborative scheme for underwater vehicles [32].

1.1 Motivation

Even when there are many studies that had successfully solved the trajectory tracking problem, most of them limit the controlled degrees of freedom (DOF) considering only the x axis for translation, and ψ angle for orientation. On the other hand, most of the controllers are model-based, which requires exact knowledge of the dynamic parameters and disturbances. This is a time consuming task, and there is always the possibility of variations and uncertainty caused by the changing underwater environment.

Related to the time of convergence, most studies presented asymptotic convergence of the error, and only a few dealt with finite-time convergence.The main difference is that the asymptotic convergence assures that the error is reduced while time tends to infinity, and the finite-time convergence allows to reduce the error to a practical 0, or in a vicinity around 0 in a given finite-time. However, this convergence time is determined by the tuning gains of the control scheme and depends on the initial conditions of the vehicle. Then, in order to establish an specific time, iterative mathematical calculations must be performed in order to obtain a desired time of convergence.

1.2 Problem Statement and Context

Underwater environments are complex, and it is not an easy task to model and consider all of their uncertainties and disturbances, since they can be considered as stochastic. To successfully perform a task, the model of the system must be as accurate as possible and a precise knowledge of the vehicle parameters is needed. Then, a model-free controller might be a better option, since it does not requires any knowledge of the physical or dynamic parameters of the vehicle [31].

Based on literature review, the work in this thesis aims to synthesize a Model-free Second Order Sliding Mode Control to achieve the finite-time convergence of the error in the trajectory tracking of an underwater vehicle using a time-variant gain, defined by a soft-polynomial, which convergence time can be set directly.

The paradigm of a finite-time convergence assures that the vehicle will converge to the desired trajectory in an specific time.

1.3 Research question

Motivated by the work described by Parra-Vega and Parra-Vega et al. [54, 55], the previous work presented by García Valdovinos et al. [31] and the research opportunities found in the literature, it is possible to synthesize the Model-free Second Order Sliding Mode Controller, with a sliding manifold parameterized by a Time Base Generator (TBG). The control will achieve finite-time convergence of tracking errors of 3D trajectories in a specific time that do not depends on the tuning of the controller and can be directly established. The control will be test considering the parameters of a BlueROV2, by BlueRobotics, controlling the x, y, z, ϕ, ψ DOFs, since θ will be considered intrinsically stable.

The approach of this work is limited the realization of computational simulations considering and neglecting the effects and disturbances caused by the marine currents. Comparisons among a Model-Based Proportional-Integral-Derivative Controller (PID), a Feedback Linearization Controller, and a Lyapunov Function Based Controller are included, evaluating the Root Mean Square (RMS) values of tracking errors of the five controlled degrees of freedom, and the RMS values of the control signals in order to obtain a parameter of energy consumption along the whole trajectory.

In a second part, the possibility of keep the simultaneous trajectory tracking of two ROVs is explored. Nevertheless, in coordinated tasks for UUVs, localization, navigation and communication are considered challenges since the underwater environment is complex and the vehicles must navigate among each other [32]. Finite-time convergence control can be one option to overcome this challenges, since the vehicles can reach to specific trajectories in a given time.

An emulation of a collaborative task between the two vehicles is performed in order to determine the effectiveness of the proposed Model-Free Second-Order Sliding Mode Controller. In order to compare the performance, the values RMS values of the tracking error and the RMS values of the control signals along the proposed trajectories. The controller will be compared against two other finite-time state-of-the-art controllers:the Non-singular Terminal Sliding Mode Control (NSTSMC) [44] and the Finite-time Second-order Sliding Mode Control (FTSOSMC) [46].

1.4 Solution Overview

To answer the research questions it is necessary to follow the methodology consisting of the next steps:

For the first part of this thesis:

- Retrieve the dynamic parameters of BlueROV2 from previous works.

- Update the Matlab-Simulink Simulator to perform the simulation with the correct parameters of the BlueROV2.

- Program and test the Proportional-Integral-Derivative Control, the Feedback Linearization Control and the Lyapunov Function Based Control for trajectory tracking.

- Synthesize and test the Model-Free Second-Order Sliding Mode Controller with the finite-time convergence approach.

- Compare the RMS values of the tracking error and control signals as a power consumption parameter of the proposed controllers and the and the proposed Model-Free Second-Order Sliding Mode Controller within a spiral trajectory.

For the second part:

- Program and test the Non-Singular Terminal Sliding Mode Control proposed by Liu et al. [44] and the Fast-Terminal Second-Order Sliding Mode Control proposed by [46]

- Compare the RMS values of the tracking error and control signals as a power consumption parameter of the proposed controllers and the and the proposed Model-Free Second-Order Sliding Mode Controller within the trajectories.

.

1.5   Contributions

1. Retrieving of the dynamic parameters of the BlueROV2 from previous reported works and update them into the proposed software for the performance of simulations.

2. Synthesizing and testing of the Model-Free Second-Order Sliding Mode Controller with finite-time convergence for Trajectory Tracking in four degrees of freedom: x, y, z and ψ. The θ angle will be considered intrinsically stable and the ϕ angle will stay in a defined reference value.

3. Comparing the RMS values of the tracking error and control signals (as a power consumption parameter) of the classical controllers: PID, Feedback-Linearization, Lyapunov Function Based and the proposed Model-Free Second-Order Sliding Mode Controller.

4. Proposing a control option for simultaneous tracking exploiting the finite-time convergence characteristic of the Model-Free Second-Order Sliding Mode Controller.

5. Comparing the RMS values of the tracking error and control signals (as a power consumption parameter) between the state-of-the-art controllers: the Non-Singular Terminal Sliding Mode Control and the Fast-Terminal Second Order Sliding Mode Control; and the proposed Model-Free Second-Order Sliding Mode Controller.

1.6   Thesis Structure

This work is structured with the next sections:

- **Chapter 1: Introduction.** In this section a scope of the project is introduced. The motivation and the objectives of the topic are also mentioned. The solution overview presents the followed methodology to solve and answer the research question. The main contributions of the work are also listed.

- **Chapter 2: Literature Review.** In this section an extensive review of the main control techniques applied for the trajectory tracking problem, giving special attention to the Sliding Mode Controller, the Model-free based controllers and the finite-time convergence paradigm.

- **Chapter 3: Theoretical Background.** The main concepts related with underwater vehicles are presented, starting with the kinematic and dynamic modeling of the vehicle, the definition of the different components of the vehicle model. Concepts about control

techniques such as the PID and the Sliding Mode Controller will be mentioned. The structure of the Finite-Time convergence approach is mentioned.

- **Chapter 4: Methodology.** The process presented in the Solution Overview are addressed. The dynamic parameters of the vehicle, as well as the constraints of the thrusters will be specified. A description of the controllers proposed to perform the simulations, as well as the parametrization of the proposed trajectories and the scope of material and software is also mentioned.

- **Chapter 5: Results.** The main results relating the performance of the controllers and showing the resulting plots for position and velocity, as well as the required torques and control inputs will be shown. The RMS values of the tracking error of the controlled DOFs and the RMS values of the control signals as a parameter to measure the energy consumption will be also presented.

- **Chapter 5: Discussion** An analysis of the results are presented in this chapter. Particular attention is given to the RMS values of the tracking errors and the RMS of the control signals. A comparison between the performance of the proposed solution and other controllers is stated.

- **Conclusions.** As the final part of the work, the main findings and contributions are presented here. Also a scope to the application of the proposed controller for future work is presented.

Chapter 2

Literature Review

Several control strategies have been found in the literature to deal with the complex underwater environment, as well as with the uncertainties and disturbances due to marine currents and to manage the variation in physical parameters of the vehicle due to a tool swap or the change in buoyancy. A revision of the state of the art control techniques is mentioned next.

2.1 Controllers

2.1.1 Proportional-Integral-Derivative (PID) Controller

The Proportional-Integral-Derivative (PID) controller have a good performance thanks to its simple structure and its preferred for its effectiveness under specific and non-variable conditions. However, the changing dynamics of the vehicle and the uncertainty of the underwater environments, it is preferred to work with more robust systems and this method is only used for performance comparison with the proposed models.

However, more robust techniques have been explored. Campos et al. [9] presented a non-linear PD and a PD+ controller with saturation functions, and an asymptotic stability. However, when the buoyancy of the vehicle is changed, the control degrades. Guerrero et al. [34] proposed a non-linear PID based on a set of saturation functions that compensates the effects of small disturbances. The controller converges in shor term, but keeps a small tracking error.

Soylu et al. [63], proposed an adaptive PID signal is included in a MIMO control law to fine tune the controller and eliminate residual errors. A hierarchical architecture is employed: an outer-loop receives the target locations and generate motion directives. The inner control-loop receive the motion commands to generate thruster commands. The controller operated with centimetre-level precision and provided stable motion.

2.1.2 Sliding Mode Control (SMC)

Unmodeled dynamics and disturbances can be efficiently managed using sliding mode control. This control strategy is compound of an equivalent control law, which is continuous and based on the dynamic model of the vehicle; and a switching term has to compensate the difference between the desired and the actual dynamics [61]. This last term may introduce a

6

high frequency switching in the actuators, called chattering, deteriorating and reducing their lifetime. The controller guarantees an asymptotic convergence of the tracking errors.

In [69], Yang et Yu proposed a control law considering the effect of states and control input quantization by introducing the bound of quantization error into the switching term of a SMC. A disturbance observer was applied to estimate the unknown disturbances. According to simulations, the trajectory tracking errors of the AUV converged to zero. Qiao et al [56], presented three exponentially convergent robust controllers based on eventual SMC. The controllers were non-linear based and compensated the dynamic uncertainties and external disturbances.

Several variations of this controller have been applied for the trajectory tracking of UUVs, including Terminal SMC, Integral SMC and High Order SMC. These variations preserve the advantages and robustness of the SMC. However, adaptive parameters are added to address the possible changes in the parameters of the vehicle and other external disturbances. Also, it is possible to obtain a faster exponential convergence rate and reduction, or even elimination, of chattering. Every of these configurations offers benefits, as chattering attenuation, finite-time convergence and robustness against unmodeled dynamics. Some of the main variations of SMC are listed on Table 3.2.

Table 2.1: Main SMC variations found in literature and their main characteristics. [57]

Controller	Characteristics	References in literature
Linear SMC	Guarantees asymptotical convergence Presence of chattering	[56]
Terminal SMC	Finite-time convergence High steady tracking precision	[13, 52]
Integral SMC	Insensitive to uncertainties and disturbances High steady state accuracy	[41, 15]

One of the strategies to reduce and even eliminate the chattering effect is by changing the discontinuous sign function in the switching term, for similar continuous function. The saturation function [4, 6, 7, 66, 52, 17, 26], as well as the hyperbolic tangent [41] and the inverse tangent functions [37],as an exponential function [73] are the ones present in the literature. However, the change of functions may reduce in the tracking performance of the vehicle [57] . Some functions are shown in Figure 2.1.

Another approaches have been considered to guarantee stability and stabilizes the tracking errors in finite time in an underactuated UUV. In [71], a PID controller as a sliding surface is proposed. To stabilize the tracking errors, a first order PI and a second order PID sliding surface are introduced to develop the dynamic tracking controller, resulting in the convergence of all tracking error to a small neighborhood of the origin even with parameter perturbation and uncertainties.

Qiao and Zhang [57], proposed an adaptive second-order fast nonsingular terminal sliding mode control that yielded local exponential convergence of the position an attitude tracking errors to zero, and included the sign function into the time derivative of the control input, eliminating chattering without reducing the tracking precision. In [52] a Time Delay Control
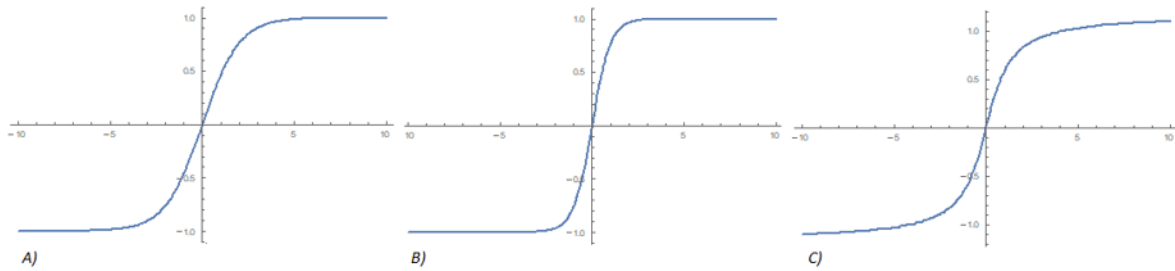
Figure 2.1: Continuous functions for the switching term in SMC to avoid chattering. A) Saturation Function. B) Hyperbolic Tangent Function. C)Inverse Tangent Function. Modifying the parameters of these functions it is possible to achieve a better approximation of the sign function.

(TDC) was proposed with the inclusion of a term based on Terminal Sliding Mode Control(TSMC) that provided a fast response and a PID term that reduced the tracking error, the controller had a good response and a free-chattering response.

In order to deal with the uncertainties and improve the trajectory tracking of the UUVs, it is common to decoupled the model of the system into two parts and thus in two independent control loops: a kinematic part and a dynamic part. Double loop SMC allows the tracking errors to converge to a small neighborhood of zero, even in the presence of external disturbances and system uncertainties. Also the chattering is considerably reduced. However, this works have been only tested by simulations. Qiao and Zhang. [58], implemented a double-loop integral terminal SMC with a kinematic and a dynamic loop. The controller tracks the desired trajectory in finite time even in the presence of uncertainties and external disturbances.

Huang and Yang [37], replaced the switching term for a inverse tangent function to reduce chattering, and the system is divided into two loops, one for controlling velocity; and the other for the position and attitude. Even in the presence of external disturbances and uncertainties, including sensor noise, the errors converge to a small neighborhood of zero. Li et al. [43], proposed a backstepping SMC where the outer-loop of the controller constructs the position error sliding surface through the desired position error and the inner-loop controller constructs the sliding surface of longitudinal, horizontal and vertical velocities. The controller presented a a faster response and shorter time of adjustment, but with a larger overshoot.

2.1.3 Visual Servoing

Also known as visual based control. This strategy uses a camera system to provide feedback signals for a robotic system. The desired configuration is reached by a set of features that moves through the image frame [26].

In [27], Gao et al. uses visual servo for positioning the vehicle with respect to a fixed target in camera-in-hand configuration. A structure of a dual loop cascade system is proposed. In a kinematic loop, the velocity is managed, and in the dynamic loop, the acceleration. Also a feed-forward neural network in conjunction to a PI controller is applied to compensate for uncertainties in the vehicle dynamics. The controller drives the vehicle to a the target successfully even in the presence of uncertainties and calibration errors.

In [28], a hierarchical image based visual servoing is used for dynamic positioning. The

desired velocity in the kinematic loop is generated by a non linear MPC, and a single, hidden layer, neural network is used to drive the vehicle to track the desired velocity based on the current velocity feedback.

2.1.4 Backstepping Control (BSC)

Backstepping has been widely used for underwater vehicles due to its simple design procedure to stabilize system states by a step-by-step recursive progress [66]. In [22], Ferreira et al. developed a controller with a kinematic/torque control law using backstepping. However, the controller does not guarantee asymptotic stability, and presented small oscillations around the equilibrium point appeared.

Karkoub et al. [39] proposed a backstepping and SMC control based on the kinematic and dynamic model of the system. The virtual reference velocity is caluated using back-stepping, while the velocity control uses SMC. The trajectory tracking is guaranteed with asymptotic stability.

2.1.5 Dynamic Surface Control (DSC)

Dynamic Surface control (DSC) is an approach similar to backstepping, which allows to avoid a high level of complexity by using first order filter to compute the derivatives of the plant model [20]. The filtered signals are calculated at each step from internal control signals, and they are used in the control law to replace analytical differentiation [5], reducing the level of complexity. Ellenrieder applied, in [20], an hyperbolic tangent function is utilized to re-scale the control input as the actuators become saturated. However, the reduction of complexity comes at the expense of a slight loss of the robustness to larger disturbances. Baldini et al. [5] aimed to control a MIMO system through three controllers. The DSC is used to generate the moment and forces required for the vehicle to perform the desired motion. Several uncertainties and external disturbances, its considered as a fault tolerant control (FTC).

2.1.6 Model Predictive Control (MPC)

Model Predictive Control (MPC) is an control methodology based on the model of the plant and its high level of flexibility allows to deal with any non-linearity or varying characteristics of the model. The model has three characteristics: prediction model, rolling optimization and feedback correction.

In [75], the problem was treated as a numerical optimization problem solved by quadratic programming, in which the system model is designed to predict the future control inputs and the future plant responses. When the AUV reached a certain position, the next optimal inputs are recalculated based on the current states and the desired trajectory. In simulation, the results showed a robustness against various disturbances. Gan et al. [25], solved the problem based on quantum-behaved particle swarm optimization, obtaining a balance between the control performance and the thrusts constraint optimization.

In [3], Anderlini et al. presented an Adaptive Model Predictive Control (AMPC). This controller selects the optimal actions at the beginning of every time step with the aim of

minimising the tracking error and prevent abrupt changes in the control action. The controller was able to track the desired trajectory, but the linearisation and the identification process affected its performance.

In [59], a nonlinear MPC was proposed to handle the strong model non-linearity of an AUV and formulated the problem trying to avoid numerical difficulties. Also, to optimize the controller, the Ohtsuka's continuation/general minimal residual is applied, and resulting in a bounded position errors. Shen et al. [60], proposed a Lyapunov based non-linear MPC that can well handle the nonlinear system dynamics and the thrust constraints, creating a trade-off between computational complexity and control performance, resulting in a better control performances and robustness and reducing considerably the mean square error of the track even in the presence of ocean current disturbances and errors in the vehicle parameters.

2.2 Adaptive Strategies

2.2.1 Neural Networks

Neural networks are widely applied due to its efficient nonlinear identification capability, as model uncertainties and external disturbances. According to Hernandez-Alvarado [35], the neural networks characteristics include: parallelism, generalization, non-linearity and adaptability. Some common structures are shown in Figure 2.2.
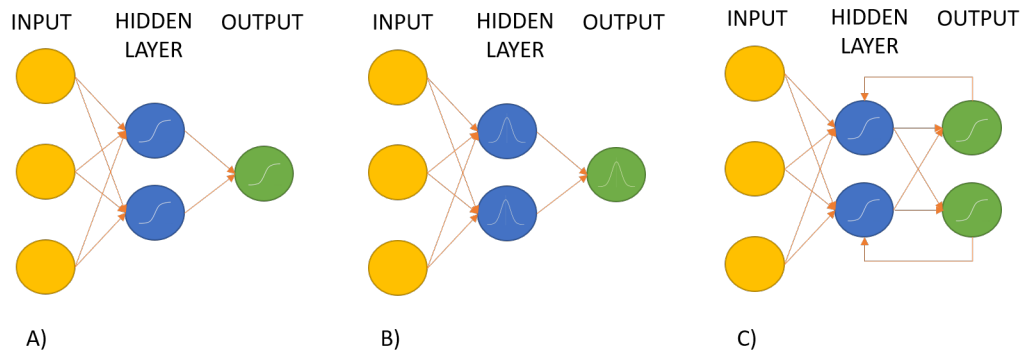
Figure 2.2: Common Neural Networks Structures with inputs, hidden layer and outputs. A) A Back-propagation NN with sigmoid activation function. B) A Radial Basis Function NN, with Gaussian activation function. C) A Recurrent NN, with feedback to the hidden layer.

Back Propagation Neural Network (BPNN)

In their work [35], Hernandez-Alvarado et al. proposed an auto-tune PID controller with a BPNN, which uses the sigmoid function as the activation function. The neural network adapted to changing environment an reduced the minimum square error compared against the traditional PID.

Recurrent Neural Network

Recurrent neural network has recurrent middle layer structure, which can reflect the time series between the input and the output variables of the system [73]. Recurrent neural networks have a faster learning speed an good learning performance [14]. In [73], a local recurrent neural network is proposed to estimate the unknown function item in controller in an adaptive SMC. The proposed approach had a higher accuracy and could track a desired trajectory without knowing the thrust model with smaller overshoot and faster convergence.

Radial Basis Function Neural Networks

The radial basis function neural network (RBFNN) Uses a radial function, i.e. a Gaussian function, as activation function instead of the common sigmoid function. This NNs are preferred due to their simplicity and linear parametrization [65]. Cui et al. [16] applied reinforcement learning to reduce the learning time of the NNs. Two NNs were used, one to evaluate the performance of the controller and the other to compensate for the unknown dynamics. In [13], Chu et al. utilized a RBFNN to identify unknown dynamics with estimation errors that can not converge to zero. The thruster's dynamics and the measurement noises of sensors are considered for simulation. As part of a Fault Tolerant Control (FTC), a RBFNN is incorporated in [66] to approximate the general uncertainty of a controller that incorporates a sliding mode algorithm and a backstepping scheme. The unknown thruster fault is treated as part of the uncertainties.

In [4], a radial basis neural network is utilized to mimic a control law in an SMC to curb the system dynamics on the sliding surface and guarantee and asymptotic stability. The neural network counted with four, twenty ad four neurons in the input, hidden and output layers, with weights initialized randomly. The parameters of the vehicle did not need to be known explicitly, and the controller follow the reference trajectory even in the occurrence of uncertainties.

In, [49], a RBFNN was employed to account for modelling errors and the controller is constructed based in a dynamic surface control and applying the minimal learning parameter. In simulation was found that the errors converge to a small neighborhood for the desired trajectory even in the presence of unmodelled dynamics and outer disturbances. Zhou et al. [76] proposed a combination of a RBFNN and state prediction using backstepping sliding mode control. The RBFNN is used to estimate the interference of model parameter uncertainties and external disturbances. The controller could track the trajectory at the fastest speed and the actual motion was smooth and stable.

2.2.2   Fuzzy Logic Controller (FLC)

Fuzzy Logic Controllers (FLC) can be applied to plants that are not so well defined mathematically [47], has a greater anti-disturbance ability and robustness, so it can be used in uncertain systems and non linear systems. In [12], Chin et al. used a fuzzy inference mechanism for a Genetic Algorithm to influence the correct evolutionary step and direction under the uncertainties and external perturbations. Huo et al. [38] proposed a fuzzy logic control scheme for speed control in a path following process. The controller reduced the complexity of the algorithm and take advantage of the robustness and anti-disturbance characteristics. In [70],
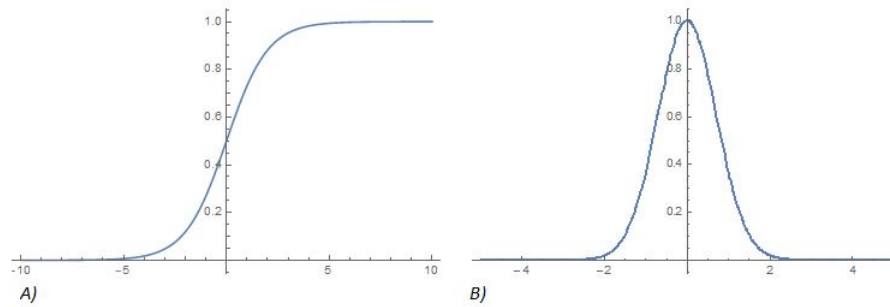
Figure 2.3: Activation functions for neural networks. A) Sigmoid function, used in most neural networks, when the value is above 0.5 the output is considered one; when is less than 0.5, the output is considered to be 0. B) Gaussian function, as a radial basis function, the output is related to a distance between a fixed center and the value.

a fuzzy function is applied to eliminate the uncertain term, and thus, reduce the chattering effect on a sliding-mode controller. At the beginning of the simulation the controller presented chattering, but in future stages it was reduced.

Fuzzy re-planing is other interesting approach of FLC. In [45], a trajectory reconstruction method is proposed. It takes into account the case where the initial position deviates from a corresponding point in a desire trajectory. For this purpose, a cubs spline function is used to reconstruct a local desired trajectory at each instant based on the AUV's current position, in order to keep the control output smooth and maintaining satisfactory tracking performance.

In, [11] is proposed a fuzzy control system of nominal dynamics based on computed-torque controller. A fuzzy compensator was also included, as a non-linear filter to compensate for uncertainties and generated a robust feedback gains variation inside the control loop. The control system is characterized by robustness and good tracking performance

2.3 Other control approaches

The presence of uncertainties can be managed by certain controllers. Other approaches include adaptive methods as neural networks or fuzzy logic. However, in

[1] an adaptive switching supervisory control combined with a non-linear Lyapunov-based tracking control is proposed. The controller does not suffer from singularities due to the parametrization of the rotation matrix and the chattering is avoided using a form of hysteresis.

In [2], a Linear Quadratic Regulator (LQR) is designed to control an AUV with two operation models: a glider mode and a thrust mode. The controller provides accurate tracking performance even in the presence of underwater currents. However, the tracking position was prioritized over orientation.

In [19], a robust adaptive control was designed for an under-actuated AUV. The control design was based on controllers for stability and of stochastic systems, potential projection functions, backstepping and Lyapunov methods. The results showed that the tracking errors converge to a circle of adjustable radius and centered in the origin.

A Nussbaum-function based controller is proposed in [64]. A high-level kinematic controller is designed for the velocity commands, and a low-level controller is designed to produce the force and torque commands for the thrusters. The controller includes an adaptation law based on Adaptive Proportional Control (APC) adaptation la to enable robustness to external disturbance and unknown environments, but the gains only can grow as a result of the adaptation and, thus, resetting the gains serves to avoid large control efforts. The controller exhibited robustness to noise and avoid overshoots and instability.

2.4 Model-Free Controllers

Bagheri and Moghadamm [4], presented a radial basis neural network that is utilized to mimic a control law in an SMC to curb the system dynamics on the sliding surface and guarantee and asymptotic stability. The neural network counted with four, twenty and four neurons in the input, hidden and output layers, with weights initialized randomly. The parameters of the vehicle did not need to be known explicitly, and the controller follow the reference trajectory even in the occurrence of uncertainties.

García-Valdovinos et al.[31], presented a model-free High Order SMC that takes advantage of the SMC and reduces the chattering effect by introducing and integral action. Based on the same model, in [36], Hosseini and Seyedtabaii presented a data fusion method, using redundant measurements and a Kalman filter, that is able to contain the varying disturbances and reaches a zero steady state tracking error. In [30], García-Valdovinos et al. included a backpropagation neural network to the model to compensate disturbances and to deal with parametric uncertainties.

Yan et al. [68], proposed a model-free PD controller that can manage the actuator saturation constraints and the time delay caused by sensors. A high proportional gain results in a large change in the output and the derivative term reduces the overshoot and improves the transient response. Martin and Withcomb [48] presented a model-free PD controller with asymptotic stability for set-point regulation. However, they found that model-based controllers' tracking errors should be significant smaller than in the model free controller.

Kumar and Rani [42] proposed a combination between a model-dependant and a model-free controller. Using a RBFNN is used for an approximation of the unknown dynamics. The control scheme has reported a strong robustness against the parametric and dynamics uncertainties.

2.5 Finite Time Convergence

Other approaches have been considered to guarantee stability and stabilize the tracking errors in finite time in an underactuated UUV. Yuo, Guo et Yan [71], presented a PID controller as a sliding surface of a SMC. To stabilize the tracking errors, a first order PI and a second order PID sliding surface are introduced to develop the dynamic tracking controller, resulting in the convergence of all tracking error to a small neighborhood near the origin even with parameter perturbation and uncertainties.

To deal with the uncertainties and improve the trajectory tracking of the UUVs, it has been found that is common to decoupled the model of the system into two parts and thus in two

independent control loops: a kinematic part and a dynamic part. Double loop SMC allows the tracking errors to converge to a small neighborhood of zero, even in the presence of external disturbances and system uncertainties. Also the chattering is considerably reduced. However, this works have been only tested on simulations. Qiao and Zhang [58], implemented a double-loop integral terminal SMC with a kinematic and a dynamic loop. The controller tracks the desired trajectory in finite time even in the presence of uncertainties and external disturbances.

Guerrero et al. [33], presented an adaptive High Order SMC. The real time experiments showed that the control signal is smoother than the control signal of other controllers as the General Super-twisting Algorithm. The finite-time convergence of the algorithm is clearly noted, counteracting against perturbations.

Parra-Vega [54] presented a 2nd Order Sliding Mode manifold with a TBG-based sliding surface applied with simulation study on a rigid 2 DOF robotic arm, obtaining finite-time convergence of tracking error. In other work, Parra-Vega et al. [55], presented a continuous chattering-free Sliding PID control law to guarantee tracking in finite time applied experimentally on a planar 2 DOFs robot.

2.6 Summary

Several control strategies have been found in the literature to deal with these conditions and make possible the performance of UUV. Even when the Proportional-Integral-Derivative (PID) is one of the most practical controllers used in linear plants due to its simplicity, the complex underwater conditions make not possible its correct operation, since the systems became non-linear and with several uncertainties, degrading its performance. Instead, the design and implementation of Sliding Mode Control (SMC) have gained a wide range of applications in the field. Linear SMC, Terminal SMC, Integral SMC and High Order SMC, have been employed due to their capacity of deal with uncertainties and disturbances. However, the reduction and elimination of chattering is also a matter of study, and several methods have been reported to avoid it, reduce it and, even, eliminate it. The change of the discontinuous sign function, for other similar-shaped and continuous functions is widely applied. The saturation function, as well as the inverse and the hyperbolic tangent function are found in literature. Other techniques as Backstepping, Visual Servoing, Dynamic Surface and Model Predictive control are also studied for the control of underwater vehicles.

Due to the lack of knowledge and the impossibility of modeling the external disturbances and vehicle dynamic uncertainties, the use of adaptive control have been widely studied. The utilization of Neural Networks is extensively applied due to their capacity of modeling uncertainties and external disturbances Back Propagation NN (BPNN), Recurrent NN (RNN), with the sigmoid functions as an activation function; and Radial Basis Function NN (RBFNN), which activation function is a radial basis function as the Gaussian function; are applied. However the RBFNNs are the most applied due to their simplicity and good learning performance. Other adaptive technique involves the application of Fuzzy Logic Controllers (FLC) due to its robustness and anti-disturbance ability.

In various studies, it is impossible to know the exact dynamic parameters of a vehicle, since this can be a complex and time consuming task. Then, it is preferred to design and

utilize model free controllers, which do not require any knowledge of these parameters. Previous strategies as SMC, PID and adaptive approaches have been found applied in the design of these type of controllers. Double-structures, where a kinematic and a dynamic controller are designed for the manage of position and velocity errors are also found in literature. In this category, the hierarchical approach is commonly treated. Other authors have design less common control techniques based on Lyapunov theory, Nussbaum functions and Linear Quadratic Regulator.

Information about the controllers used in several studies for dynamic positioning and trajectory tracking is shown in Tables 2.2 and 2.3. As well, the type of vehicle utilized in the study, the level of approach, denoted by an E when the study included Real Time Experiments, and an S, when the study included simulations. The strategies marked with the symbol $*$ are the studies based on a model-free controller. The controlled DoF are also included.

Table 2.2: Control Techniques with at least one form of Sliding Mode Control applied for dynamic positioning

Reference	Vehicle	Controllers	Approach	DOF
Bessa, Dutra et Kreuzer. (2008*, 2010) [6, 7]	ROV	FLC SMC	S	z x, y, z
Chin et Lin (2018) [12]	ROV	FLC SMC	S	z, ψ
Gao et al. (2017) [26]	ROV	SHL-FFNN SMC (VSC)	S	x, y, z, ψ
García-Valdovinos et al. (2019)* [30]	ROV	BPNN HOSMC	E	z
Hernández-Alvarado et al. (2019)* [35]	ROV	BPNN PID	E	z

Table 2.3: Control Techniques involving at least one form of Sliding Mode Control applied for Path Following and Trajectory Tracking.

Reference	Vehicle	Controller	Approach	DOF
Bagheri and Moghadamm (2009)* [4]	ROV	SMC NN	S	x, y, z, ψ
Chin et Lin (2018) [12]	ROV	FLC SMC	S	x, y
Chu et al. (2019) [13]	ROV	RBFNN SMC	S	x, y, z, ψ
Chu, Zhu et Yang (2017) [14]	ROV	RNN ATSMC	S	x, y, ψ

Table 2.3: Control Techniques involving at least one form of Sliding Mode Control applied for Path Following and Trajectory Tracking.

Reference	Vehicle	Controller	Approach	DOF
Cui et al. (2017) [15]	ROV	ISMC	S	$x, y, z, \phi, \theta, \psi$
Cui, Zhang et Cui (2016) [17]	AUV	SMC	S/E	θ, ψ
Elmokadem et al. (2017) [21]	AUV	TSMC	S	x, y, ψ
Gan et al. (2018) [25]	ROV	MPC (PSO) SMC	S	x, y, z, ψ
García-Valdovinos et al. (2014)* [31]	ROV	HOSMC	S E	x, y, z, ψ z
García-Valdovinos et al. (2019)* [30]	ROV	BPNN HOSMC	E	z
Guerrero et al. (2019) [34]	AUV	HOSMC	E	z, ψ
Hernández-Alvarado et al. (2019)* [35]	ROV	BPNN PID	S	x, y, z, ψ
Hosseini et Seyedtabaii (2016)* [36]	ROV	HOSMC	S	$x, y, z, \phi, \theta, \psi$
Huang et Yang (2019) [37]	ROV	SMC	S	x, y, z, ψ
Karkoub, Wu et Huang (2017) [39]	AUV	BSC SMC	S	$x, y, z, \phi, \theta, \psi$
Kim et al. (2015) [41]	AUV	ISMC	S/E	x, y, ψ
Li et al. (2019) [43]	AUV	BSC ISMC	S	$x, y, z, \phi, \theta, \psi$
Martin et Whitcomb (2018)* [48]	AUV	PD* PD	S	x, y, ψ
Esfahani et al. (2015) [52]	AUV	TSMC PID /FLC	S	x, y, z, ψ
Qiao et al. (2017) [56]	AUV	SMC	S	$x, y, z, \phi, \theta, \psi$

Table 2.3: Control Techniques involving at least one form of Sliding Mode Control applied for Path Following and Trajectory Tracking.

Reference	Vehicle	Controller	Approach	DOF
Qiao et Zhang (2019) [58]	AUV	ITSMC	S	$x, y, z, \phi, \theta, \psi$
Qiao et Zhang (2019) [57]	AUV	TSMC	S	$x, y, z, \phi, \theta, \psi$
Soylu et al. (2016) [63]	ROV	SMC PID	E	x, y
Wang et al. (2015) [66]	AUV	RBFNN SMC/BSC	S	$x, y, z, \phi, \theta, \psi$
Yan et al. (2019)* [68]	ROV	PD	S/E	x, y, z, ψ
Yan et Yu (2018) [69]	AUV	SMC	S	x, y, ψ
Yan et al. (2019) [70]	AUV	BSC SMC-FLC	S	z, θ
Yu, Guo et Yan (2019) [71]	AUV	PID-SMC	S	x, y, z, θ, ψ
Zhang et Chu (2012) [73]	ROV	SMC RNN	S	z
Zhou et al. (2019) [76]	AUV	RBFNN BSC-TSMC	S	x, y, ψ

Only studies that include the application of a Sliding Mode Controller where included in these tables. The inclusion of a finite time convergence approach was also considered.

Chapter 3

Theoretical Background

3.1 Mathematical Modeling

An underwater vehicle, has six degrees of freedom (DOF), defined as the set of independent displacements and rotations that specify completely the position and orientation of the vehicle. The motion in the horizontal plane is referred to as *surge* (*x* axis), the sideways motion is *sway* (*y* axis) and the vertical motion (*z* axis) is referred to as *heave*. Now, the rotations on each of these axes are *roll*, *pitch* and *yaw*, respectively. According to the Society of Naval Architects and Marine Engineers (SNAME) [62], the notation for the movement of underwater vehicles and the used variables is shown in Table 3.1.

Table 3.1: Notation for the modeling of the vehicle dynamics according to SNAME [62]

Degrees of Freedom (DOF)		Forces and Torques	Position and Euler Angles	Linear and angular velocities
Surge	Motion in the x direction	X	x	u
Sway	Motion in the y direction	Y	y	v
Heave	Motion in the z direction	Z	z	w
Roll	Rotation about the x axis	K	ϕ	p
Pitch	Rotation about the y axis	M	θ	q
Yaw	Rotation about the z axis	N	ψ	r

According to Fossen [24], the model of an UUV has to be referred to two reference frames, as shown in Figure 3.1. One is the earth-fixed frame known as North-East-Down (NED), defined as a the tangent plane on the surface of the Earth. The other is the body-fixed frame, located in the center of buoyancy of the vehicle, and defined as a moving coordinate frame that is fixed to the vehicle. Fossen [23], proposed a compact model in the 6 DOFs using a vectorial setting shown by the equation 3.1.

Fossen [23], proposed a compact model in the 6 DOFs using a vectorial setting shown by the equation 3.1.

18
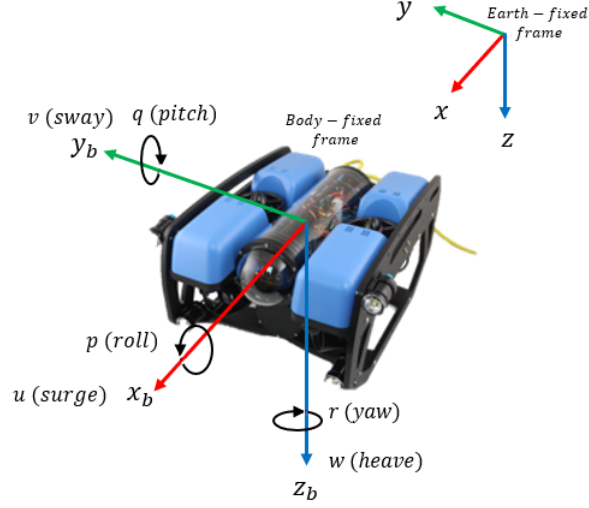
Figure 3.1: ROV's basic Degrees of Freedom for movement, as explained by Fossen [24].

$$M\dot{\nu} + C(\nu)\nu + D(\nu)\nu + g(\eta) = \tau \tag{3.1}$$

Considering that:

$$\eta = [x, y, z, \phi, \theta, \psi]^T \tag{3.2}$$

and

$$\nu = [u, v, w, p, q, r]^T \tag{3.3}$$

Where $M \in \mathbb{R}^{6\times6}$ represents a matrix of inertia. $C(\eta) \in \mathbb{R}^{6\times6}$ and $D(\eta) \in \mathbb{R}^{6\times6}$ represent the Coriolis and Damping matrices respectively. Finally, vectors $g(\eta) \in \mathbb{R}^{6\times1}$ and $\tau \in \mathbb{R}^{6\times1}$ are the compensation for gravity and buoyancy, and the vector with the control inputs, respectively. η is a vector with the components of position respect to the earth-fixed frame and ν is the vector of the velocities respect to the vehicle body-fixed frame. The transformation between this two reference frames is performed by Eq. 3.4.

$$\dot{\eta} = J(\eta)\nu \tag{3.4}$$

Where $J(\eta)$ is the Jacobian matrix, and it is defined as:

$$J(\eta) = \begin{bmatrix} J_1(\eta_2) & 0_{3\times3} \\ 0_{3\times3} & J_2(\eta_2) \end{bmatrix} \tag{3.5}$$

With $\eta_2 = [\phi, \theta, \psi]$. The matrices J_1 and J_2 are defined as:

$$J_1(\eta_2) = \begin{bmatrix} c\psi c\theta & -s\psi c\theta + c\psi s\theta s\phi & s\psi s\theta + c\psi c\phi s\theta \\ s\psi c\theta & c\psi c\phi + s\phi s\theta spsi & -c\psi s\phi + s\theta s\psi c\phi \\ -s\theta & c\theta s\phi & c\theta c\phi \end{bmatrix} \tag{3.6}$$

and:

$$J_2(\eta_2) = \begin{bmatrix} 1 & s\phi t\theta & c\phi t\theta \\ 0 & c\phi & -s\phi \\ 0 & \frac{s\phi}{c\theta} & \frac{c\phi}{c\theta} \end{bmatrix} \tag{3.7}$$

Where $s = \sin(a)$, $c = \cos(a)$ and $t = \tan(a)$.

3.2 Kinetic Model

The equation 3.1 considers the Newton-Euler formulation for rigid bodies. This formulation is based on the Newton's Second Law. However, it is necessary to consider the motion of rigid bodies, hydrodynamics and hydrostatics in order to completely define this equation.

3.2.1 Inertia Matrix

The inertia matrix M is expressed as:

$$M = M_{RB} + M_A \tag{3.8}$$

Where M_{RB} is the rigid-body mass matrix and it is defined by:

$$M_{RB} = \begin{bmatrix} m I_{3\times3} & -m S(r_g^b) \\ m S(r_g^b) & I_b \end{bmatrix} = \begin{bmatrix} m & 0 & 0 & 0 & mz_g & -my_g \\ 0 & m & 0 & -mz_g & 0 & -mx_g \\ 0 & 0 & m & my_g & -mx_g & 0 \\ 0 & -mz_g & my_g & I_x & -I_{xy} & -I_{xz} \\ mz_g & 0 & -mx_g & -I_{yx} & I_y & -I_{yz} \\ -my_g & mx_g & 0 & -I_{zx} & -I_{zy} & I_z \end{bmatrix} \tag{3.9}$$

Where the $S(r_g^b)$ term is the skew symmetric matrix, with $r_g^b = [x_g, y_g, z_g]^T$ which are the distances from the origin of the body-fixed frame to the center of gravity. m is the mass of the ROV, I_x, I_y, I_z are respectively the moments of inertia about x_b, y_b and z_b axes in the body-fixed frame. Also with $I_{xy} = I_{yx}$, $I_{xz} = I_{zx}$, $I_{yz} = I_{zy}$ are the inertia products [24].

The matrix M_A involves the added mass, which can be considered as pressure-induce forces due to a forced harmonic motion of the vehicle body proportional to its acceleration, and for vehicles that are completely submerged the coefficients are constant [24]. The matrix is defined as shown in equation 3.11.

$$M_A = - \begin{bmatrix} X_{\dot u} & X_{\dot v} & X_{\dot w} & X_{\dot p} & X_{\dot q} & X_{\dot r} \\ Y_{\dot u} & Y_{\dot v} & Y_{\dot w} & Y_{\dot p} & Y_{\dot q} & Y_{\dot r} \\ Z_{\dot u} & Z_{\dot v} & Z_{\dot w} & Z_{\dot p} & Z_{\dot q} & Z_{\dot r} \\ K_{\dot u} & K_{\dot v} & K_{\dot w} & K_{\dot p} & K_{\dot q} & K_{\dot r} \\ M_{\dot u} & M_{\dot v} & M_{\dot w} & M_{\dot p} & M_{\dot q} & M_{\dot r} \\ N_{\dot u} & N_{\dot v} & N_{\dot w} & N_{\dot p} & N_{\dot q} & N_{\dot r} \end{bmatrix} \tag{3.10}$$

Where, for example the term $Y_{\dot u} := \frac{\partial Y}{\partial \dot u}$.

However, in several applications the ROV will only move at a low speed. Also, considering symmetry, the off-diagonal elements of the matrix $\boldsymbol{M_A}$ can be neglected [23]. Resulting in:

$$\boldsymbol{M_A} = \boldsymbol{M_A}^T = -diag\{X_{\dot{u}}, Y_{\dot{v}}, Z_{\dot{w}}, K_{\dot{p}}, M_{\dot{q}}, N_{\dot{r}}\} \tag{3.11}$$

3.2.2 Coriolis Matrix

The Coriolis Matrix is defined by:

$$\boldsymbol{C}(\boldsymbol{\nu}) = \boldsymbol{C_{RB}}(\boldsymbol{\nu}) + \boldsymbol{C_A}(\boldsymbol{\nu}) \tag{3.12}$$

Where $\boldsymbol{C_{RB}}$ is the rigid-body Coriolis and centripetal matrix due to the rotation of the body-fixed frame about the inertial Earth-fixed frame [24] and can always be expressed such that $\boldsymbol{C}_{RB}$ is skew-symemtric:

$$\boldsymbol{C_{RB}}(\boldsymbol{\nu}) = -\boldsymbol{C}_{RB}^T(\boldsymbol{\nu}) = \begin{bmatrix} 0_{3\times3} & -m\boldsymbol{S}(\boldsymbol{\nu}_1) - m\boldsymbol{S}(\boldsymbol{S}(\boldsymbol{\nu}_2)\boldsymbol{r}_g^b) \\ -m\boldsymbol{S}(\boldsymbol{\nu}_1) - m\boldsymbol{S}(\boldsymbol{S}(\boldsymbol{\nu}_2)\boldsymbol{r}_g^b) & m\boldsymbol{S}(\boldsymbol{S}(\boldsymbol{\nu}_1)\boldsymbol{r}_g^b - \boldsymbol{S}(\boldsymbol{I}_o\boldsymbol{\nu}_2)) \end{bmatrix} \tag{3.13}$$

However, considering the same symmetry conditions, the matrix shown in Eq. 3.13 can be written as 3.14 [67]:

$$\boldsymbol{C}_{RB}(\boldsymbol{\nu}) = \begin{bmatrix} 0 & 0 & 0 & 0 & mw & 0 \\ 0 & 0 & 0 & -mw & 0 & 0 \\ 0 & 0 & 0 & mv & -mu & 0 \\ 0 & mw & -mv & 0 & I_z r & -I_y q \\ -mw & 0 & -mu & -I_z r & 0 & I_x p \\ mv & -mu & 0 & I_y q & -I_x p & 0 \end{bmatrix} \tag{3.14}$$

For a rigid-body moving through an ideal fluid the Coriolis matrix $\boldsymbol{C_A}(\boldsymbol{\nu})$ can be always parameterized such that it is skew-symmetric [23], such that:

$$\boldsymbol{C_A}(\boldsymbol{\nu}) = \boldsymbol{C}_A^T(\boldsymbol{\nu}) = -\begin{bmatrix} 0_{3\times3} & -\boldsymbol{S}(\boldsymbol{A}_{11}\boldsymbol{\nu}_1 + \boldsymbol{A}_{12}\boldsymbol{\nu}_2) \\ -\boldsymbol{S}(\boldsymbol{A}_{11}\boldsymbol{\nu}_1 + \boldsymbol{A}_{12}\boldsymbol{\nu}_2) & -\boldsymbol{S}(\boldsymbol{A}_{21}\boldsymbol{\nu}_1 + \boldsymbol{A}_{22}\boldsymbol{\nu}_2) \end{bmatrix} \tag{3.15}$$

Taking in consideration that:

$$\boldsymbol{M} = \boldsymbol{M}_A = \begin{bmatrix} \boldsymbol{A}_{11} & \boldsymbol{A}_{12} \\ \boldsymbol{A}_{21} & \boldsymbol{A}_{22} \end{bmatrix} \tag{3.16}$$

However, the same consideration of velocity and symmetry arise, simplifying Eq. 3.15 into 3.17.

$$\boldsymbol{C}_A(\boldsymbol{\nu}) = \boldsymbol{C}_A^T(\boldsymbol{\nu}) = \begin{bmatrix} 0 & 0 & 0 & 0 & -Z_{\dot{w}}w & Y_{\dot{v}}v \\ 0 & 0 & 0 & Z_{\dot{w}}w & 0 & -X_{\dot{u}}u \\ 0 & 0 & 0 & -Y_{\dot{v}}v & X_{\dot{u}}u & 0 \\ 0 & -Z_{\dot{w}}w & Y_{\dot{v}}v & 0 & -N_{\dot{r}}r & M_{\dot{q}}q \\ Z_{\dot{w}}w & 0 & -X_{\dot{u}}u & N_{\dot{r}}r & 0 & -K_{\dot{p}}p \\ Y_{\dot{v}}v & X_{\dot{u}}u & 0 & -M_{\dot{q}}q & K_{\dot{p}}p & 0 \end{bmatrix} \tag{3.17}$$

3.2.3 Hydrodynamic Damping

Fossen [23] recalls four different types of damping:

- **Potential Damping:** This damping is encountered when a body is forced to oscillate with the wave excitation frequency. The contribution of this term are usually neglectable.

- **Skin Friction:** This damping is due to the laminar boundary layer when considering the low-frequency motion of the vehicle. A quadratic contribution can be added due to a turbulent boundary layer.

- **Wave Drift Damping:** This is added resistance for surface vessels advancing in waves.

- **Damping due to Vortex Shedding:** In a viscous fluid, the frictional forces make the system not conservative with respect to energy. The viscous damping force depends on the speed of the vehicle, the projected cross-sectional area under water, the density of the water and the drag-coefficient based on the representative area.

In general, it is not an easy task to separate the damping effects. So, it is then convenient to write the hydrodynamic damping as:

$$\boldsymbol{D}(\nu) = \boldsymbol{D} + \boldsymbol{D}_n(\boldsymbol{\nu}) \tag{3.18}$$

Where $\boldsymbol{D}$ is the linear damping matrix, and $\boldsymbol{D}_n(\boldsymbol{\nu})$ is the nonlinear damping matrix. For slow speed underwater vehicle, this matrix is expressed as Eq. 3.19.

$$\begin{aligned}
\boldsymbol{D}(\boldsymbol{\nu}) = &- diag\{X_u, Y_v, Z_w, K_p, M_q, N_r\} \\
&- diag\{X_{|u|u}|u|, Y_{|v|v}|v|, Z_{|w|w}|w|, K_{|p|p}|p|, M_{|q|q}|q|, N_{|r|r}|r|\}
\end{aligned} \tag{3.19}$$

3.2.4 Restoring Forces and Moments

Gravity and buoyancy forces also affect underwater vehicles. This forces are called restoring forces. According to SNAME notation, the submerged weight of the body and buoyancy force are defined as:

$$W = mg \tag{3.20}$$

$$B = \rho g \nabla \tag{3.21}$$

Where m is the mass of the vehicle, g is the constant gravity acceleration of $9.8\frac{m}{s^2}$ (positive downwards), ρ is the density of water, and ∇ is the volume of fluid displaced by the vehicle.

Considering that the center of the body-fixed frame is located in the center of flotation, and the considerations mentioned by Wu[67],the resulting matrix is shown in Eq. 3.22.

$$g(\eta) = \begin{bmatrix} (W-B)sin(\theta) \\ -(W-B)cos(\theta)sin(\phi) \\ -(W-B)cos(\theta)cos(\phi) \\ z_g W cos(\theta)sin(\phi) \\ z_g W sin(\theta) \\ 0 \end{bmatrix} \tag{3.22}$$

3.2.5   Ocean Currents

According to Fosen [24], the forces of the ocean currents can be implemented using relative velocity, between the difference of the real velocity and the current velocity:

$$\boldsymbol{\nu_r} = \boldsymbol{\nu} - \boldsymbol{\nu_c} \tag{3.23}$$

Where ν is the velocity of the vehicle, and ν_c is the velocity of the currents.

The generalized vector for an irrotational ocean current velocity is given by:

$$\boldsymbol{\nu_c} = [u_c, v_c, w_c, 0, 0, 0]^T \tag{3.24}$$

Defining the angles α_c as the angle of attack, β_c as the slideslip angle and V_c as the magnitude of the velocity of the marine current, every element of the velocity vector can be calculated as:

$$\begin{aligned} u_c &= V_c \cos(\alpha_c) \cos(\beta_c) \\ v_c &= V_c \sin(\beta_c) \\ w_c &= V_c \sin(\alpha_c) \cos(\beta_c) \end{aligned} \tag{3.25}$$

Where u_c is a current velocity produced from north, v_c is the current from east, and w_c is the current from down.

Since the velocity vector is expressed in the Earth-Fixed frame, Eq. 3.1, can be modified, resulting in:

$$\boldsymbol{M\dot{\nu}_r} + \boldsymbol{C(\nu_r)\nu_r} + \boldsymbol{D(\nu_r)\nu_r} + \boldsymbol{g(\eta)} = \boldsymbol{\tau} \tag{3.26}$$

3.2.6   Thruster Allocation

The underwater vehicles are equipped with thrusters in order to generate the forces and torques for movement. The force produced by these thrusters can be calculated using the Eq. 3.27

$$\boldsymbol{\tau} = \boldsymbol{TKu} \tag{3.27}$$

Where $\boldsymbol{u}$ is the vector with the control inputs, K is a diagonal matrix with the thrust coefficients such that $K = diag\{K_1, K_2, K_3, K_4, K_5, K_6\}$ and T is the allocation matrix.

The matrix $\boldsymbol{T}$ includes the distances and angles to calculate the required torques according to the control inputs.

3.2.7 Control Allocation

From Eq.3.27 it is possible to solve for $\boldsymbol{u}$ in order to find the corresponding control signals to be applied for each thruster. This vector is determined as Eq.3.28.

$$\boldsymbol{u} = \boldsymbol{K}^{-1}\boldsymbol{T}^{-1}\boldsymbol{\tau} \tag{3.28}$$

Nevertheless, the matrix $\boldsymbol{T}$ is singular, due to the roll-row filled with 0s. For this case, the Moore-Penrose pseudo inverse is applied.

3.3 Control Strategies

All the different control strategies apply a torque on the system based on the difference between the desired position and the real position. In order to obtain the desired accelerations $\dot{\boldsymbol{\nu}}$, it is necessary to solve from Eq. 3.1. Resulting in:

$$\dot{\boldsymbol{\nu}} = \boldsymbol{M}^{-1}\left(\boldsymbol{\tau} - \boldsymbol{C}(\boldsymbol{\nu})\boldsymbol{\nu} - \boldsymbol{D}(\boldsymbol{\nu})\boldsymbol{\nu} - \boldsymbol{g}(\boldsymbol{\eta})\right) \tag{3.29}$$

However, with the modifications proposed by [67], the $\boldsymbol{M}^{-1}$ is now singular, and the Moore-Penrose pseudoinverse matrix must be applied in this case.

3.3.1 Proportional Integral Derivative Controller

The Proportional-Integral-Derivative (PID) is one of the most practical controllers used in linear plants due to its simplicity. It is composed of a proportional term, which is proportional to the present error; an integral term, which accumulates the past errors, and thus eliminates the steady state error; and a derivative term, which works with the rate of change of the error, and thus reduces the overshoot, since it acts as a predictive term. Equation **??** presents a basic PID structure presented by Ogata [53], where K_p represents a proportional gain, τ_i represents an integral time constant, and τ_d represents a derivative time constant.

$$G_c = K_c\left(e(t) + \frac{1}{\tau_i}\int e(t) + \tau_d\frac{de(t)}{dt}\right) \tag{3.30}$$

However, the complex underwater conditions make not possible its correct operation, since the systems became non-linear and with several uncertainties, degrading its performance.

3.3.2 Sliding Mode Controller (SMC)

Uncertainty can be classified into to major kinds [61]:

- Structured: Which are inaccuracies on the modeling.

- Unstructured: Inaccuracies of the system order.

However, both type of inaccuracies have undesired effects on the vehicles. The Sliding Mode controller can deal with uncertainty since it is composed of a nominal part, and additional terms capable of deal with model uncertainty. The task of designing a control law starts with getting the state x to track a specific time varying state x_d in the presence of model imprecision [61]. However to achieve this task successfully the initial desired state $x_d(0)$ must be equal to the real $x(0)$ state.

$$x_d(0) = x(0) \tag{3.31}$$

The aim of sliding mode control is to define a time-varying surface $S(t)$ in the state-space by a scalar equation $s(x, t) = 0$ or:

$$s(x,t) = \left(\frac{d}{dt} + \lambda \right)^{n-1} \tilde{x} \tag{3.32}$$

Where $\tilde{x} = x - x_d$ and with λ strictly positive.

Graphically, the sliding surface is a line in the phase plane, with a slope $-\lambda$ and containing the point x_d.
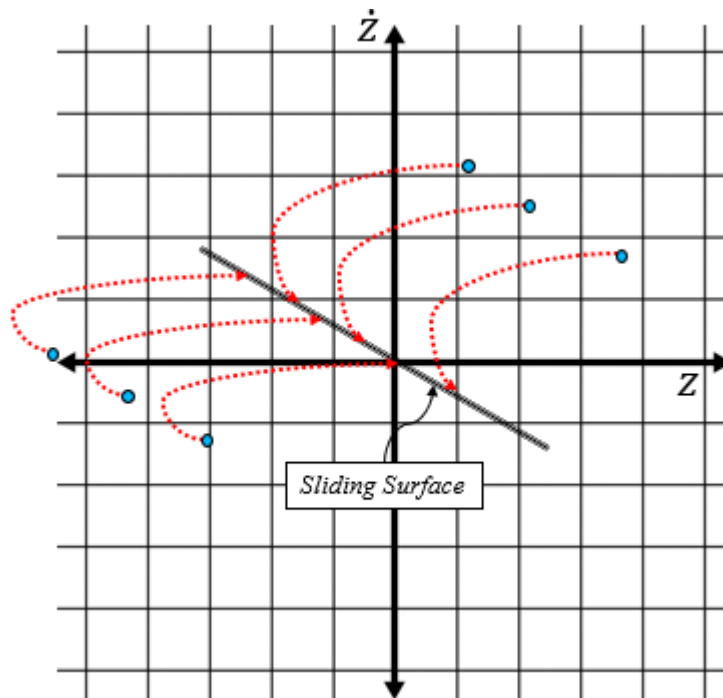
Figure 3.2: Phase plane with a sliding Surface with outside points that reach the surface.

However, it is necessary for the control law to be discontinuous across $S(t)$. This discontinuity term may introduce a high frequency switching in the actuators, called chattering, deteriorating and reducing their lifetime. The controller guarantees an asymptotic convergence of the tracking errors. Unmodeled dynamics and disturbances can be efficiently managed using SMC.

Several variations of this controller have been applied for the trajectory tracking of UUVs, including Terminal SMC, Integral SMC and High Order SMC. These variations preserve the advantages and robustness of the SMC. However, adaptive parameters are added to address the possible changes in the parameters of the vehicle and other external disturbances. Also, it is possible to obtain a faster exponential convergence rate and reduction, or even elimination, of chattering. Every of these configurations offers benefits, as chattering attenuation, finite-time convergence and robustness against unmodeled dynamics. Some of the main variations of SMC are listed on Table 3.2.

Table 3.2: Some SMC variations and their main characteristics. [57]

| Controller	Characteristics
Conventional SMC	Guarantees asymptotic convergence
	Presence of chattering
Terminal SMC	Finite-time convergence
	High steady tracking precision
Integral SMC	Insensitive to uncertainties and disturbances
	High steady state accuracy

3.4 Finite Time Convergence

If the vehicle is placed outside the initial point of the desired trajectory, it must be able to reach the trajectory in an determined time, or converge and reduce the error in finite-time. For this task, it is necessary to establish a sliding surface using a Time Base Generator (TBG), which, according to Morasso [50], is a scalar time function, characterized by a smooth transition from 0 to 1, with a controllable duration t_b and the desired bell-shaped speed profile. Mathematically, it implies that the trajectory is reached at the same time in which the TBG concludes the transition between 0 and 1 as shown in Fig. 3.3.

Garcia-Valdovinos [29], proposed a fifth order soft polynomial for the TBG, with conditions $\xi(t_0) = \dot{\xi}(t_b) = 0$, where t_0 represents the initial time, which is usually equal to 0. The shape of this function, Eq. 3.33, and its derivative, Eq. 3.34, accomplish the conditions presented above.

$$\xi(t) = 10\frac{(t-t_0)^3}{(t_b-t_0)^3} - 15\frac{(t-t_0)^4}{(t_b-t_0)^4} + 6\frac{(t-t_0)^5}{(t_b-t_0)^5} \tag{3.33}$$

$$\dot{\xi}(t) = 30\frac{(t-t_0)^2}{(t_b-t_0)^2} - 60\frac{(t-t_0)^3}{(t_b-t_0)^3} + 30\frac{(t-t_0)^4}{(t_b-t_0)^4} \tag{3.34}$$

The derivative of the TBG function has a bell-shaped form, which satisfies the conditions $\dot{\xi}(t_0) = \dot{\xi}(t_b) = 0$. This functions are shown in Fig. 3.4. The time t_b can be arbitrarily established and does not depend on the initial condition of the system. Equations 3.35 and 3.36 define a well posed TBG as a sliding surface for SMC, with $\alpha_0 = 1+\epsilon$, which represents an initial gain, $0 < \epsilon \ll 1$ and $0 < \delta \ll 1$ [54], which represent adaptive parameters.
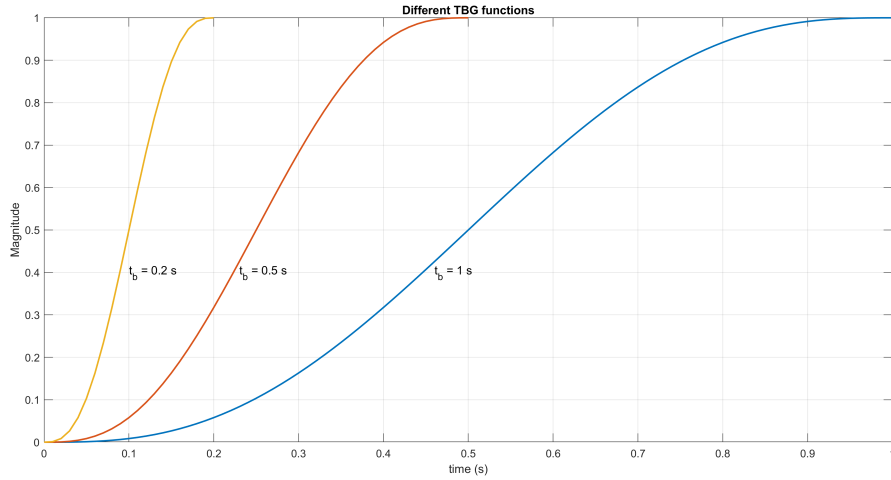
Figure 3.3: Function of the TBG with different values of t_b.
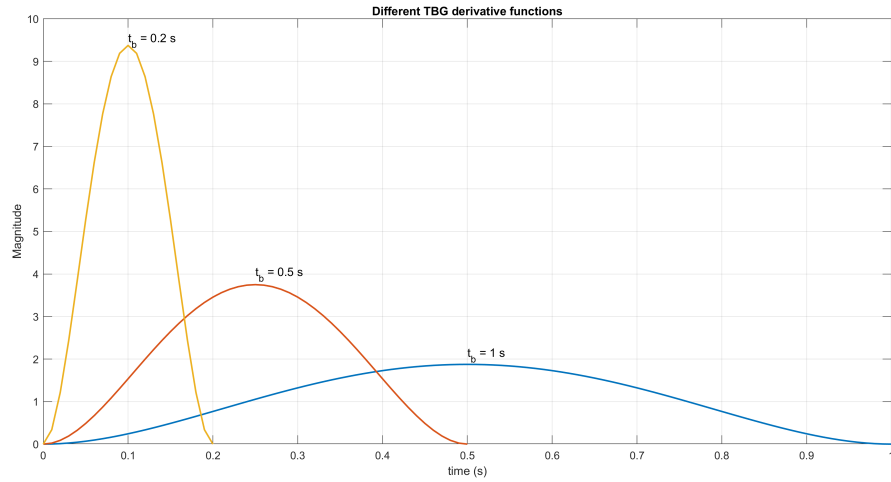
Figure 3.4: Derivatives of the TBG functions with different values of t_b.

$$\dot{z} = -\alpha(t)z \tag{3.35}$$

where

$$\alpha(t) = \alpha_0 \frac{\dot{\xi}}{(1 - \xi) + \delta} \tag{3.36}$$

The solution of the differential equation, shown in eq. 3.36, represents a family of functions that softly converge to a arbitrary small value in the time t_b, and thus convergence in finite time is achieved. The solution is then:

$$z(t) = z(t_0)[1 - \xi + \delta]^{\alpha_0} \tag{3.37}$$

when $t = t_b$, then $\xi(t_b) = 1$ which leads to the solution:

$$z(t_b) = z(t_0)\delta^{\alpha_0} \tag{3.38}$$

Chapter 4

Methodology

In order to successfully synthesize and test the 2nd Order Sliding Mode Controller with finite time convergence some specifications and precisions about the BlueROV2 model will be presented. The parametrization of the trajectory to be tracked, and the description of the used controllers are also described.

4.1 The BlueROV2

The BlueROV2 is a small underwater and affordable vehicle that have been used in other studies [18],[51]. The vehicle have 6 thrusters (T200 model): 4 vectored thrusters for horizontal translation and two vertical thrusters for vertical movement. It is ideal to perform tasks in moderate waters at a maximum depth of 100 m. The model of this vehicle is considered, and its dynamic and hydrodynamic parameters are used in this work to perform the trajectory tracking simulations.

Figure 4.1: BlueROV2 underwater vehicle.

For the operation of the BlueROV2 in this work, the next considerations are taken into account:

- The BlueROV2 operates at relatively low speeds, and thesn lift forces can be neglected.

- BlueROV2 is assumed to have port-starbord and fore-aft symmetry. Thus, the center of gravity is located in the symmetry planes.

- The thruster allocation of the BlueROV2 does not permit an active control of the *pitch* DOF. Since the values of angular position θ and angular velocity q are considered intrinsically stable. Resulting in a system of velocity:

$$\nu = [u, v, w, p, 0, r]^T \tag{4.1}$$

This considerations result in the simplification of the matrices presented in the Chapter 2. Following the work of Wu [67] and Binugroho [8] the matrices M, C, D, and, g applied for this work are:

$$\boldsymbol{M}_{RB} = \begin{bmatrix} m & 0 & 0 & 0 & mz_g & 0 \\ 0 & m & 0 & -mz_g & 0 & 0 \\ 0 & 0 & m & 0 & 0 & 0 \\ 0 & -mz_g & 0 & I_x & 0 & 0 \\ 0 & 0 & 0 & 0 & 0 & 0 \\ 0 & 0 & 0 & 0 & 0 & I_z \end{bmatrix} \tag{4.2}$$

$$\boldsymbol{M_A} = \boldsymbol{M_A}^T = -diag\{X_{\dot{u}}, Y_{\dot{v}}, Z_{\dot{w}}, K_{\dot{p}}, 0, N_{\dot{r}}\} \tag{4.3}$$

As well as with the Mass matrices, the row of the θ DOF, must be changed to 0. The matrices shown in Eq. 3.14 and 3.17 are then:

$$\boldsymbol{C}_{RB}(\boldsymbol{\nu}) = \begin{bmatrix} 0 & 0 & 0 & 0 & mw & 0 \\ 0 & 0 & 0 & -mw & 0 & 0 \\ 0 & 0 & 0 & mv & -mu & 0 \\ 0 & mw & -mv & 0 & I_z r & -I_y q \\ 0 & 0 & 0 & 0 & 0 & 0 \\ mv & -mu & 0 & I_y q & -I_x p & 0 \end{bmatrix} \tag{4.4}$$

$$\boldsymbol{C}_A(\boldsymbol{\nu}) = \begin{bmatrix} 0 & 0 & 0 & 0 & -Z_{\dot{w}}w & Y_{\dot{v}}v \\ 0 & 0 & 0 & Z_{\dot{w}}w & 0 & -X_{\dot{u}}u \\ 0 & 0 & 0 & -Y_{\dot{v}}v & X_{\dot{u}}u & 0 \\ 0 & -Z_{\dot{w}}w & Y_{\dot{v}}v & 0 & -N_{\dot{r}}r & M_{\dot{q}}q \\ 0 & 0 & 0 & 0 & 0 & 0 \\ Y_{\dot{v}}v & X_{\dot{u}}u & 0 & -M_{\dot{q}}q & K_{\dot{p}}p & 0 \end{bmatrix} \tag{4.5}$$

Now, for the damping matrix, after changing to 0 all the parameters in the θ row:

$$\begin{aligned} \boldsymbol{D}(\boldsymbol{\nu}) = & -diag\{X_u, Y_v, Z_w, K_p, 0, N_r\} \\ & -diag\{X_{|u|u}|u|, Y_{|v|v}|v|, Z_{|w|w}|w|, K_{|p|p}|p|, 0, N_{|r|r}|r|\} \end{aligned} \tag{4.6}$$

Finally applying the same technique to decouple the θ DOF for the gravity matrix, it results in:

$$\boldsymbol{g}(\boldsymbol{\eta}) = \begin{bmatrix} (W - B)sin(\theta) \\ -(W - B)cos(\theta)sin(\phi) \\ -(W - B)cos(\theta)cos(\phi) \\ z_g W cos(\theta)sin(\phi) \\ 0 \\ 0 \end{bmatrix} \tag{4.7}$$

4.1.1   Dynamic Parameters

Based on the data from the manufacturer of the BlueROV2, the parameters shown in table 4.1 were obtained.

Table 4.1: Physical parameters and equipment of the BlueROV2

Parameter	Value
Dimensions	457 x 338 x 254 mm
Weight in Air	10-11 kg
Net Buoyancy	0.2 kg

The values of weight and buoyancy can be obtained using Eq.3.20 and Eq.3.21. Solving then:

$$w = mg = 10.5 \ kg \times 9.81 \ \frac{m}{s^2} = 103.005 \ N \tag{4.8}$$

$$B = B_n + w = 0.2 \ N + 103.005 \ N = 105.005 \ N \tag{4.9}$$

Where B_n is the net buoyancy proportioned by the manufacturer.

The information related to the dynamic parameters of the BlueROV2 is not presented exhaustively in the literature. However, information about the BlueROV and BlueROV2 Heavy is presented in the works of Amorim [18] and Laranjeira [51] and Wu [67]. As considered as Wu, the roll and pitch motions of the ROV are passively stable, such that a representative value of $z_g = 0.02 \ m$, which is the distance from the center of the body-fixed frame, located at the center of buoyancy, and the center of gravity, assuming that $r_b = [0, 0, 0]^T$ and $r_g = [0, 0, 0.02]^T$. The information applied for the simulations is shown in Tables

Table 4.2: Used parameters for the BlueROV2 simulation.

Parameter	Value
$\boldsymbol{r}_b$	$[0, 0, 0]^T$
$\boldsymbol{r}_g$	$[0, 0, 0.02]^T$
I_x	$0.16 \ kg \ m^2$
I_y	$0.16 \ kg \ m^2$
I_z	$0.16 \ kg \ m^2$

Table 4.3: Added mass parameters for the BlueROV2 simulation.

Added mass	Value
$X_{\dot{u}}$	$-5\ kg$
$Y_{\dot{v}}$	$-12.7\ kg$
$Z_{\dot{w}}$	$-14.57\ kg$
$K_{\dot{p}}$	$-0.12\ \frac{kg\ m^2}{rad}$
$M_{\dot{q}}$	$-0.12\ \frac{kg\ m^2}{rad}$
$N_{\dot{r}}$	$-0.12\ \frac{kg\ m^2}{rad}$

Table 4.4: Damping parameters for the BlueROV2 simulation.

Linear Damping	Value	Quadratic Damping	Value
X_u	$-4.03\ kg$	$X_{u\|u\|}$	$-18.18\ \frac{Ns^2}{m^2}$
Y_v	$-6.22\ kg$	$Y_{v\|v\|}$	$-21.66\ \frac{Ns^2}{m^2}$
Z_w	$-5.18\ kg$	$Z_{w\|w\|}$	$-36.99\ \frac{Ns^2}{m^2}$
K_p	$-0.07\ kg$	$X_{p\|p\|}$	$-1.55\ \frac{Ns^2}{rad^2}$
M_q	$-0.07\ kg$	$X_{q\|q\|}$	$-1.55\ \frac{Ns^2}{rad^2}$
N_r	$-0.07\ kg$	$X_{r\|r\|}$	$-1.55\ \frac{Ns^2}{rad^2}$

4.1.2 Thruster Allocation

The BlueROV2 has a four vectored thrusters configuration for the horizontal displacement, and two vertical thrusters for the vertical displacement. As it was stated before, the BlueROV2 is intrinsically stable in the *pitch*, θ angle. Considering the same restrictions that Binugroho et al. [8] the matrix $\boldsymbol{T} \in \mathbb{R}^{6 \times 6}$ but with $rank = 5$, since the row corresponding to the roll angle is filled with 0. Matrix $\boldsymbol{T}$ is shown in Eq. 4.10. And the position of the Thrusters are shown in Fig. 4.2.

$$\boldsymbol{T} = \begin{bmatrix} cos(\gamma) & cos(\gamma) & -cos(\gamma) & -cos(\gamma) & 0 & 0 \\ -sin(\gamma) & sin(\gamma) & -sin(\gamma) & sin(\gamma) & 0 & 0 \\ 0 & 0 & 0 & 0 & -1 & -1 \\ 0 & 0 & 0 & 0 & -d_y & d_y \\ 0 & 0 & 0 & 0 & 0 & 0 \\ -d_\psi & d_\psi & -d_\psi & d_\psi & 0 & 0 \end{bmatrix} \quad (4.10)$$

It is important to obtain the position of the thrusters in order to calculate correctly the forces applied by every actuator. The positions are shown in Table 4.5.
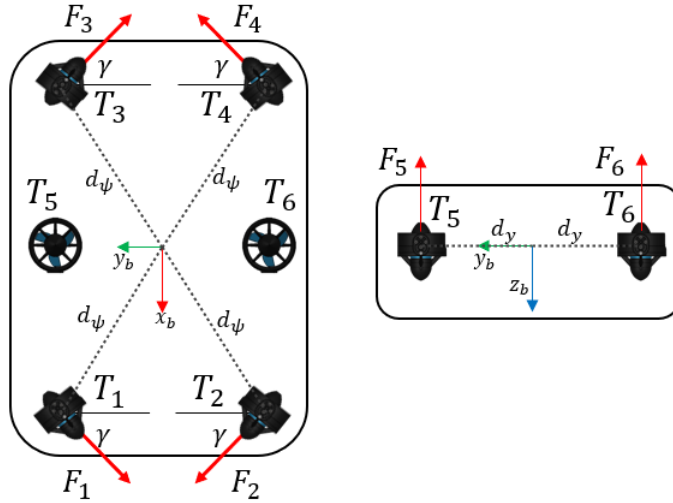
Figure 4.2: Thruster location and numeration used in this work.

Table 4.5: BlueROV2 thrusthers positions with respect of the body-fixed frame [51].

Positions	X (m)	Y (m)	Z (m)
T_1	0.135	-0.115	0.0
T_2	0.135	0.115	0.0
T_3	-0.135	-0.115	0.0
T_4	-0.135	0.115	0.0
T_5	0	-0.115	0.070
T_6	0	0.115	0.070

Applying the matrix from Eq.4.10 with $d_y = 0.115$ and $d_\psi = d_x sin(\gamma) + d_y cos(\gamma)$ with $d_x = 0.135$ [51], the matrix T can be successfully applied for the control of the BlueROV2. The BlueROV2 has six identical thrusters (model T200), which at an operating voltage of 16 V produce approximately 40 N of torque. According to Wu [67],the matrix K can be approximated as shown in Eq. 4.11.

$$K = diag\{40, 40, 40, 40, 40, 40\} \tag{4.11}$$

4.1.3 Saturation of Thrusters

The necessary control signals are calculated with Eq. 3.28. However, in order to make the simulations more realistic the saturation constraints of the thrusters must be taken in account. Since the vector u only can have values between such as $-1 \leq u \leq 1$. The value of u must be constrained, for the 4 horizontal thrusters, which corresponds to the first 4 elements of the vector, if the maximum absolute value of all this four elements is greater than one, all the

values are divided by this value. Then for thrusters T_1, T_2, T_3, T_4:

$$u(i) = \left\{ \frac{u(i)}{\max(u(1:4))} \quad \text{if } \max(|u(1:4)|) > 1 \right. \tag{4.12}$$

with $i = 1, 2, 3, 4$.

Now for the elements of the vertical thrusters, T_5 and T_6, if the value is greater than 1 it is limited only to 1, and if the value is lesser than -1, it is limited to -1. Then:

$$u(i) = \begin{cases} u(i) = 1 & \text{if } u(i) > 1 \\ u(i) = -1 & \text{if } u(i) < -1 \end{cases} \tag{4.13}$$

with $i = 5, 6$.

Now the torques are calculated again using Eq. 3.27.

4.2 Simulations

4.2.1 Software

A simulation program based on a Matlab/Simulink environment was implemented by Hernández-Alvarado [35]. However, this software needs to be adapted for the *BlueROV2*, since the current parameters were obtained for the *6 DoF Kaxan* vehicle. The process presented by Wu [67] will be followed in order to model and update the parameters of the *BlueROV2* into the simulation software. Among other characteristics, this software allows to simulate external disturbances, as ocean currents. For this task, some of the main parameters of the ROV are shown in Tables 4.1, 4.2, 4.3, 4.4 and 4.5.

4.2.2 Parameterized Trajectory

The desired trajectory was chose in order to control the four DOFs of the ROV: x, y, z and ψ. An spiral trajectory was parameterized, as function of time. For the xy plane, the- equations of a circle where used as shown in Eq. 4.14.

$$\begin{aligned} x_d &= R\,cos(\omega t) + h \\ y_d &= R\,sin(\omega t) + k \end{aligned} \tag{4.14}$$

Where $R = 1\ m$, $\omega = \frac{\pi}{6}\ \frac{rad}{s}$, $h = 0$ and $k = 0$, since it is centered in the origin.

For the z axis position, a final depth of $10\ m$ was chose. The parametrization of this component followed a simple line depending on time as shown in Eq. 4.15.

$$z_d = 10\,\frac{t}{t_{total}} \tag{4.15}$$

Where t_{total} is the desired time of simulation.

For a time of simulation, $t_{total} = 30\ s$, the resultant trajectory is shown in Fig.4.3.
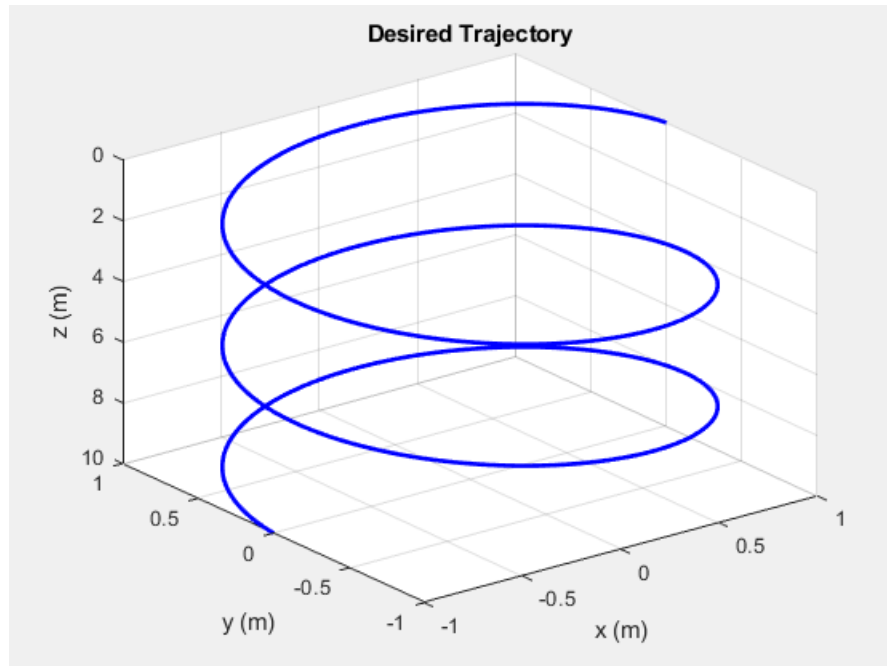
Figure 4.3: Desired trajectory parametrized by Eq. 4.14 and Eq. 4.15.

4.2.3   Parameterized Trajectory for Simultaneous Scheme

To test the trajectory tracking of two BlueROV2 vehicles, a task of gripping, transporting and depositing an object was designed. For successfully accomplish the task, the UUVs must converge to their desired trajectories in a given time, and must keep a constant euclidean distance between them. The heading of both vehicles must remain constant along the time of the task.

The following considerations were made for the design of the task:

1. A tank of $6m \times 6m \times 3m$ is considered as workspace.

2. Only the geometry of the object is considered, neglecting its physical and dynamic properties. The object is considered to be non-deformable and static under the action of marine currents.

3. The position and dimensions of the object are completely known, requiring a distance of 0.5 m between the UUVs to grip it.

4. Both UUVs must grip the object with their front, in such a way that their x axis must be aligned but in opposite directions, having a difference of $180°$ in the heading orientations.

5. The gripping of the object occurs when the UUVs approach to a certain distance of the object, considering high friction at the gripping.

6. The UUVs can start in any initial position, but they finish their trajectories in the opposite corners of the tank.

7. The environment is completely observable, there are not obstacles and it is possible to access to the position states $\eta = [x, y, z, \phi, \theta, \psi]^T$.

Design of the task

The complete coordinated task has a total duration of 40 s and it is divided into 9 intervals:

1. **Interval 1:** $t \leq 6s$
   The vehicles start in an arbitrary initial position and they approximate to the object and converging in finite-time. The initial position of the object is given by $O_i(1.5, 3.5, 3)$. The UUVs arrive one meter above the initial location of the object and with a distance of 0.5 m between their body-reference-frame center point. The heading of the UUVs at this point is given by $\psi_1 = -\frac{\pi}{2}$ and $\psi_2 = \frac{\pi}{2}$.

2. **Interval 2:** $6s < t \leq 9s$
   Descending to the object: The UUVs descend to the depth $z = 3m$ where the object is located.

3. **Interval 3:** $9s < t \leq 12s$
   Gripping of the object: Both vehicles get slightly closer on the y axis reaching the gripping points which are $G_1(1.5, 3.75, 3)$ for UUV1 and $G_2(2.5, 3.25, 3)$ for UUV2.

4. **Interval 4:** $12s < t \leq 15s$
   Carrying of the object: The UUVs ascend to one meter ($z = 2m$) above of the gripping point.

5. **Interval 5:** $15s < t \leq 21s$
   Moving of the object: Both UUVs translates the object to the point above the releasing point $O_f(4.5, 1.5, 3)$.

6. **Interval 6:** $21s < t \leq 24s$
   Descending to the releasing position: The UUVs descend to a depth of $z = 3m$ to release the object. The realising points are $R_1(4.5, 1.75, 3)$ for UUV1 and $R_2(4.5, 1.25, 3)$ for UUV2.

7. **Interval 7:** $24s < t \leq 27s$
   Releasing of the object: The UUVs separate slightly on the y axis to release the object.

8. **Interval 9:** $27s < t \leq 30s$
   Ascending to a safe point: The UUVs ascend slightly to a depth of $z = 2m$.

9. **Interval 6:** $t > 30s$
   The UUVs finish the task moving to their final positions, located at $F_1(0, 0, 0)$ for UUV1 and $F_2(6, 6, 0)$ for UUV2.
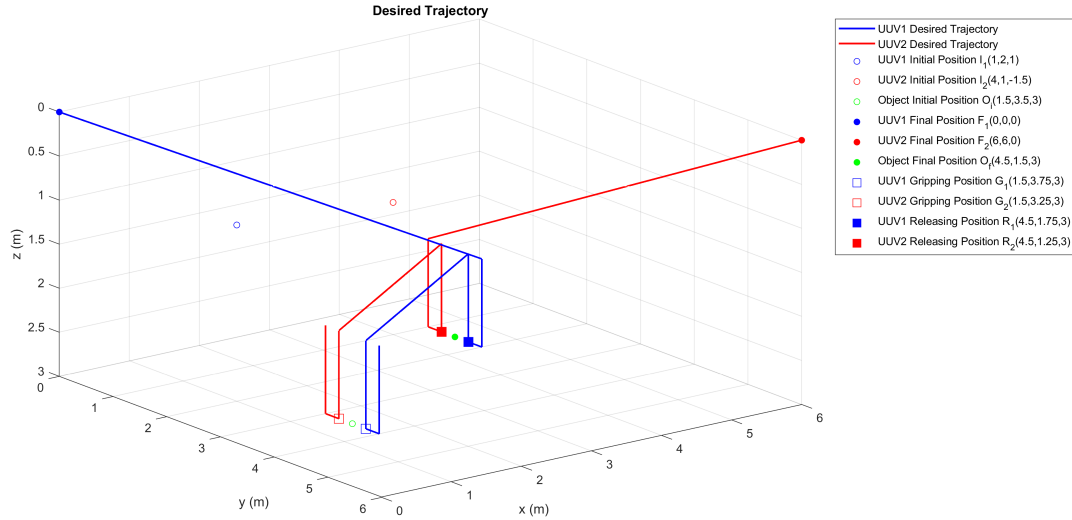
The whole trajectory set is shown in Fig. 4.4.

Figure 4.4: Desired trajectories for simultaneous trajectory tracking.

4.3 Classic Controllers

Once the software is adapted with the right parameters, the control laws based on the PID controller, the Feedback Linearization Controller, the Lyapunov-function based controller and the 2nd order SMC were implemented. These controllers were tested in the Matlab/Simulink program for validation with the previously defined trajectory.

4.3.1 Proportional Integral Derivative Controller

The PID controller is widely used in plants that are linear since it has a simple structure. The controller was applied using Eq. 3.30 can be expanded in order to obtain a structure where the gains K_d and a K_i arise. In the case of the 6 DOF model, $\boldsymbol{K_p}$, $\boldsymbol{K_d}$, $\boldsymbol{K_i}$ are matrices such that the gains are located on the main diagonal.

$$\boldsymbol{G}_{PID} = \boldsymbol{K}_p \boldsymbol{e}(t) + \boldsymbol{K}_i \int \boldsymbol{e}(t) + \boldsymbol{K}_d \frac{d\boldsymbol{e}(t)}{dt} \tag{4.16}$$

Where $\boldsymbol{e}(t) = \boldsymbol{\eta}_d - \boldsymbol{\eta}$ is the error between the desired positions and the actual positions on the Earth-fixed frame.

Now, to obtain the respective torques the Eq. 4.17 is applied.

$$\boldsymbol{\tau} = \boldsymbol{J}^T(\boldsymbol{\nu})\boldsymbol{G}_{PID} \tag{4.17}$$

The controller was tuned manually since the Ziegler-Nichols methods did not apply for the system.

4.3.2 Feedback Linearization Controller

This controller is also called Computed Torque, it is a model-based controller and its main purpose is to cancel the non-linear dynamics of the vehicle, obtaining a closed-loop decoupled

and linear dynamic. Considering the dynamics of the vehicle, presented in Eq. 3.1, the non-linearities can be cancelled using the control law from Eq. 4.18.

$$\boldsymbol{\tau} = \boldsymbol{M}\boldsymbol{a}^b + \boldsymbol{C}(\boldsymbol{\nu})\boldsymbol{\nu} + \boldsymbol{D}(\boldsymbol{\nu})\boldsymbol{\nu} + \boldsymbol{g}(\boldsymbol{\eta}) \tag{4.18}$$

Where the term $\boldsymbol{a}^b$ is called a commanded acceleration [23], that can be designed in order to obtain a linear closed-loop dynamic. This term was implemented in this work as a PID controller, as shown in the Eq.4.19.

$$\boldsymbol{a}^b = \dot{\boldsymbol{\nu}}_d - \boldsymbol{K}_p\tilde{\boldsymbol{\nu}} - \boldsymbol{K}_d\dot{\tilde{\boldsymbol{\nu}}} - \boldsymbol{K}_i \int_0^t \tilde{\boldsymbol{\nu}} dt \tag{4.19}$$

Where $\tilde{\boldsymbol{\nu}} = \boldsymbol{\nu} - \boldsymbol{\nu}_d$ is the tracking error. And the term with commanded accelerations, considering Eq. 4.14 and 4.15, the resulting terms are:

$$\begin{aligned} \ddot{x}_d &= -R\omega^2 cos(\omega t) \\ \ddot{y}_d &= -R\omega^2 sin(\omega t) \\ \ddot{z}_d &= 0 \end{aligned} \tag{4.20}$$

Thus the commanded acceleration vector is $\dot{\boldsymbol{\nu}}_d = [\ddot{x}_d, \ddot{y}_d, \ddot{z}_d, 0, 0, 0]^T$.

The value of gains where exactly the same than the ones used with the PID controller. Also, there is not any parametric uncertainty considered for the control scheme.

4.3.3 Lyapunov Based Controller

The Lyapunov based controller looks for the asymptotic convergence of the tracking error. Proposing a change of coordinates as shown in Eq.4.21 and 4.22.

$$\dot{\boldsymbol{\eta}}_r = \dot{\boldsymbol{\eta}}_d - \alpha\tilde{\boldsymbol{\eta}} \tag{4.21}$$

$$\boldsymbol{S}_\eta = \dot{\boldsymbol{\eta}} - \dot{\boldsymbol{\eta}}_r = \dot{\tilde{\boldsymbol{\eta}}} + \alpha\tilde{\boldsymbol{\eta}} \tag{4.22}$$

Where $\tilde{\boldsymbol{\eta}} = \boldsymbol{\eta} - \boldsymbol{\eta}_d$ is the tracking error respect of the Earth-fixed frame and $\alpha > 0$ is a constant diagonal matrix $\in \mathbb{R}^{6\times6}$. The applied control law is expressed in Eq.4.26.

$$\boldsymbol{\tau}_\eta = \boldsymbol{M}_\eta\ddot{\boldsymbol{\eta}}_r + \boldsymbol{C}_\eta\dot{\boldsymbol{\eta}}_r + \boldsymbol{D}_\eta\dot{\boldsymbol{\eta}}_r + \boldsymbol{g}(\boldsymbol{\eta}) - \boldsymbol{K}_d\boldsymbol{S}_\eta \tag{4.23}$$

To express the control in the body-fixed frame the next transformations are implemented:

$$\dot{\boldsymbol{\eta}}_r = \boldsymbol{J}\boldsymbol{\nu}_r \rightarrow \boldsymbol{\nu}_r = \boldsymbol{J}^{-1}\dot{\boldsymbol{\eta}} \tag{4.24}$$

$$\ddot{\boldsymbol{\eta}}_r = \boldsymbol{J}\dot{\boldsymbol{\nu}}_r + \dot{\boldsymbol{J}}\boldsymbol{\nu}_r \rightarrow \dot{\boldsymbol{\nu}}_r = \boldsymbol{J}^{-1}\left[\dot{\boldsymbol{\eta}}_r - \dot{\boldsymbol{J}}\boldsymbol{\nu}_r\right] \tag{4.25}$$

Considering Eq.4.24 and 4.25 the control law in the body-fixed frame is:

$$\boldsymbol{\tau} = \boldsymbol{M}\dot{\boldsymbol{\nu}}_r + \boldsymbol{C}\boldsymbol{\nu}_r + \boldsymbol{D}\boldsymbol{\nu}_r + \boldsymbol{g}(\boldsymbol{\eta}) - \boldsymbol{K}_d\boldsymbol{S} \tag{4.26}$$

Where $\boldsymbol{S} = \boldsymbol{\nu} - \boldsymbol{\nu}_r$.

4.4 State-of-the-art Controllers

4.4.1 Non-singular Terminal Sliding Mode Control

The work presented by Liu et al [46], includes a non-singular sliding mode manifold defined by:

$$S = e_2 + \beta F_f(e_1) \tag{4.27}$$

where $e_2 = \eta - \eta_d$, $e_2 = \dot{\eta} - \dot{\eta}_d$ with η_d and eta_d are the desired position vector and the desired velocity vector, β is a positive constant and $F_f(e_1)$ is given by:

$$F_f(e_1) = \begin{cases} \sqrt{|A(e_1)|}\frac{(I+e^{-e_1})^2}{e^{-e_1}}\text{sign}(e_1) & \text{if } |e_1| > \epsilon_1 \\ A_1\sin\left(\frac{\pi}{2}\frac{e_1}{\epsilon_1}\right) + \frac{\epsilon_1}{2\pi}A_2\sin\left(2\pi\frac{e_1}{\epsilon_1}\right) & \text{if } |e_1| \leq \epsilon_1 \end{cases} \tag{4.28}$$

where ϵ_1 is a constant vector, I is a ones vector of compatible dimensions, $|e_1|$ is the absolute value of each element in e_1, and:

$$A(e_1) = \frac{I - e^{-e_1}}{I + e^{-e_1}} \tag{4.29a}$$

$$A_1 = \sqrt{|A(\epsilon_1)|}\frac{(I + e^{-\epsilon_1})^2}{e^{-\epsilon_1}} \tag{4.29b}$$

$$A_2 = \frac{1}{\sqrt{|A(\epsilon_1)|}} + \sqrt{|A(\epsilon_1)|}\frac{I - e^{-2\epsilon_1}}{e^{-\epsilon_1}} \tag{4.29c}$$

Considering an AUV subject to modelling uncertainty and external disturbances, the action of control law with the sliding manifold and the adaptive rate is:

$$u = u_{eq} + u_{ad} \tag{4.30a}$$

$$u_{eq} = B^+ J^T((\hat{C}_{RB\eta} + \hat{C}_{A\eta})\dot{\eta} + \hat{D}_\eta\dot{\eta} + \hat{g}_\eta) + \\ B^+ J^T \hat{M}_\eta\left(\dot{\eta}_d - \beta\frac{\partial F_f(e_1)}{\partial e_1}e_2\right) \tag{4.30b}$$

$$u_{ad} = -B^+ J^T \hat{M}_\eta\left(\alpha_1 S + \alpha_2|S|^\gamma\text{sign}(S) + \frac{\hat{L}_m^T\Theta}{2\epsilon_0}S\right) \tag{4.30c}$$

with

$$\dot{\hat{L}}_m = \lambda_m^{-1}\left(\frac{\|S\|^2}{2\epsilon_0^2}\Theta - K_m^2\hat{L}_m\right) \tag{4.31a}$$

$$\dot{K}_m = -\lambda_p^{-1}K_m \tag{4.31b}$$

Where the superscript + denotes a pseudo-inverse operation; α_1 and α_2 are diagonal matrices: ϵ_0 is a positive constant and γ is a constant between 0 and 1; and $\Theta = [1; \|\dot{\eta}\|; \|\dot{\eta}^2\|]^2$

Now the partial derivative $\frac{\partial F_f(e_1)}{\partial e_1}$ is given by:

$$\frac{\partial F_f(e_1)}{\partial e_1} = \begin{cases} \frac{1}{\sqrt{|A(e_1)|}} + \sqrt{|A(e_1)|}\frac{I-e^{-2e_1}}{e^{-e_1}}\text{sign}(e_1) & \text{if } |e_1| > \epsilon_1 \\ \frac{\pi}{2\epsilon_1}A_1\cos\left(\frac{\pi}{2}\frac{e_1}{\epsilon_1}\right) + \frac{\epsilon_1}{2\pi}A_2\cos\left(2\pi\frac{e_1}{\epsilon_1}\right) & \text{if } |e_1| \leq \epsilon_1 \end{cases} \tag{4.32}$$

4.4.2 Finite-Time Second-Order Sliding Mode Control

Liu et al [44] presented a finite-time second-order sliding mode control (FTSOSMC) for trajectory tracking of underwater vehicles subject to system uncertainties and unknown disturbances. The model expressed in the body coordinate system is:

$$\dot{\eta} = J(\eta)\nu \tag{4.33}$$

$$M'\dot{\nu} + C'(\nu)\nu + D'(\nu)\nu g'(\eta) = \tau + \tau_{ex} \tag{4.34}$$

And the underwater vehicle dynamics can be rewritten as:

$$\ddot{\eta} = F(\eta, \dot{\eta}) + G(\eta)\tau + \tau_d \tag{4.35}$$

where $F(\eta, \dot{\eta}) = M^{-1}(-C\dot{\eta}) - D\dot{\eta} - g$ and $G(\eta) = M^{-1}$. Also, $M = M'J^{-1}(\eta)$, $C(\nu, \dot{\eta}) = [C' - M'J^T\dot{J}]J^{-1}(\eta)$, $D(\nu, eta) = D'J^{-1}(\eta)$ and $g(\eta) = g'(\eta)$.

The tracking error is then:

$$e(t) = \eta(t) - \eta_d(t) \tag{4.36}$$

The sliding surface is defined as:

$$s = \dot{e} + \lambda e \tag{4.37}$$

where λ is a positive scalar.

The control law has the form:

$$\tau = \tau_e + M\tau_s \tag{4.38}$$

where $\tau_e = -G^{-1}(F + \lambda\dot{e} - \ddot{\eta}_d)$ and τ_s is defined as:

$$\begin{aligned} \tau_s = &- k_1\text{sign}^b(s) - \int_0^t \left(k_2\text{sign}^{2b-1}(s(\tau))\right. \\ &+ k_3 s(\tau) + k_4\text{sign}^b s(\tau)d\tau \end{aligned} \tag{4.39}$$

4.5 Proposed Model-free Second Order Sliding Mode Control

To develop this controller, a transformation between the body-fixed frame model(Eq.3.1) can be transformed into a Earth-fixed frame model.

$$M_\eta \ddot{\eta}_r + C_\eta(\eta, \nu)\dot{\nu}_r + D_\eta(\eta, \nu)\dot{\nu}_r + g_\eta(\eta) = \tau_\eta \qquad (4.40)$$

Where:

$$M_\eta(\eta) = J^{-T}(\eta)MJ^{-1}(\eta)$$
$$C_\eta(\eta, \nu) = J^{-T}(\eta)J^{-T}(\eta)\left[C(\nu) - MJ^{-1}(\eta)\dot{J}(\eta)\right]J^{-1}(\eta)$$
$$D_\eta(\eta, \nu) = J^{-T}(\eta)D(\nu)J^{-1}(\eta) \qquad (4.41)$$
$$g_\eta(\eta) = J^{-T}(\eta)g(\eta)$$
$$\tau_\eta(\eta) = J^{-T}(\eta)\tau(\eta)$$

García-Valdovinos et al [31] established that equation 3.1 is linearly parametrizable by the product of a regressor $Y(\eta, \dot{\eta}, \ddot{\eta})$ composed of known no linear functions and a vector θ of constant parameters.

$$M_\eta \ddot{\eta}_r + C_\eta(\eta, \nu)\dot{\nu}_r + D_\eta(\eta, \nu)\dot{\nu}_r + g_\eta(\eta) = Y(\eta, \dot{\eta}, \ddot{\eta})\theta \qquad (4.42)$$

The open loop error dynamics are obtained by the substraction of Eq. 4.40 and 4.42. Obtaining:

$$M_\eta \dot{s}_r + C_\eta(\eta, \nu)s_r + D_\eta(\eta, \nu)s_r = \tau_\eta - Y(\eta, \dot{\eta}, \ddot{\eta})\theta \qquad (4.43)$$

Where $s_r = \dot{\eta} - \dot{\eta}$ is the extended error and thus the problem is to design a controller finding a τ that generates exponential convergence when the term $Y(\eta, \dot{\eta}, \ddot{\eta})\theta$ is not available. Now, considering the nominal reference:

$$\dot{\eta}_r = \dot{\eta}_d - \alpha\tilde{\eta} + s_d - K_i \int_0^t sign(s_\eta)d\sigma \qquad (4.44)$$

The position tracking error is described by $\tilde{\eta} = \eta - \eta_d$, as the difference between the actual position and the desired position. α is a diagonal positive definite matrix, which can be manipulated to implement the finite time convergence. K_i is also a diagonal positive definite matrix of gains. Now, considering that:

$$s = \dot{\tilde{\eta}} + \alpha\tilde{\eta}$$
$$s_d = s(t_0)e^{-\kappa t} \qquad (4.45)$$
$$s_\eta = s - s_d$$

The extended error s_r can be expressed as:

$$s_r = s_\eta + K_i \int_0^t sign(s_n)d\sigma \qquad (4.46)$$

Considering Eq.4.47 the proposed control law has the structure:

$$\tau_\eta = -K_d s_r \qquad (4.47)$$

García-Valdovinos et al. [31] presented a stability test of the system and demonstrates the existence of the sliding mode. It concludes that if K_d has a big enough value and the

initial error is small enough the stability arises. To apply the torque correctly to the model it is necessary to transform it back to the Body-fixed frame, using the expression:

$$\boldsymbol{\tau} = \boldsymbol{J}^T \boldsymbol{\tau}_\eta \tag{4.48}$$

Since the diagonal matrix of gains $\boldsymbol{\alpha}$ is constant, the proposed approach from [29] applied to manipulators, is considered to modify and make the gain variable as a function of time and it is parameterized by a time-base generator (TBG) that has the same form of the fifth-order polynomial shown in Eq. 3.33 and its derivative shown in Eq. 3.34. The time base t_b can be set arbitrarily to establish different convergence times. Then, α is defined in Eq. 4.49:

$$\alpha = \begin{cases} \alpha_0 \frac{\dot{\xi}}{1-\xi+\delta} & \text{if } t \le t_b \\ \alpha_c & \text{if } t > t_b \end{cases} \tag{4.49}$$

Where α_0 is $1 + \epsilon$, with $0 < \epsilon \ll 1$ and $0 < \delta \ll 1$ and α_c is a constant gain. The parameters for the implementation are:

4.6 Marine currents

In order to better compare the performance of the proposed controller with finite-time convergence, a simulated marine current was proposed in order to determine the robustness of the controller. The proposed current has the three components of the directions in order to better simulate the effects of the current in a real ocean environment.

In the work presented by Zhang [74], the ocean currents were measured and registered. The depth proposed in the mentioned study has a final value of 800 m, and thus variable currents, dependant on the depth are presented. For the purposes of this study, the depth is only 10 m, and then, the proposed values of velocity are taken as constants, considering the max values reported in [74]:

$$u_c = 0.7\frac{m}{s} \quad v_c = 0.2\frac{m}{s} \quad w_c = 0.3\frac{m}{s} \tag{4.50}$$

4.7 RMS values for comparisons

The results of the performance of the controllers will be examined in terms of the Mean Root Squared (RMS) values of the tracking errors, and the RMS value of the control signal, u. The tracking error is defined as the difference between the desired position and the real position. The formula used to calculated these values will be:

$$x_{RMS} = \sqrt{\frac{1}{N} \sum_{n-1}^{N} |x_n|^2} \tag{4.51}$$

Where x_n is the value of error or the value of control signal, respectively, and N represents the total number of values obtained in the t_{total} simulation time.

Chapter 5

Results

5.1 Spiral Trajectory

Since the main contribution of this thesis is to synthesize the Model-Free Second-Order Sliding Mode Controller with finite-time convergence, the vehicle must start outside of the desired trajectory. The initial proposed point has the structure $\eta_0 = [x_0, y_0, z_0, \phi_0, \theta_0, \psi_0]$, considering the trajectory described before, was the point $\eta_0 = [2, -1, 2, 0, 0, 0]$. Three different times t_b were tested: $t_b = 3$ s, $t_b = 5$ s and $t_b = 3$ s. The time of simulation is always $t_{total} = 30$ s. The results of the implementations of the controllers on the proposed trajectory and with the desired initial point are shown in the next section.

This section will present the behavior of the four control schemes: PID, Feedback Linearization, Lyapunov-Function based, and the Model-Free Second Order Sliding Mode, while reaching the trajectory from the proposed point, and without disturbances. After the proposed marine currents are added to the simulation only with the Second Order Sliding Mode controller in order to test its robustness. The control gains were tuned heuristically to guaranty a good performance in the simulations that do not consider the marine currents. The resulting tuned gains are shown in the Table 5.1.

Table 5.1: Control gains for every control scheme.

Control Scheme	
PID	$\boldsymbol{K}_p = diag\{140, 140, 140, 140, 0, 140\}$ $\boldsymbol{K}_i = diag\{120, 120, 120, 120, 0, 120\}$ $\boldsymbol{K}_d = diag\{180, 180, 180, 180, 0, 180\}$
Feedback Linearization	$\boldsymbol{K}_p = diag\{140, 140, 140, 140, 0, 140\}$ $\boldsymbol{K}_i = diag\{120, 120, 120, 120, 0, 120\}$ $\boldsymbol{K}_d = diag\{180, 180, 180, 180, 0, 180\}$
Lyapunov-Based	$\boldsymbol{\alpha} = diag\{0.8, 0.8, 0.8, 0, 0.8\}$ $\boldsymbol{K}_d = diag\{80, 80, 80, 80, 0, 80\}$
2nd Order SMC	$\boldsymbol{K}_d = diag\{800, 800, 800, 800, 0, 800\}, \boldsymbol{K}_i = diag\{5, 5, 5, 5, 0, 5\}$ $\kappa = 5, \alpha_0 = 1.01, \alpha_c = 25, \delta = 0.001$

5.1.1 Proportional Integral Derivative Controller

The main results of the PID controller on the proposed trajectory are shown next. The linear position behavior is shown in Fig. 5.1, while the angular position comparison is shown in Fig. 5.2. It can be seen that the PID converges to the trajectory with an overshoot in all the degrees of freedom, except the ψ angle, since it is already in the desired value. Since θ is not controllable, the movement in this DOF is caused by the displacement of the vehicle. The errors are not maintain in 0 along the whole trajectory.
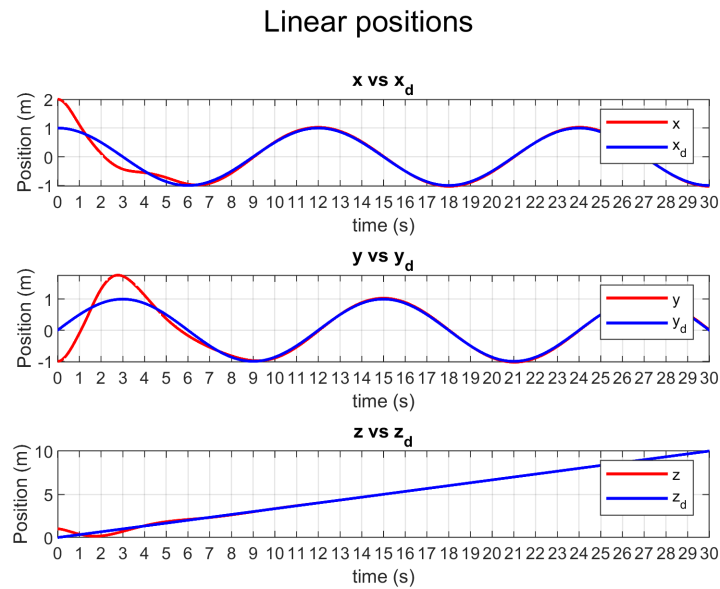
Figure 5.1: Resulting linear positions with the PID controller.
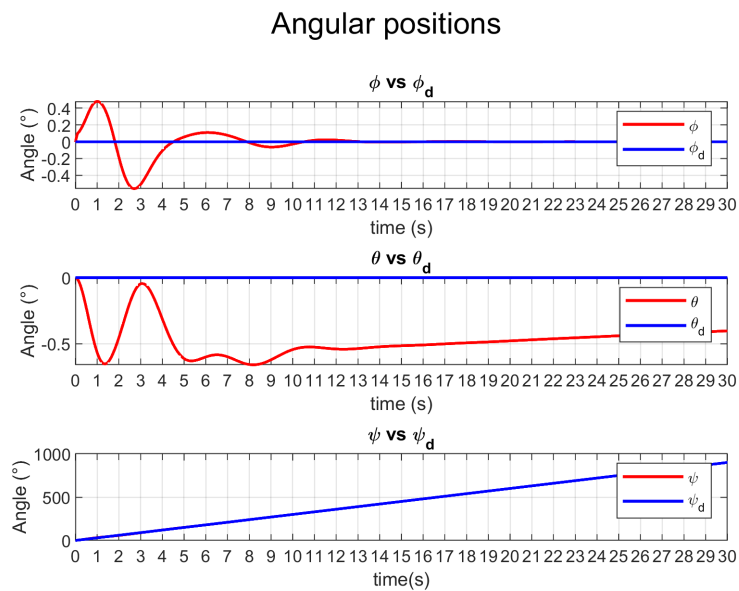
Figure 5.2: Resulting angular positions with the PID controller. Note that θ is not controllable.

Linear and angular velocities in the body-fixed frame are shown in Fig. 5.3 and 5.4. As well as with the positions, the velocities reach their desired values with overshoot and a small error is maintain along the whole trajectory. As well as θ, q is not controllable.
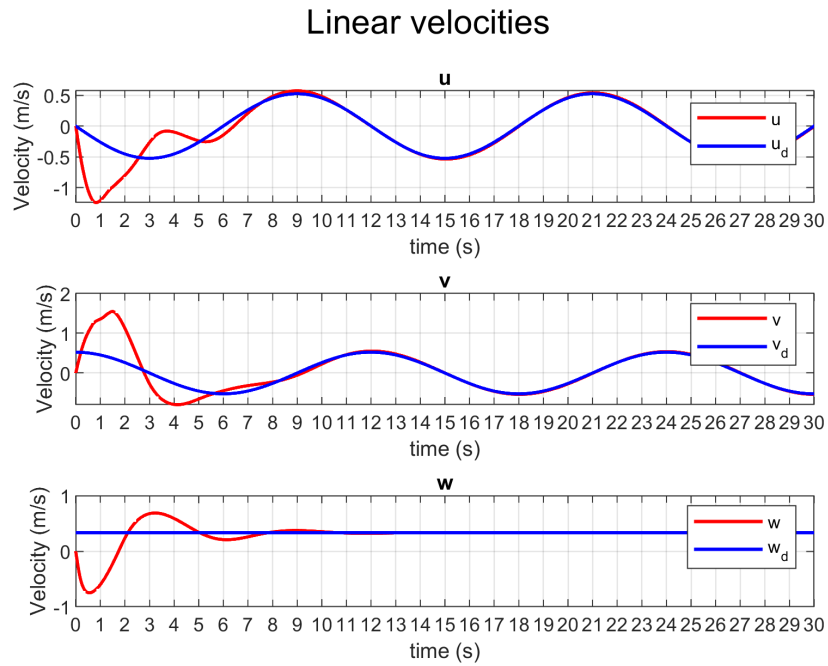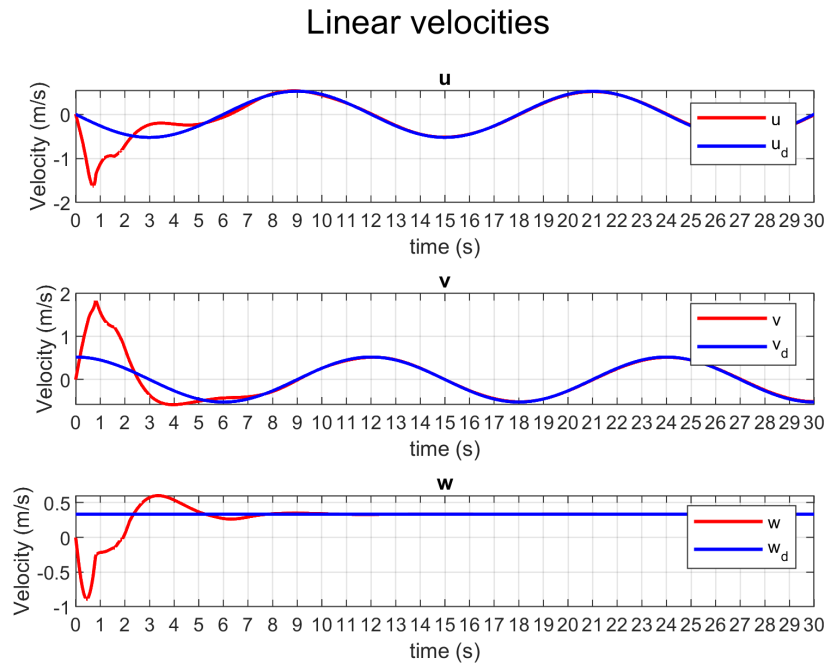

Figure 5.3: Resulting linear velocities with the PID controller.
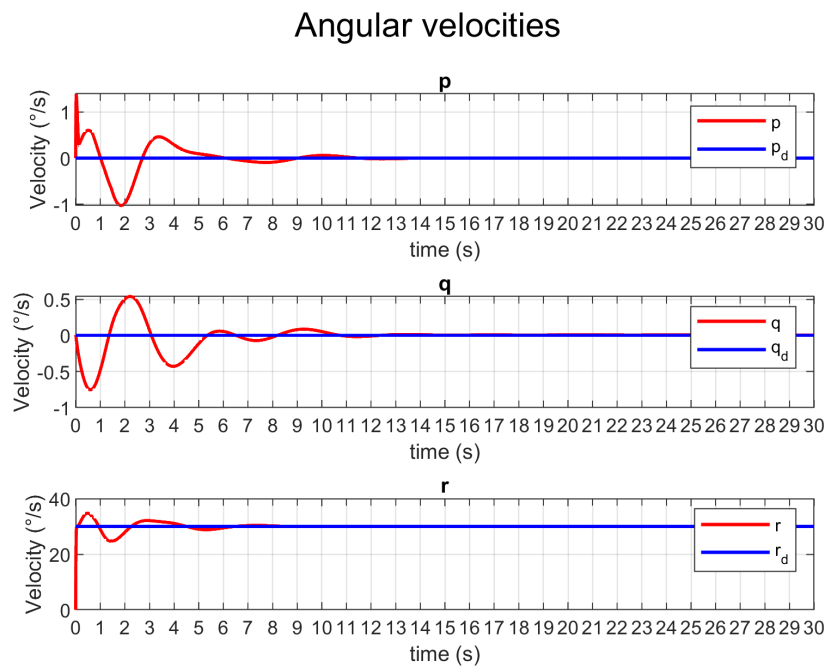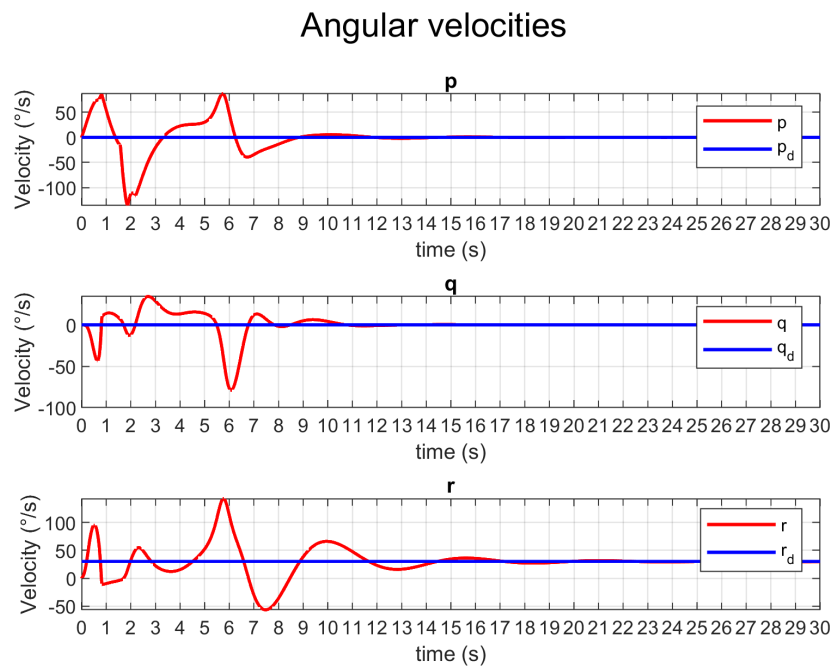

Figure 5.4: Resulting angular velocities positions with the PID controller. Note that q is not controllable.

The comparison between the desired trajectory and the actual trajectory performed by the controller is shown in Fig. 5.5. It can be seen that the obtained trajectory does not follow the desired trajectory, since a small error is maintained between them.
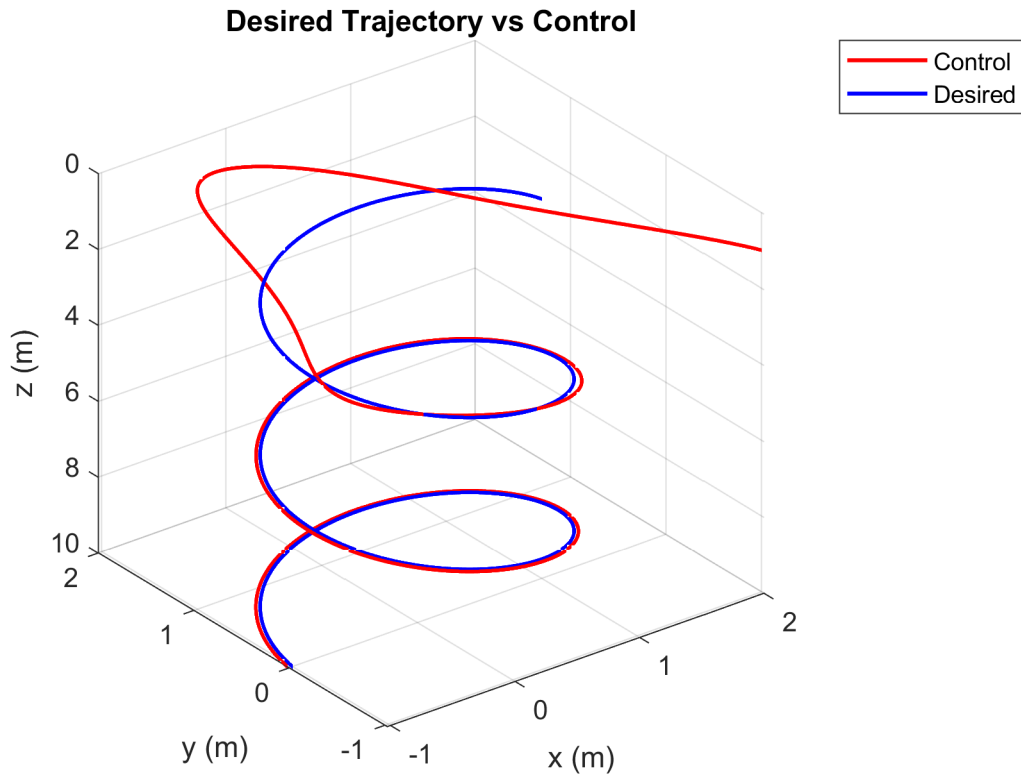
Figure 5.5: Comparison of Trajectories with the PID controller.

The applied torques and the control signals for every thruster are shown in Fig. 5.6 and 5.7. It can be seen that only in the beginning a strong control signal and thus, a strong torque, is applied to force the ROV to converge to trajectory. However, once the vehicle is in a vicinity near to 0, the control signals and the torques becomes constant and smooth.

Required torques per DOF
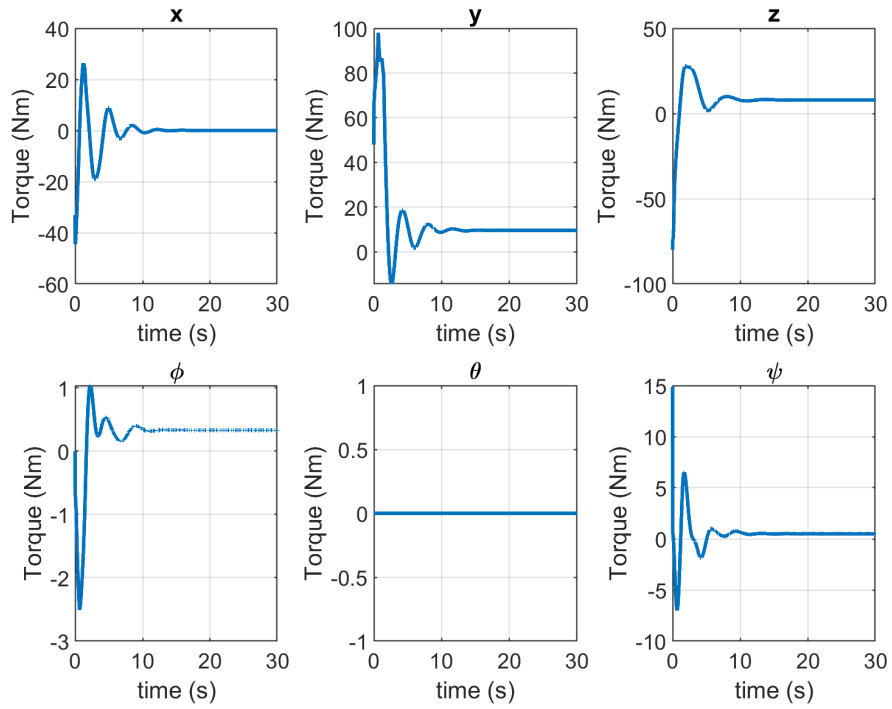
Figure 5.6: Required Torques with the PID controller.

Control signals for each thruster
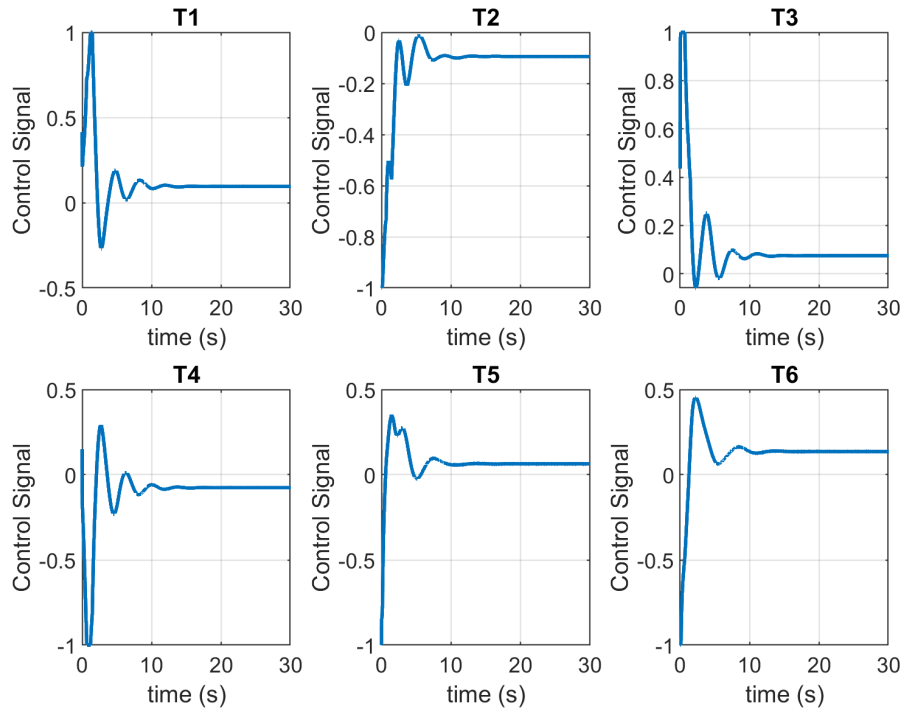
Figure 5.7: Control signals u behavior with the PID controller.

5.1.2 Feedback Linearization Controller

The main results of the Feedback Linearization Controller on the proposed trajectory are shown next. The linear position behavior is shown in Fig. 5.8, while the angular position comparison is shown in Fig. 5.9. The behavior of this controller also presented overshoots in all the DOF. Specially, the angular positions of the ϕ angle has an overshoot of $\pm 50°$. Even when θ is not controllable, the fast movement of the vehicle to converge to the trajectory causes an overshoot of $40°$, but after a while it stabilizes to value of $\theta \approx 10°$.
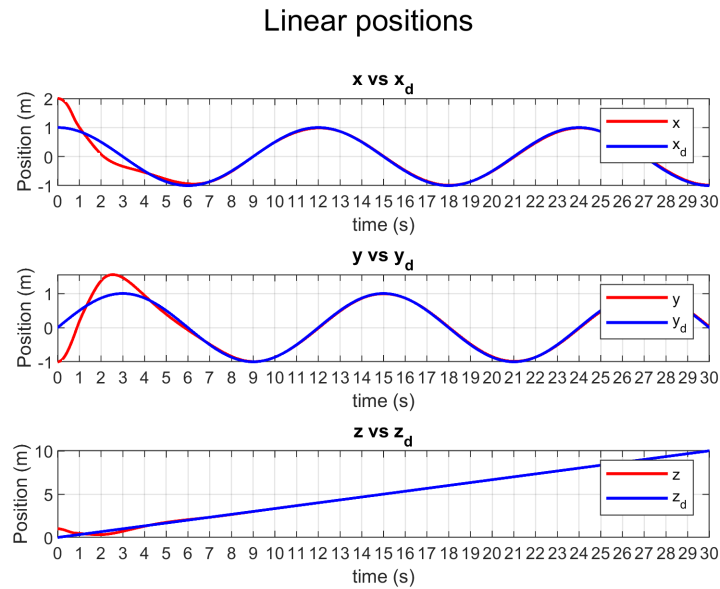
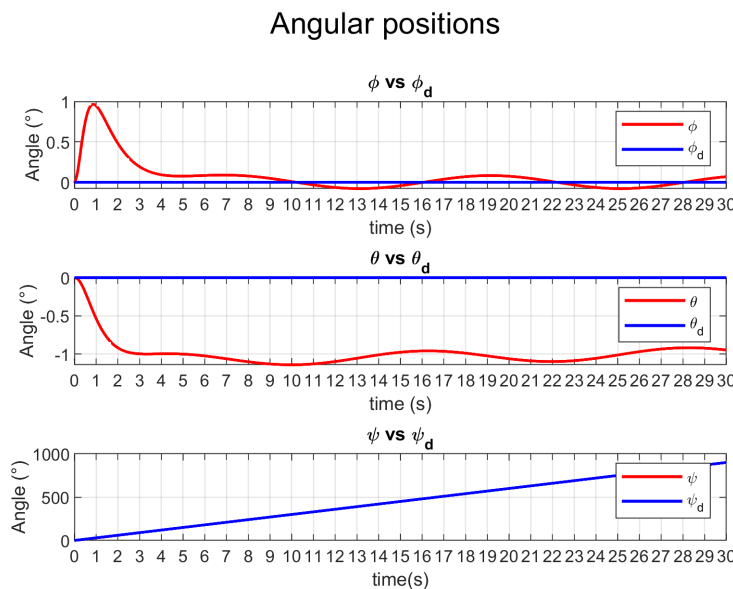Figure 5.8: Resulting linear positions with the Feedback Linearization controller.
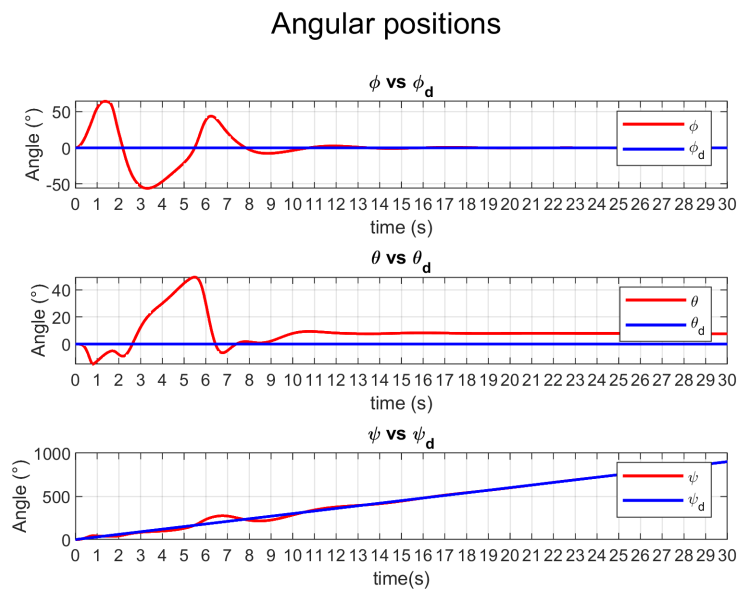
Figure 5.9: Resulting angular positions with the Feedback Linearization controller.

Linear and angular velocities in the Body-fixed frame are shown in Fig. 5.3 and 5.4. it can be seen that velocities u, v and w have a sharp behavior. Angular velocities have also abrupt behaviors, having maximum values greater than $100\frac{\circ}{s}$.
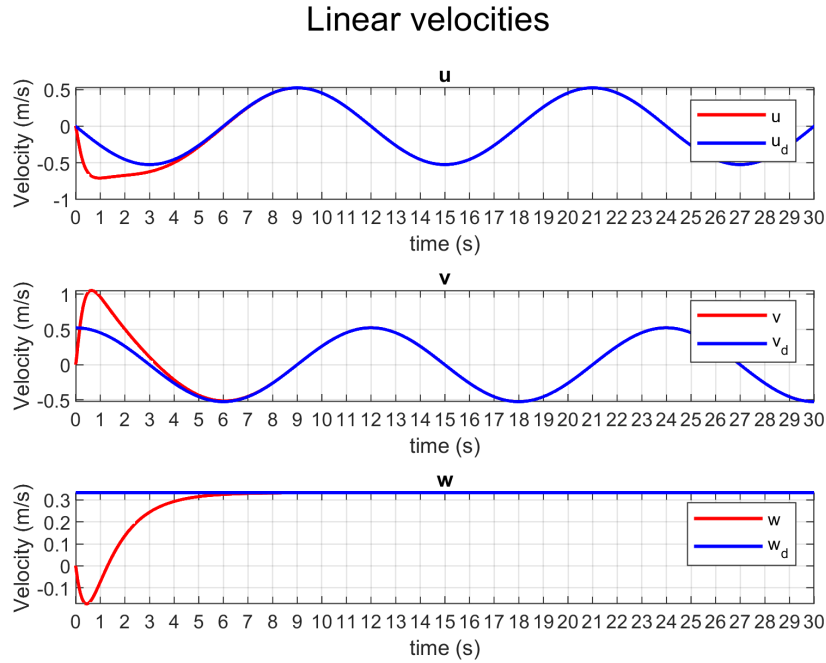

Figure 5.10: Resulting linear velocities with Feedback Linearization controller.

Figure 5.11: Resulting angular velocities positions with the Feedback Linearization controller. Note that only q is not controllable.

The comparison between the desired trajectory and the actual trajectory performed by the controller is shown in Fig. 5.12.
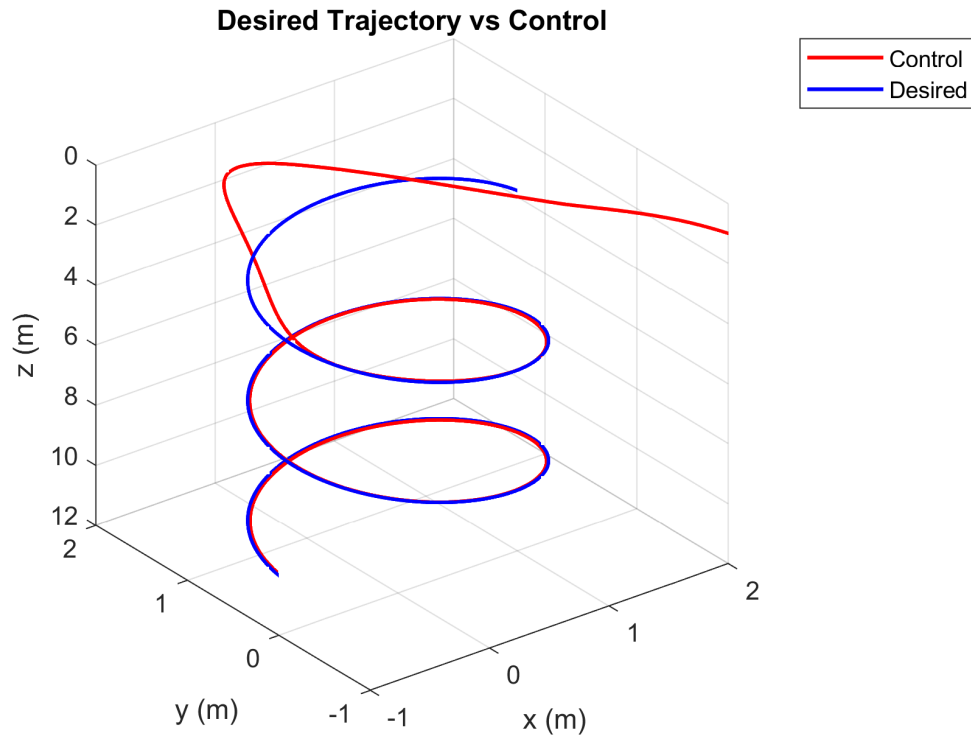
Figure 5.12: Comparison of Trajectories with the Feedback Linearization controller.

The applied torques and the control signals for every thruster are shown in Fig. 5.13 and 5.14. It can be seen that at the beginning both control signals and required torques presented abrupt changes and oscillations. Approximately, after $t = 10s$ the signals become smoother and constant.

Required torques per DOF
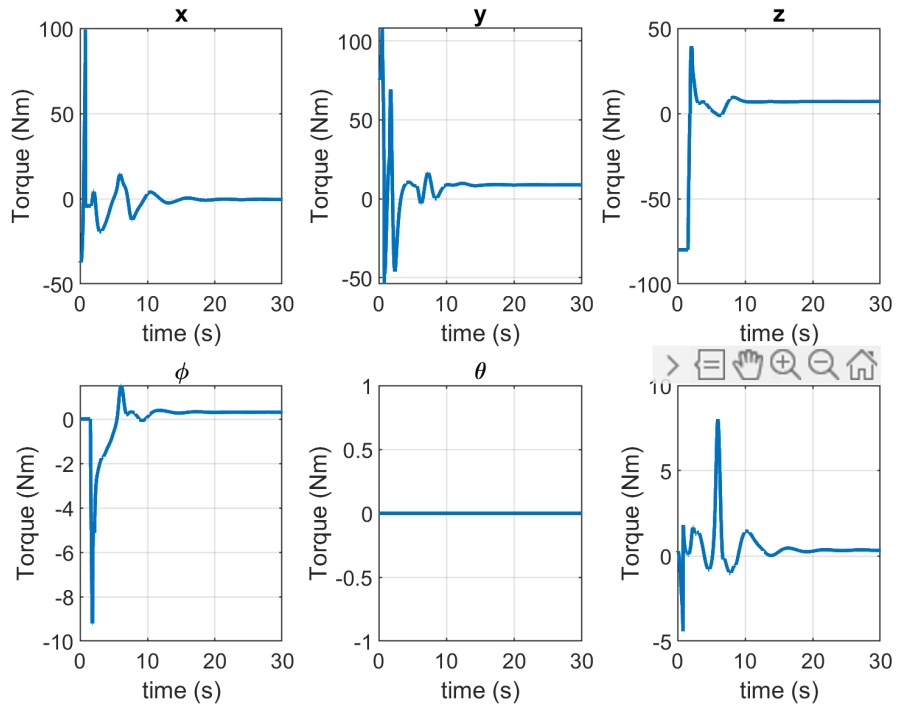
Figure 5.13: Required Torques with the Feedback Linearization controller.

Control signals for each thruster
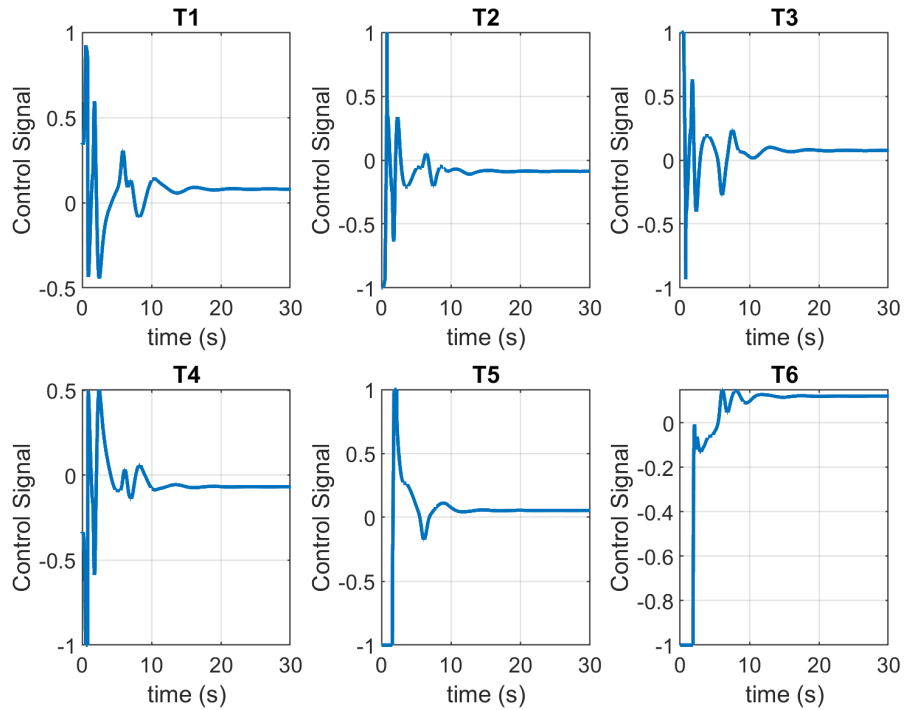
Figure 5.14: Control Signals with the Feedback Linearization controller.

5.1.3 Lyapunov Based Controller

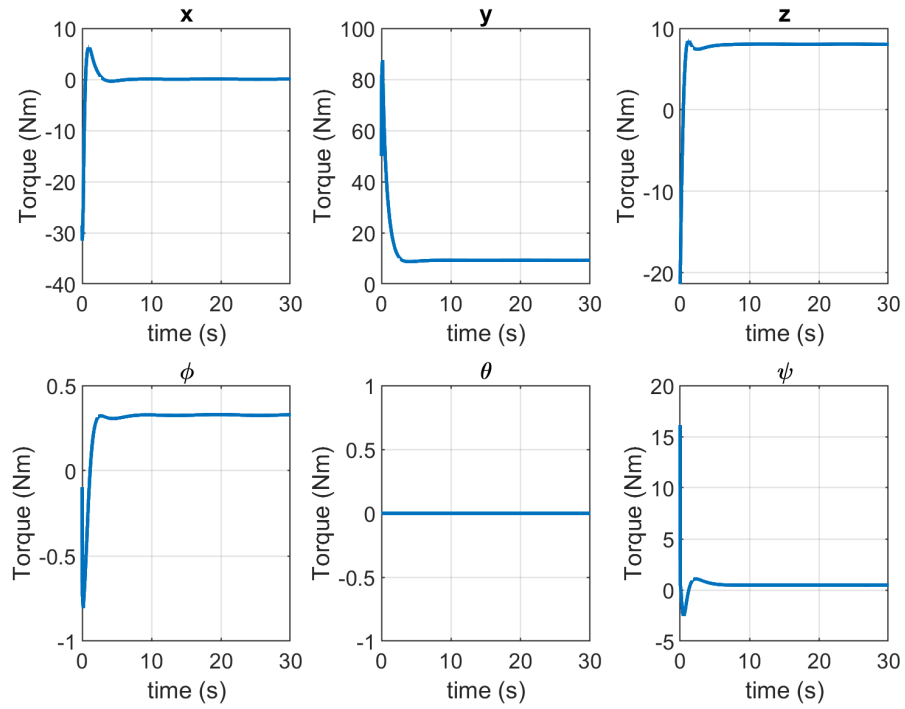The main results of the Lyapunov Based Controller on the proposed trajectory are shown next. The linear positions behavior is shown in Fig. 5.15, while the angular position comparison is shown in Fig. 5.16. The Lyapunov based controller offers exponential convergence, which is seen in the convergence of the errors. The linear position errors converge to 0 in a time $t \approx 6s$. This convergence is smooth and following the exponential behavior. In the angular positions, the errors are kept oscillating in a small vicinity near to 0 for ϕ.
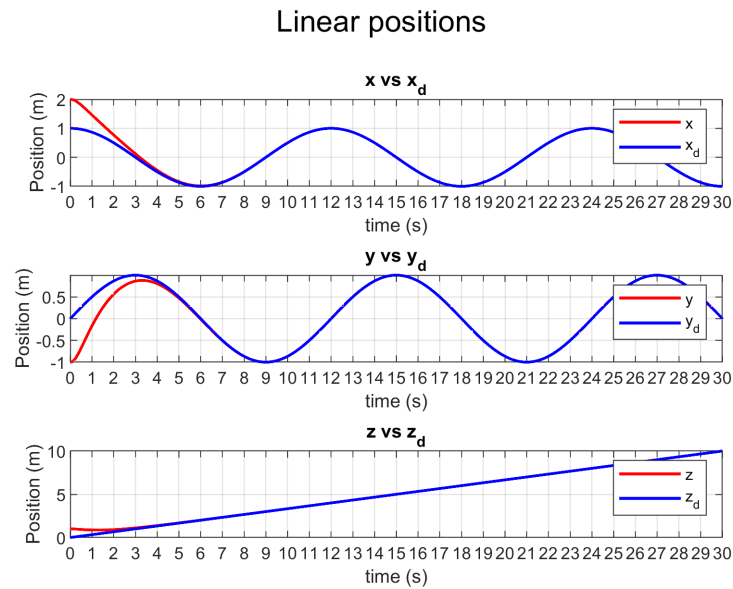
Figure 5.15: Resulting linear positions with the Lyapunov-function based controller.

Figure 5.16: Resulting angular positions with the Lyapunov-function based controller.

Linear and angular velocities in the Body-fixed frame are shown in Fig. 5.17 and 5.18. Velocities also converge exponentially, except for velocity r, which have an abrupt behavior. For the case of p, the velocity present small oscillations around the desired value. Recall that q is not controllable.

Figure 5.17: Resulting linear velocities with the Lyapunov-function based controller.
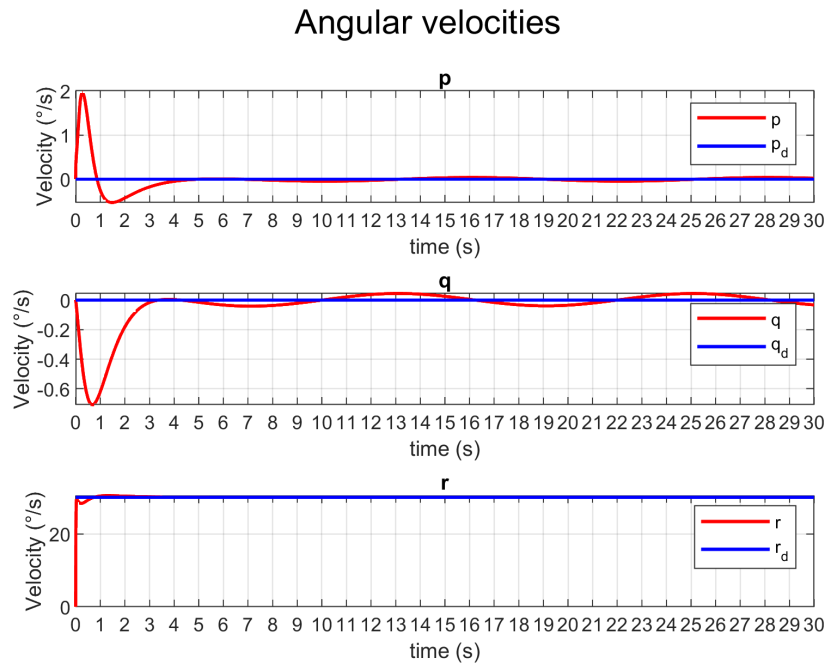
Figure 5.18: Resulting angular velocities positions with the Lyapunov-function based controller. Note that only q is not controllable.

The comparison between the desired trajectory and the actual trajectory performed by the controller is shown in Fig. 5.19.
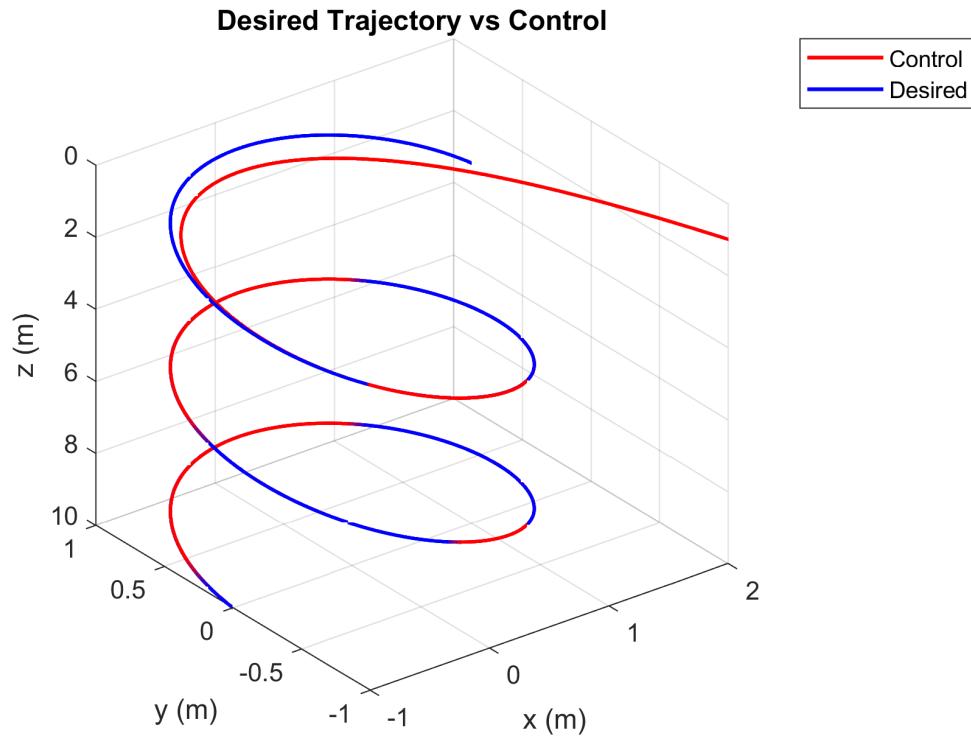
Figure 5.19: Comparison of Trajectories with the Lyapunov-function based controller.

The applied torques and the control signals for every thruster are shown in Fig. 5.20 and 5.21. Both the control signal u and the torques for each thruster presented an exponential and behavior. After the time of converge both of this variables remain constant. As a special remark the variation of the parameter α modifies the convergence time.

Required torques per DOF

Figure 5.20: Required Torques with the Lyapunov-function based controller.

Control signals for each thruster
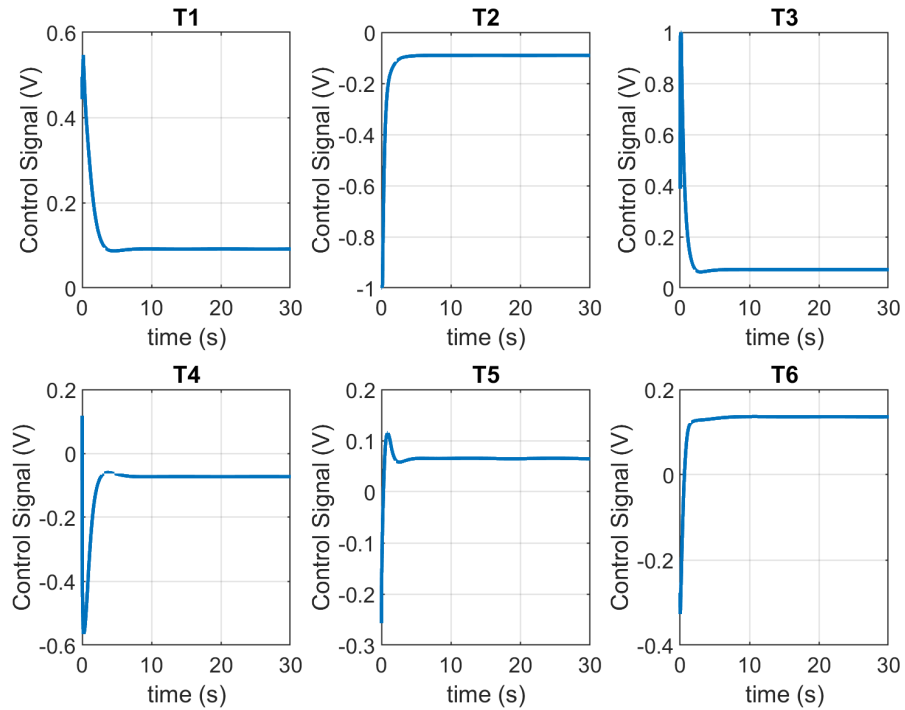
Figure 5.21: Control Signals with the Lyapunov-function based controller.

5.1.4 Model-free Second Order Sliding Mode Controller

There where three different arbitrarily selected time to perform the simulations. These times were $t_b = 3\ s$, $t_b = 5\ s$, $t_b = 7\ s$.

$t_b = 3\ s$

The results of the 2nd Order SMC on the proposed trajectory with a $t_b = 3\ s$ are shown next. The linear position behavior is shown in Fig. 5.22, while the angular position comparison is shown in Fig. 5.23. The behavior of the convergence is completely smooth and is done in the proposed time $t_b = 3s$ for all the degrees of freedom. The error is kept at 0 along the whole trajectory.
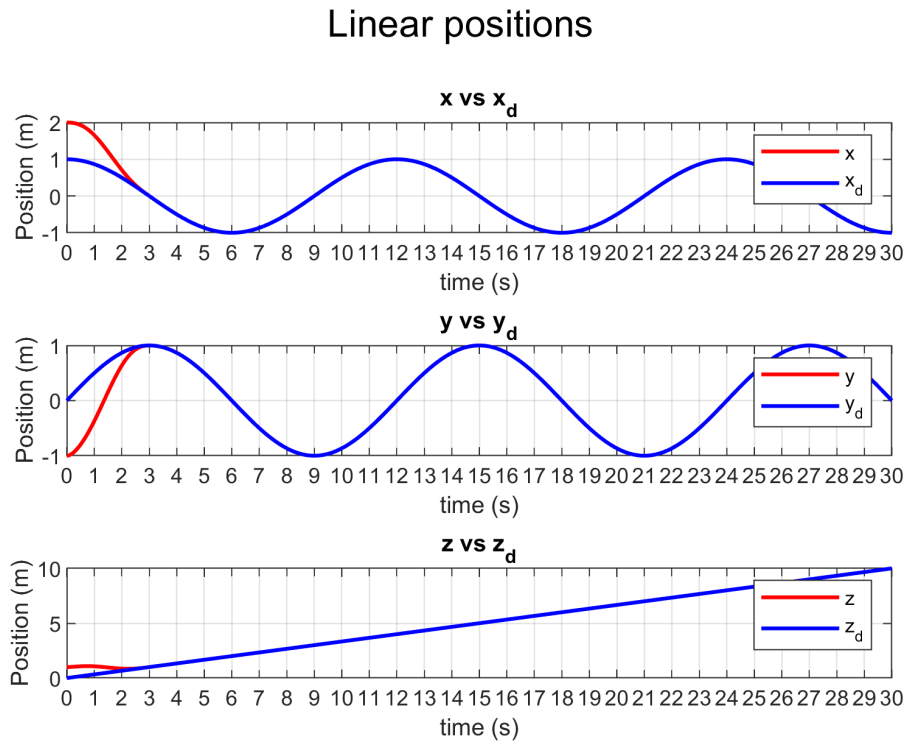
Figure 5.22: Resulting linear positions with the 2nd Order SMC with a $t_b = 3\ s$

Angular positions
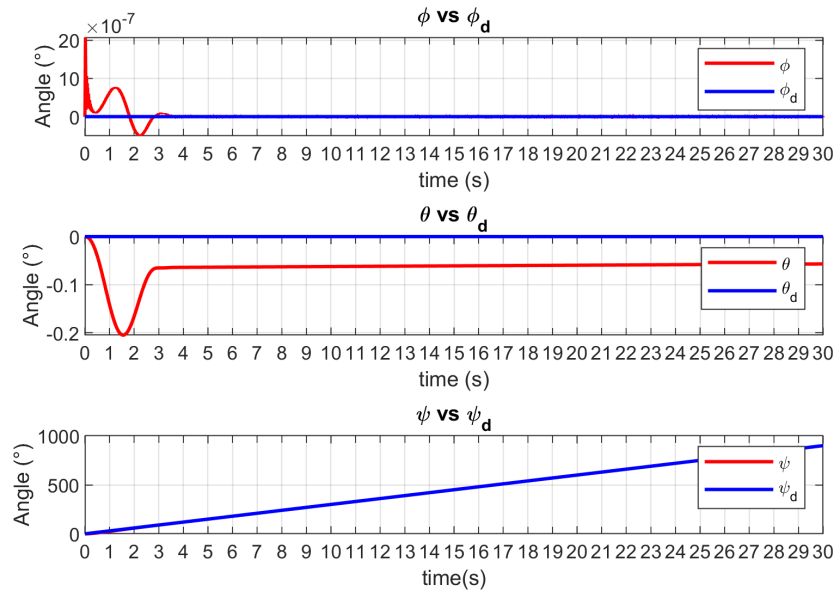
Figure 5.23: Resulting angular positions with the 2nd Order SMC with a $t_b = 3\ s$

Linear and angular velocities in the Body-fixed frame are shown in Fig. 5.24 and 5.25. It can be seen that velocities converge in the same proposed time $t_b = 6s$, and its values are maintain at 0 along the whole trajectory.
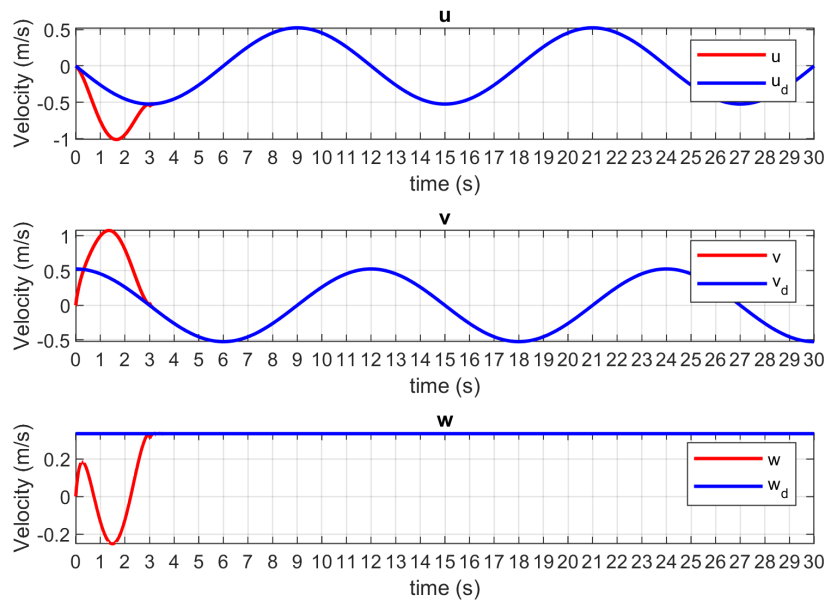
Linear velocities

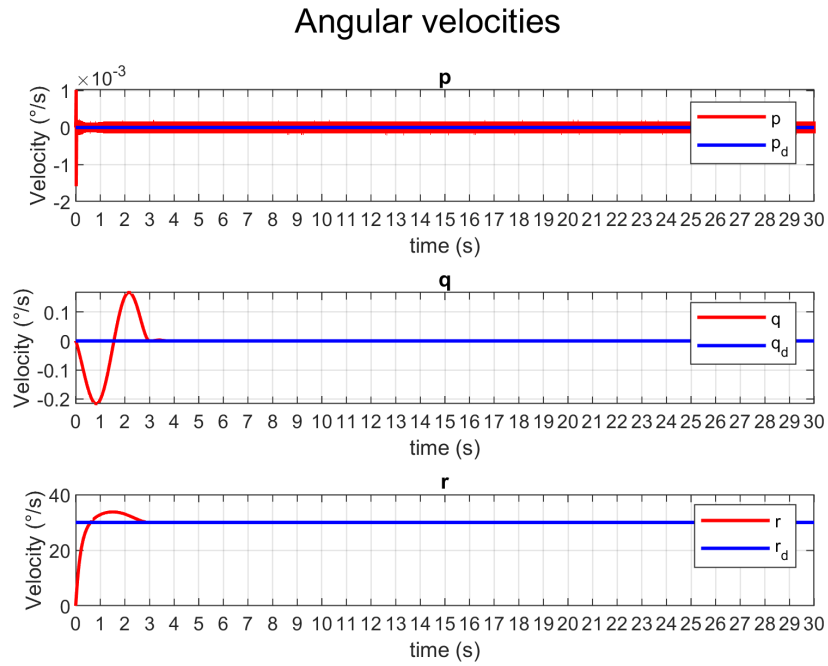Figure 5.24: Resulting linear velocities with the 2nd Order SMC with a $t_b = 3\ s$

Figure 5.25: Resulting angular velocities positions with the 2nd Order SMC with a $t_b = 3$ s. Note that only q is not controllable.

The comparison between the desired trajectory and the actual trajectory performed by the controller is shown in Fig. 5.26.
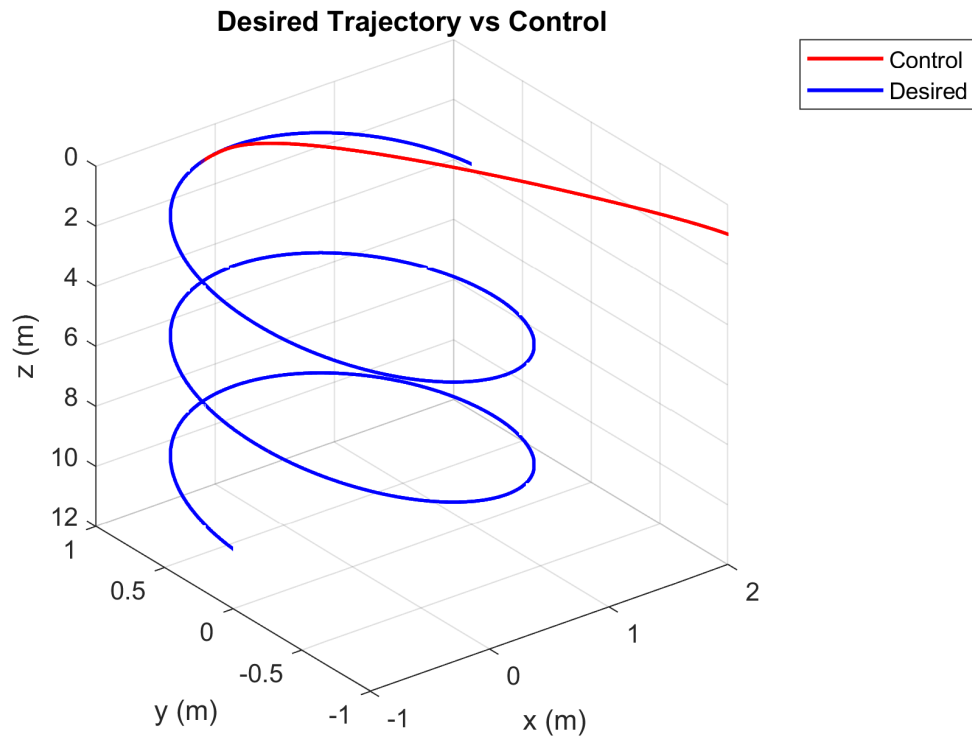

Figure 5.26: Comparison of Trajectories with the 2nd Order SMC with a $t_b = 3$ s

The applied torques and the control signals for every thruster are shown in Fig. 5.27 and 5.28. The plots shown that the control signals are smooth and continuous, avoiding the saturation of the actuators. After the convergence is achieved, the values of torques are maintain constant.
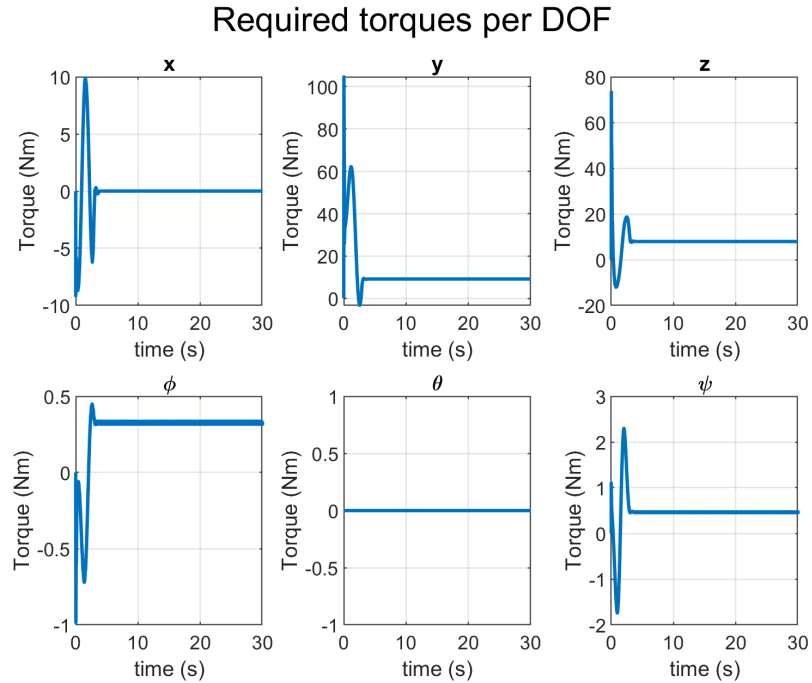

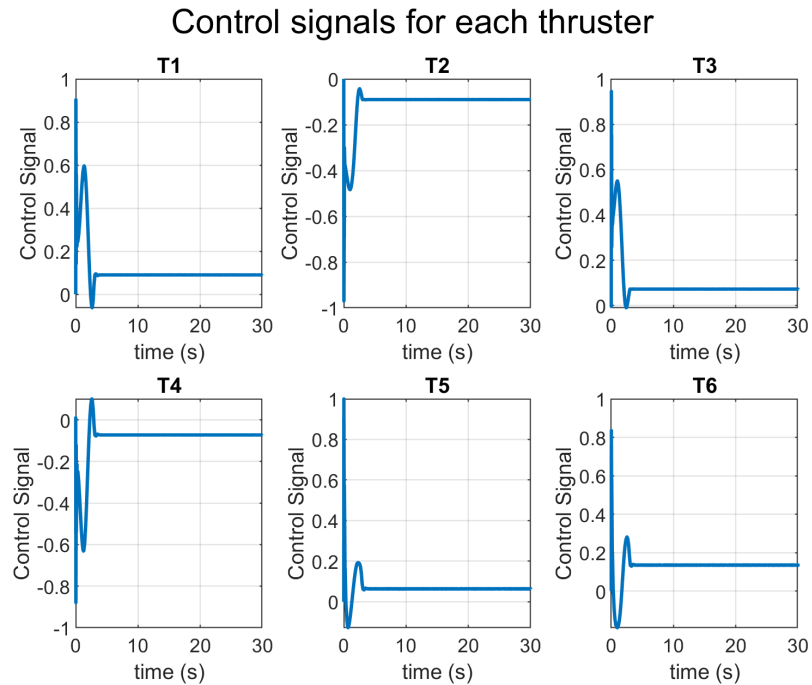Figure 5.27: Required Torques with the 2nd Order SMC with a $t_b = 3\ s$

Figure 5.28: Control Signals with the 2nd Order SMC with a $t_b = 3\ s$

$t_b = 5\ s$

The results of the 2nd Order SMC on the proposed trajectory with a $t_b = 5\ s$ are shown next. The linear position behavior is shown in Fig. 5.29, while the angular position comparison is shown in Fig. 5.30. The same behavior is expected, even when the time t_b was modified, the vehicle converge to the desired trajectory in the proposed time.
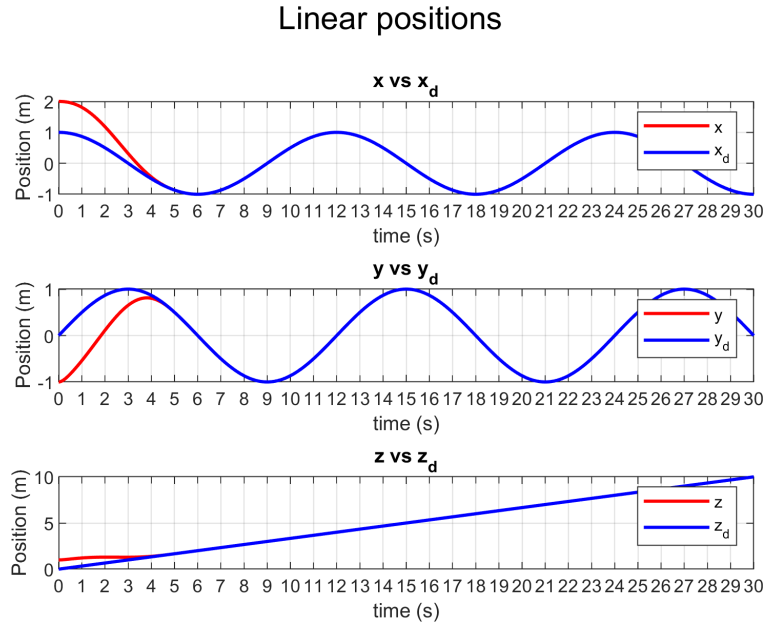

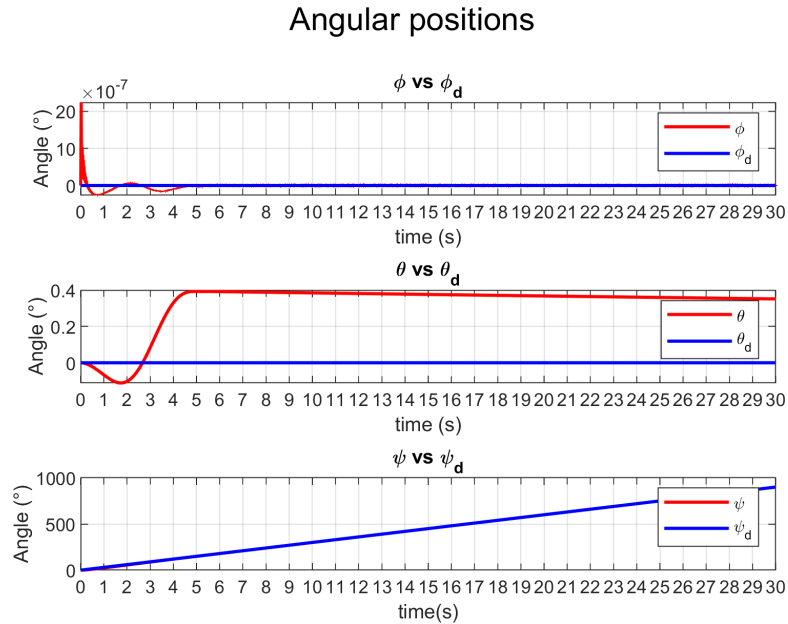Figure 5.29: Resulting linear positions with the 2nd Order SMC with a $t_b = 5\ s$

Figure 5.30: Resulting angular positions with the 2nd Order SMC with a $t_b = 5\ s$

Linear and angular velocities in the body-fixed frame are shown in Fig. 5.31 and 5.32, and they have the same behavior, converging in the proposed time $t_b = 5s$.
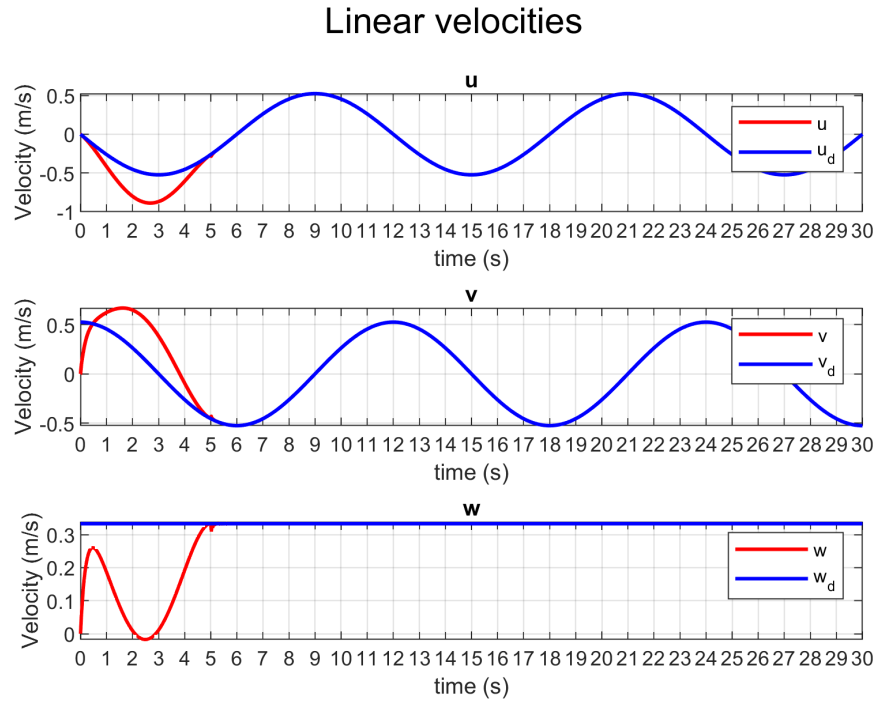
Linear velocities

Figure 5.31: Resulting linear velocities with the 2nd Order SMC with a $t_b = 5$ s
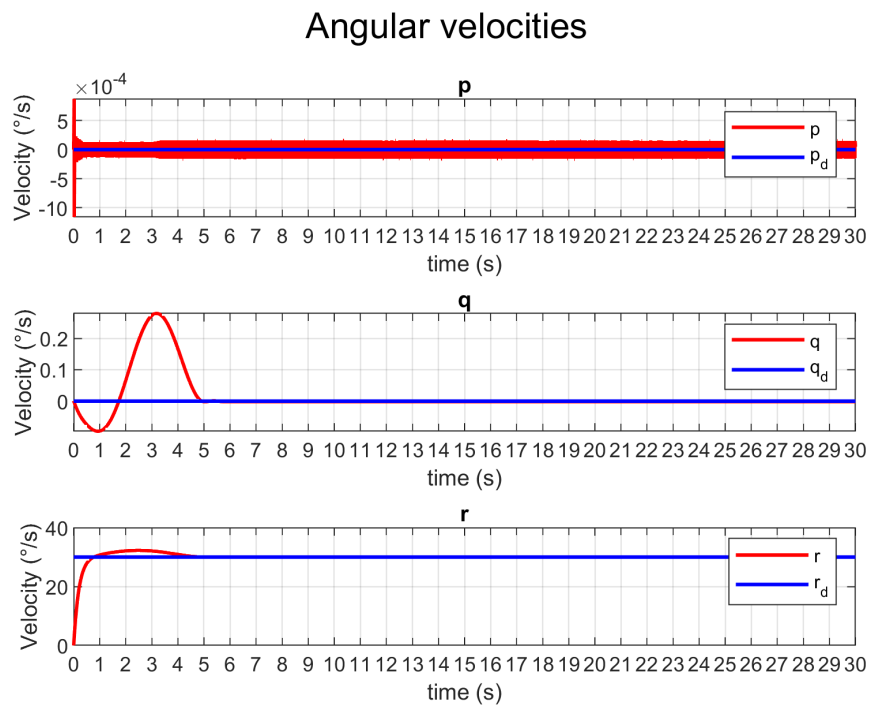
Angular velocities

Figure 5.32: Resulting angular velocities positions with the 2nd Order SMC with a $t_b = 5$ s. Note that only q is not controllable.

The comparison between the desired trajectory and the actual trajectory, performed by the controller, is shown in Fig. 5.33.
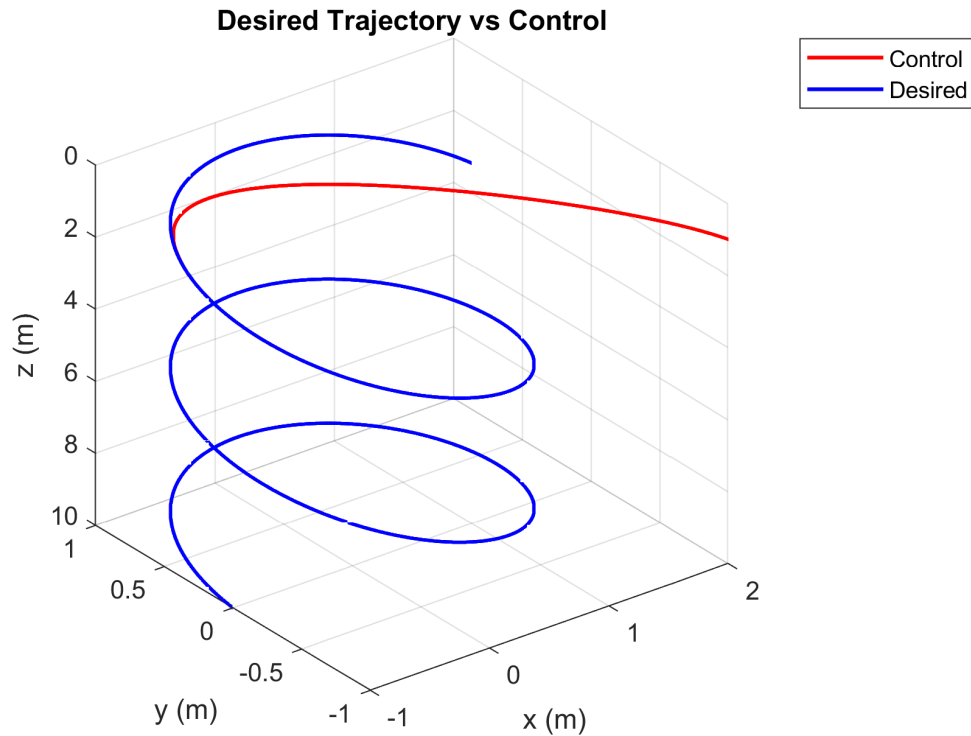

Figure 5.33: Comparison of Trajectories with the 2nd Order SMC with a $t_b = 5\ s$

The applied torques and the control signals for every thruster are shown in Fig. 5.34 and 5.35. The graphs show a relaxation in the torques, since the t_b is bigger, and the vehicle has more time to converge to the desired trajectory.

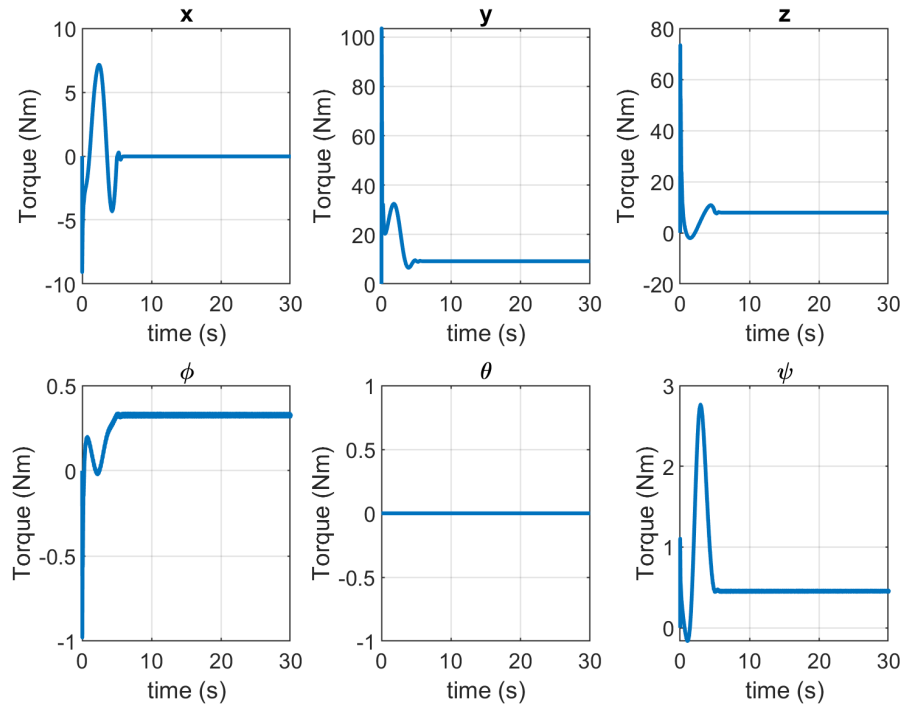Figure 5.34: Required Torques with the 2nd Order SMC with a $t_b = 5\ s$
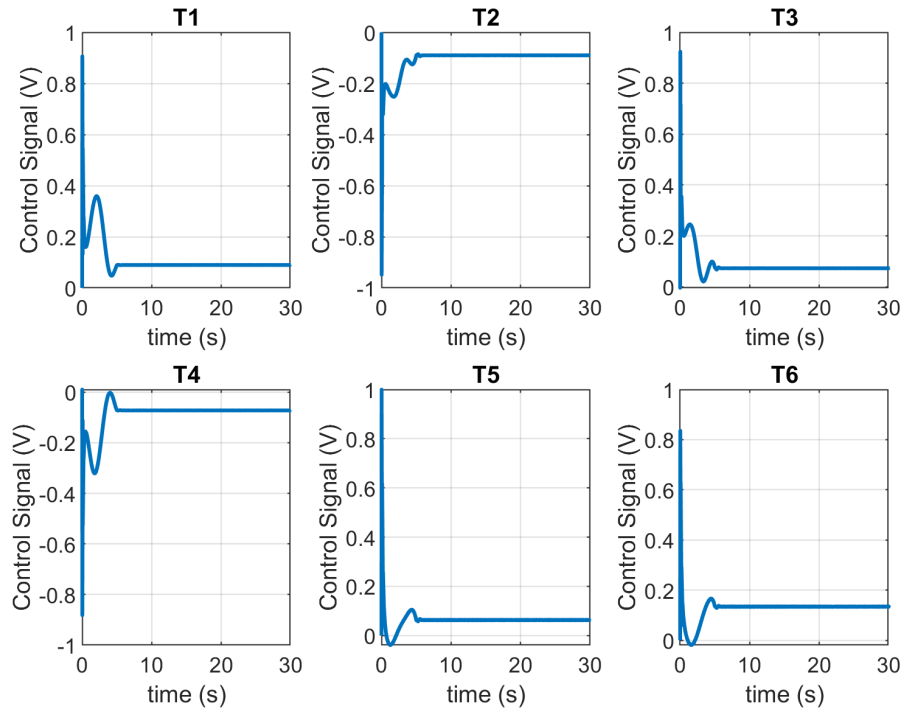

Figure 5.35: Control Signals with the 2nd Order SMC with a $t_b = 5\ s$

$t_b = 7\ s$

The results of the 2nd Order SMC on the proposed trajectory with a $t_b = 7\ s$ are shown next. The linear position behavior is shown in Fig. 5.36, while the angular position comparison is shown in Fig. 5.37. Again, the vehicle converge to the desired trajectory in the established time t_b, in a smooth way.
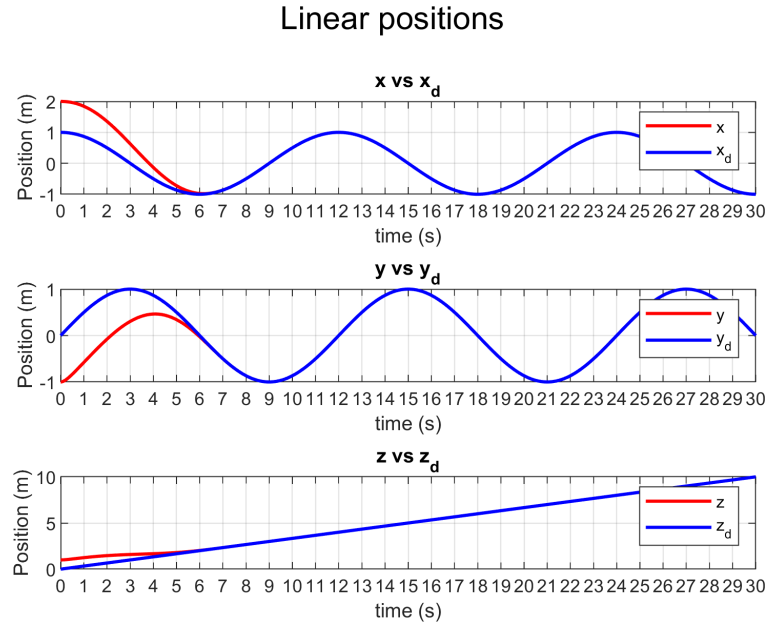

Figure 5.36: Resulting linear positions with the 2nd Order SMC with a $t_b = 7\ s$
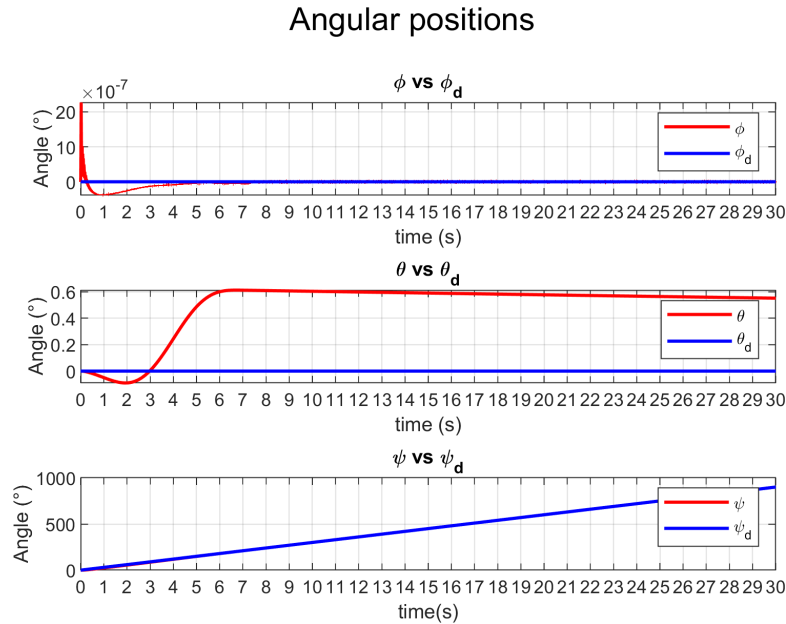
Figure 5.37: Resulting angular positions with the 2nd Order SMC with a $t_b = 7\ s$

Linear and angular velocities in the body-fixed frame are shown in Fig. 5.38 and 5.39 respectively and shown the same behavior, converging to the desired value in the time $t_b = 5s$. Recall that θ is not controllable.
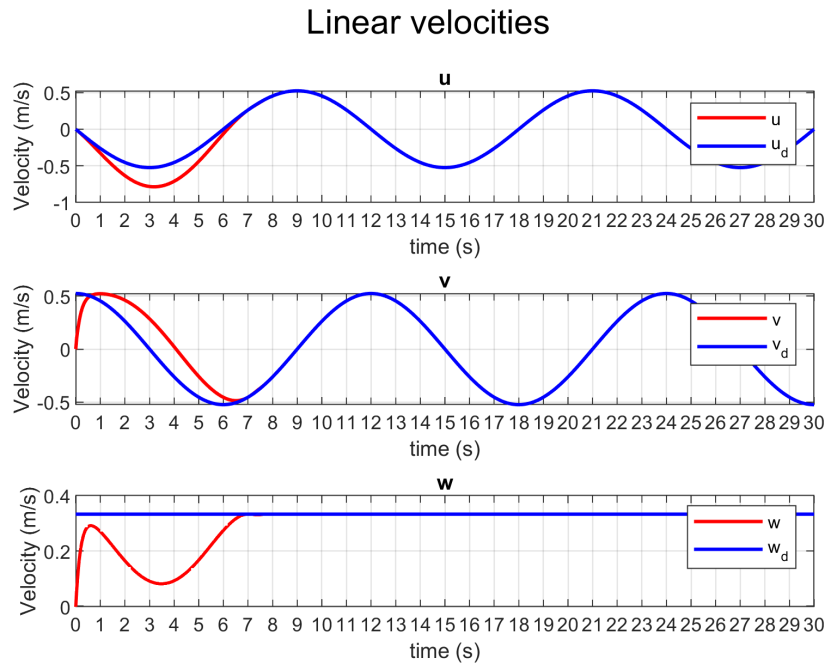
Figure 5.38: Resulting linear velocities with the 2nd Order SMC with a $t_b = 7 \ s$
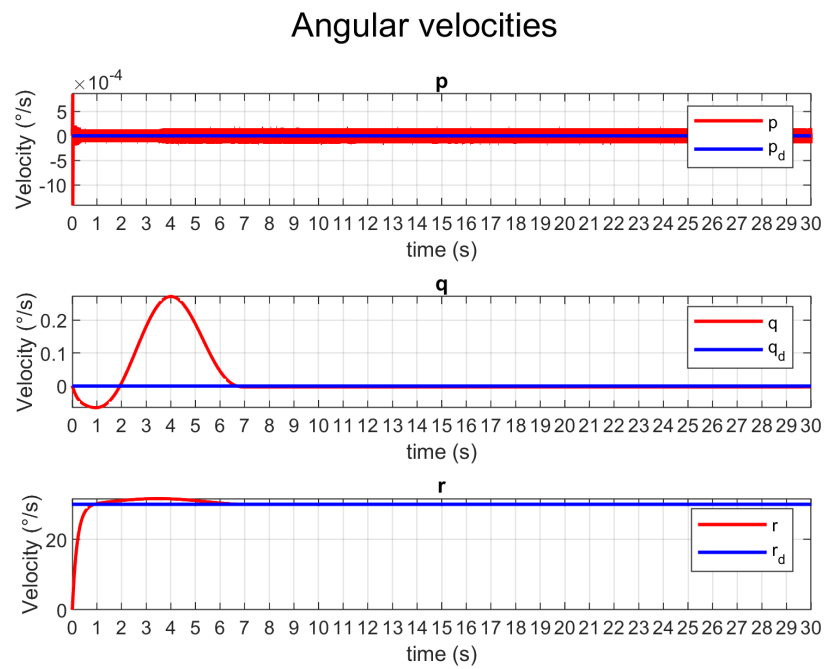
Figure 5.39: Resulting angular velocities positions with the 2nd Order SMC with a $t_b = 7 \ s$. Note that only q is not controllable.

The comparison between the desired trajectory and the actual trajectory performed by the controller is shown in Fig. 5.40.

Figure 5.40: Comparison of Trajectories with the 2nd Order SMC with a $t_b = 7\ s$

The applied torques and the control signals for every thruster are shown in Fig. 5.41 and 5.42. The required torques and control signals are less aggressive, since the time t_b has been increased.

Figure 5.41: Required Torques with the 2nd Order SMC with a $t_b = 7\ s$

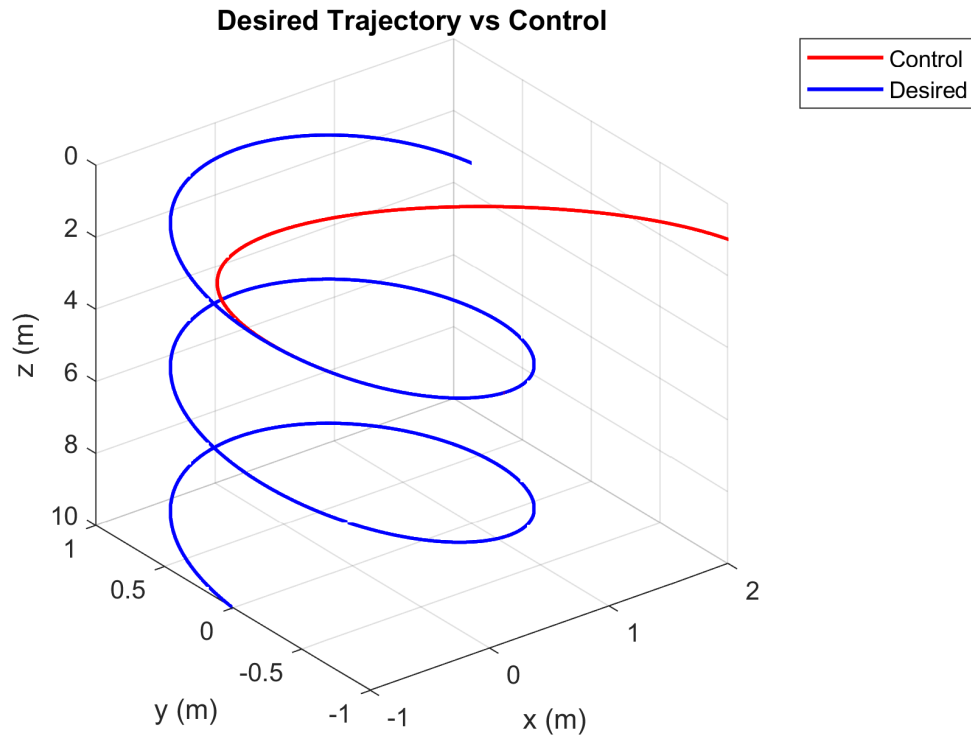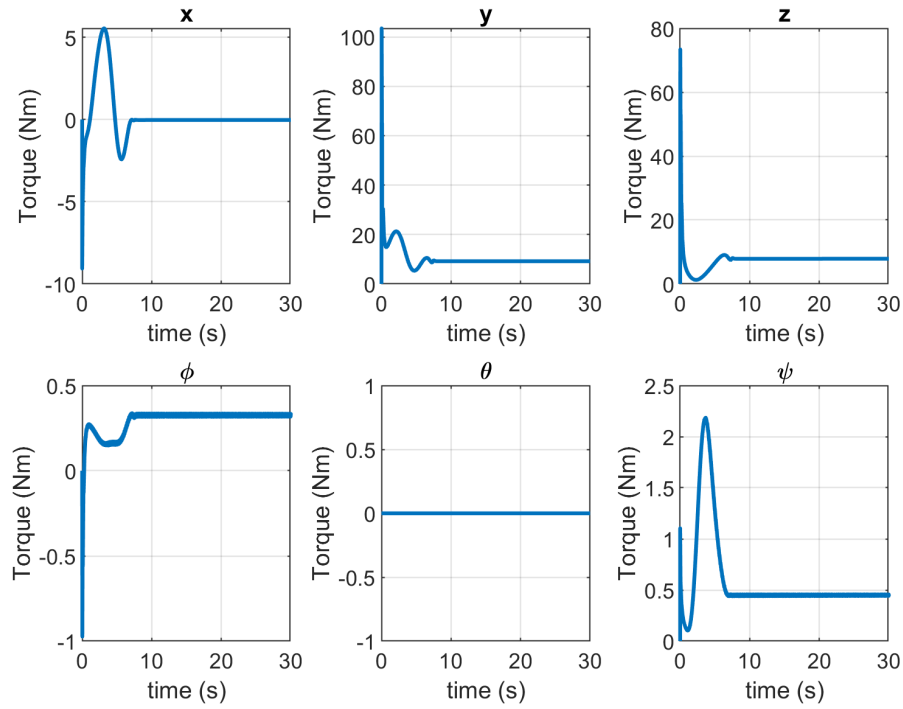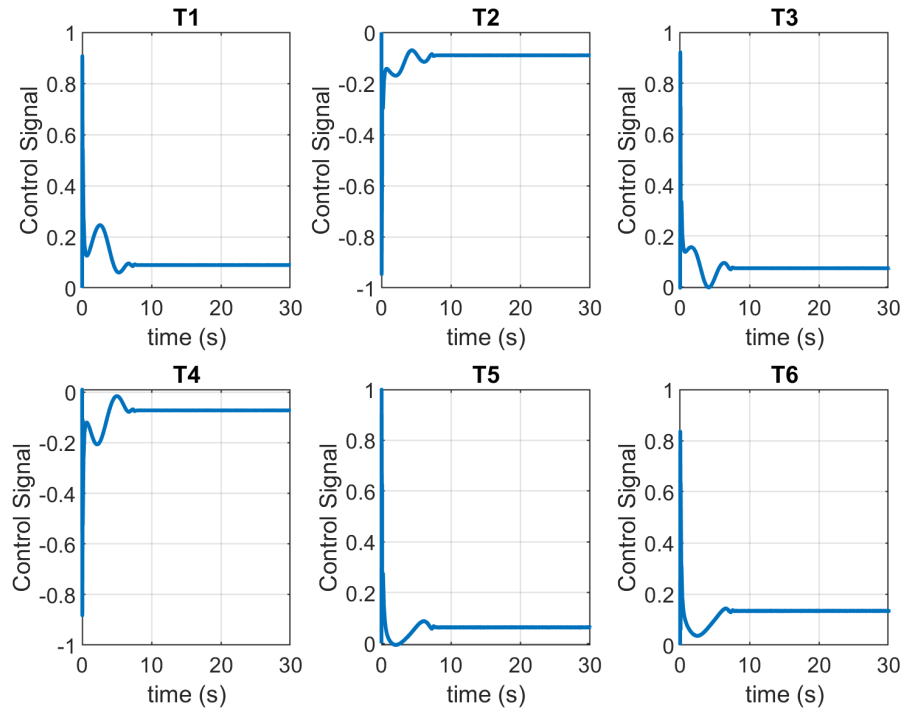Figure 5.42: Control Signals with the 2nd Order SMC with a $t_b = 7\ s$

5.1.5   RMS values

As stated before, the parameters to analyze are related with the RMS values of the tracking error and the RMS values of the control signal, as a parameter of energy consumption. The RMS values are calculated with Eq.4.51.

The summary of the results are reported in the tables 5.2, 5.3 and 5.4.

Linear positions

Table 5.2: RMS error for the linear positions x,y and z

Controller	RMSE x (m)	RMSE y (m)	RMSE z (m)	Mean
PID	0.1788	0.2482	0.1628	0.1966
Feedback Linearization	0.1695	0.2028	0.1442	0.1722
Lyapunov-Based	0.1829	0.1993	0.1707	0.1843
2nd Order SMC with $t_b = 3\ s$	0.1989	0.2163	0.1879	0.2011
2nd Order SMC with $t_b = 5\ s$	0.2563	0.2804	0.2410	0.2592
2nd Order SMC with $t_b = 7\ s$	0.3032	0.3326	0.2645	0.3068

The smaller RMS values of linear errors was obtained by the Feedback Linearization Controller, and then is followed by the Lyapunov function-based controller. The third place is obtained by the 2nd Order SMC with $t_b = 3\ s$. However, the first two controllers are model-based and this condition requires an exact knowledge of the model of the vehicle. The 2nd Order SMC is model-free, which means that in the presence of dynamic uncertainty will still have a good performance. This difference must take into account that the 2nd Order SMC controller makes the vehicle to be outside the desired trajectory until the convergence time. For this reason, the RMS tracking error is also greater that with other controllers.

Angular positions

Table 5.3: RMS error for the angular positions ϕ,θ and ψ

Controller	RMSE ϕ (°)	RMSE θ (°)	RMSE ψ (°)	Mean (°)
PID	0.1363	0.4911	0.5159	0.3811
Feedback Linearization	19.1639	13.6952	18.8877	17.2489
Lyapunov-Based	0.2048	1.0021	0.1837	0.4635
2nd Order SMC with $t_b = 3\ s$	0	0.0706	1.0366	0.3691
2nd Order SMC with $t_b = 5\ s$	0	0.3500	1.4142	0.5881
2nd Order SMC with $t_b = 7\ s$	0	0.5362	1.7100	0.7487

In the case of the angular position, the Best performance was obtained for the 2nd Order SMC. Even when the controllable DOF are ψ and ϕ, the values of θ are also near to 0 since it is intrinsically stable. In the case of the 2nd Order SMC, as the time t_b increases, the angular error also increases.

Control Signals

Considering the saturation constraints for all the controllers, the highest RMS value was obtained by the Feedback Linearization Controller. The RMS values obtained by the Lyapunov function-based Controller and the 2nd Order SMC has similar values. However, when the time t_b increases, the RMS values reduces. This occurs since the controller gives the vehicle more time to reach the desired trajectory, and thus less work is demanded on thrusters.

Table 5.4: RMS values of control signals for each thruster.

Controller	T_1	T_2	T_3	T_4	T_5	T_6	Mean
PID	0.2078	0.1946	0.2010	0.0.2105	0.0.1311	0.2041	0.1915
Feedback Linearization	0.1676	0.1876	0.1909	0.1693	0.2851	0.2760	0.2127
Lyapunov Based	0.1278	0.1500	0.1380	0.1192	0.0678	0.1358	0.1231
2nd Order SMC with $t_b = 3\ s$	0.1475	0.1417	0.1351	0.1404	0.0853	0.1450	0.1325
2nd Order SMC with $t_b = 5\ s$	0.1275	0.1199	0.1015	0.1071	0.0801	0.1355	0.1119
2nd Order SMC with $t_b = 7\ s$	0.1163	0.1096	0.0915	0.0958	0.0794	0.1324	0.1042

5.1.6   Convergence of the error

In this part the analysis the time of convergence of every controller will be analysed in order to compare the first three controllers: PID, Feedback Linearization and the Lyapunov function-based will be compared with the different configurations of the 2nd Order SMC. These comparisons are shown in Fig. 5.43 for x, Fig. 5.44 for y, Fig. 5.45 for z. In this case it is observable the PID behavior, since it can not completely eliminate the steady state error, but instead it keeps oscillating in a vicinity near to 0.
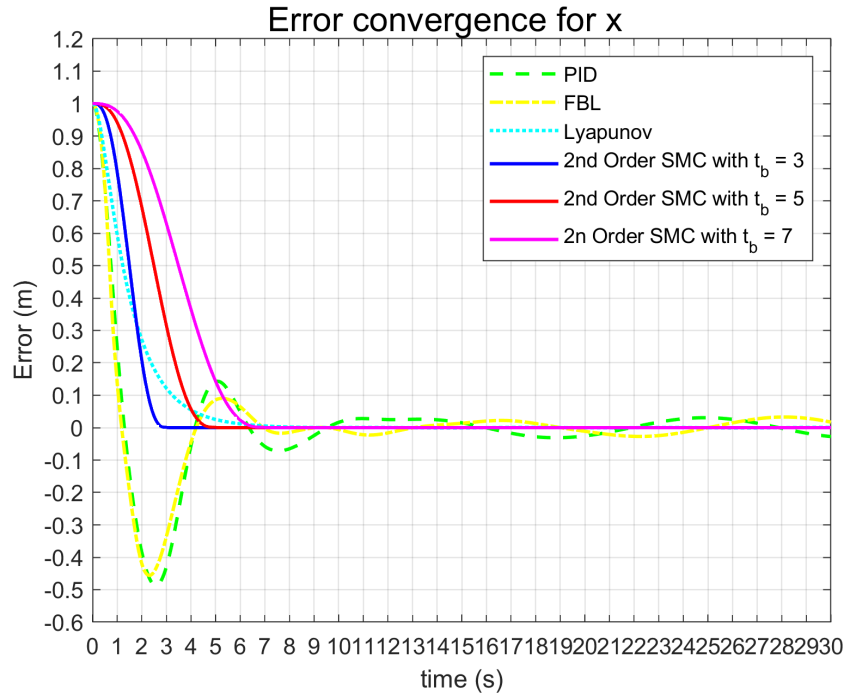
Figure 5.43: Comparison of the error convergence of all the controllers in the x DOF.

Figure 5.44: Comparison of the error convergence of all the controllers in the y DOF.

Figure 5.45: Comparison of the error convergence of all the controllers in the z DOF.

In Fig.5.46, the error convergence of ϕ. For the case of the Feedback Linearization Controller, the behavior of the ϕ DOF is one order of magnitude greater that the others controllers. Fig. 5.47 shows the comparison in this DOF on magnification.
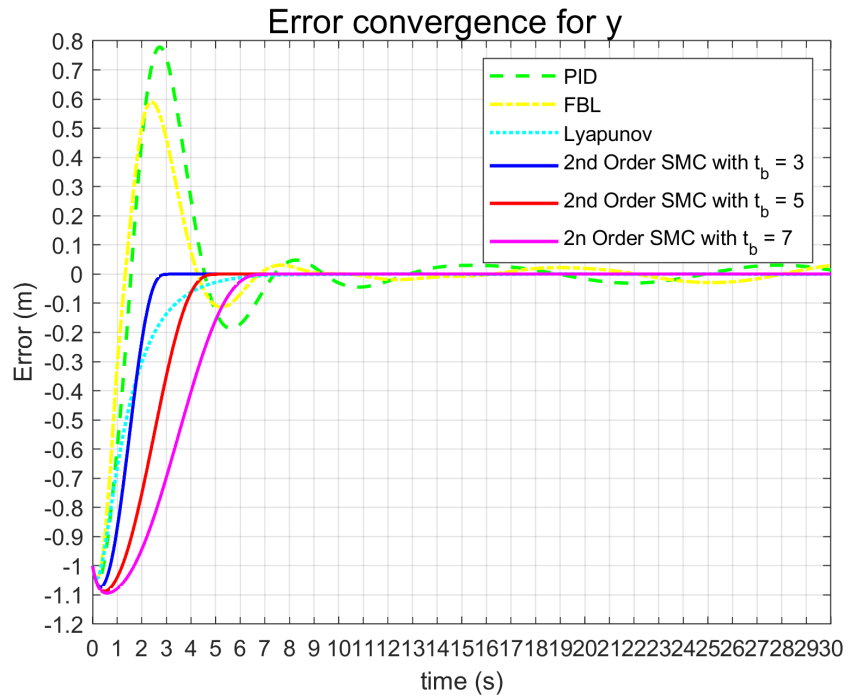

Figure 5.46: Comparison of the error convergence of all the controllers in the ϕ DOF.

Figure 5.47: Magnification of the error convergence of all the controllers in the ϕ DOF (without Feedback Linearization Controller).

In Fig.5.48, the error convergence of ψ. For the case of the Feedback Linearization Controller, the behavior of the ψ DOF is one order of magnitude greater that the others controllers. Fig. 5.49 shows the comparison in this DOF on magnification.

Figure 5.48: Comparison of the error convergence of all the controllers in the ψ DOF.

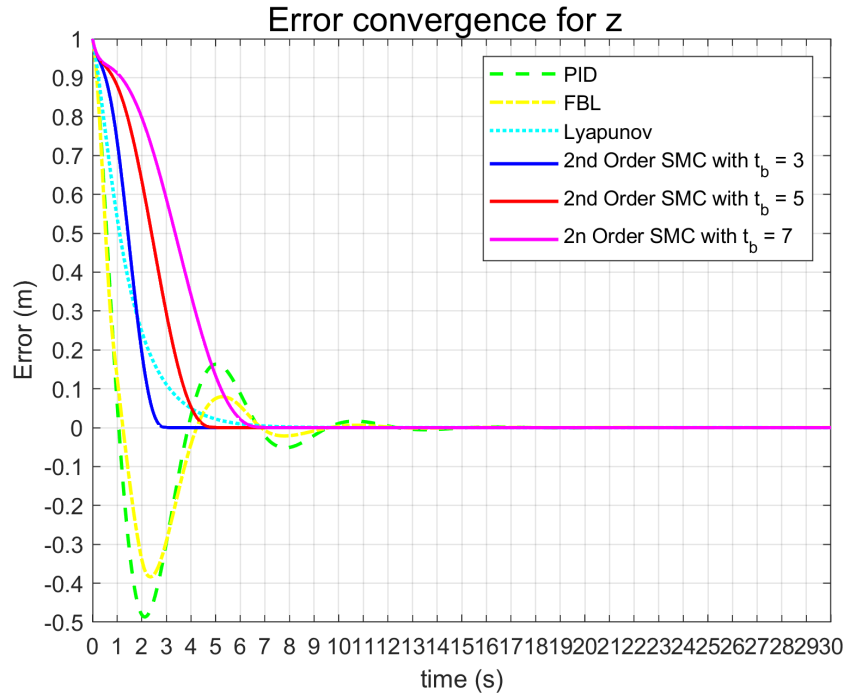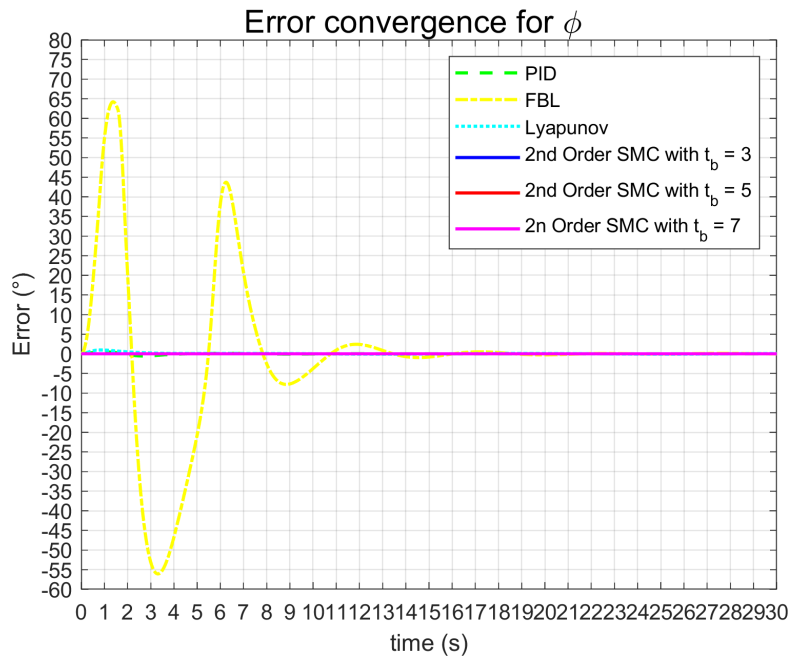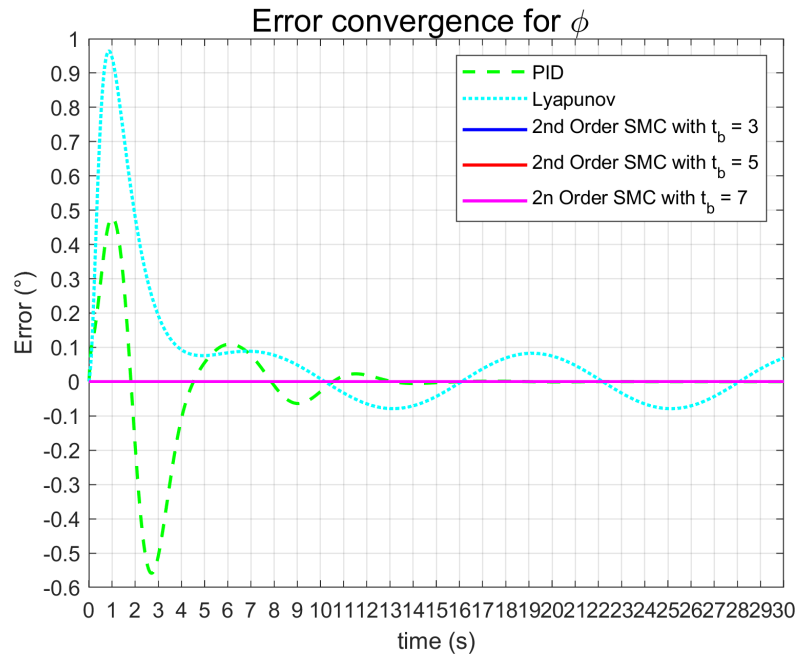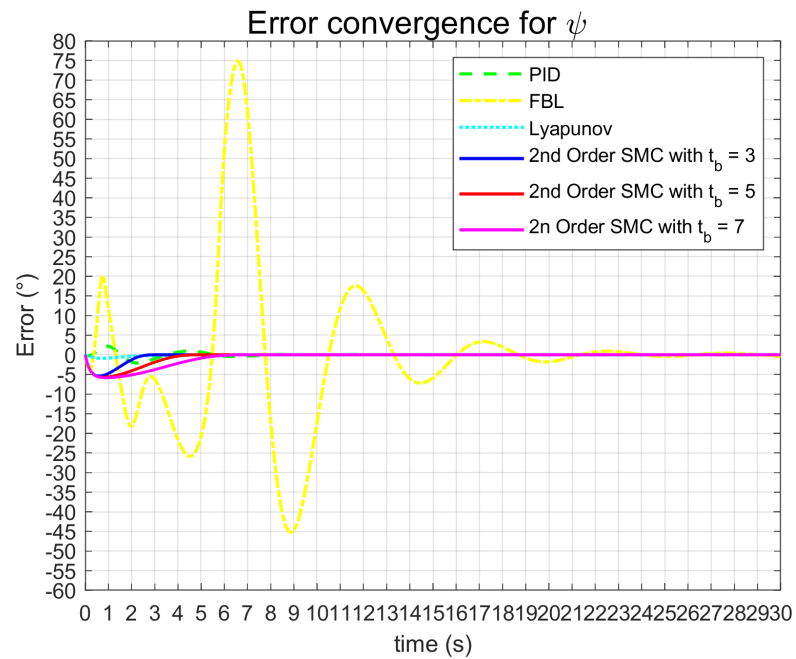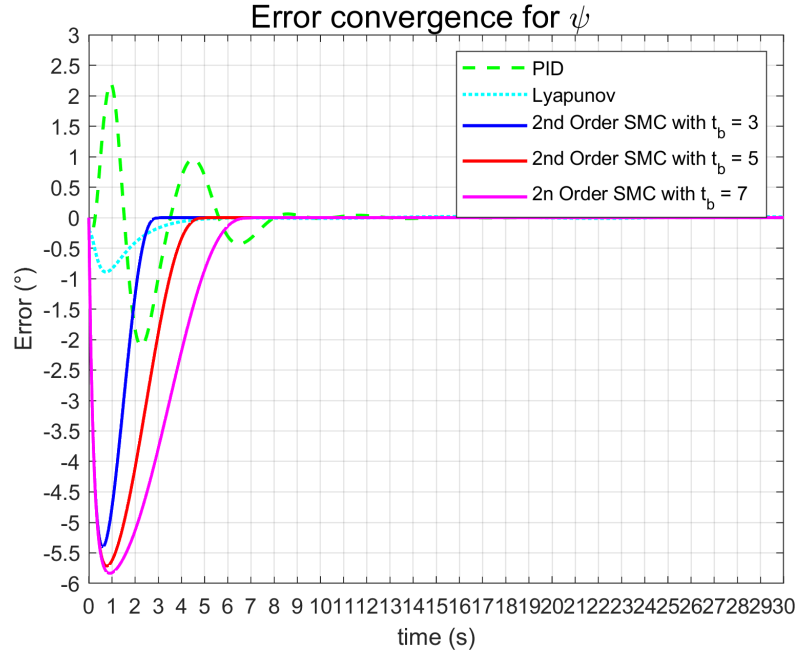Figure 5.49: Magnification of the error convergence of all the controllers in the ψ DOF (without Feedback Linearization Controller).

The 2nd Order SMC controllers are included in these figures in order to verify the finite-time convergence. The chose parameters could dealt with the regressor term proposed by Eq.4.42, and thus the finite time convergence is achieved.

5.2 Spiral Trajectory considering the effects of marine currents

The effects of marine currents are considered in this section. The values of marine currents proposed by Zhang et al. [75] are considered. These values are given as:

$$u_c = 0.7\frac{m}{s} \quad v_c = 0.2\frac{m}{s} \quad w_c = 0.3\frac{m}{s} \tag{5.1}$$

The same control gains proposed in the Table 5.1 are kept in order to verify the effects of the marine currents in the controllers.

5.2.1 Convergence of the error

As in the previous section, the analysis the time of convergence of every controller will be analysed in order to determine the effects caused by marine currents. The same three classical schemes are considered, as well as the three configurations of the 2nd Order SMC. These comparisons are shown in Fig. 5.50 for x, Fig. 5.51 for y, Fig. 5.52 for z. In this case, the PID, the Feedback Linearizaton and the Lyapunov based controller degrade, since they can not completely eliminate the steady state error, and the vehicle keeps oscillating and never

eliminating the errors in the three linear DOFs. The 2nd Order SMC is robust, since the time of convergence is kept even in the presence of marine currents.
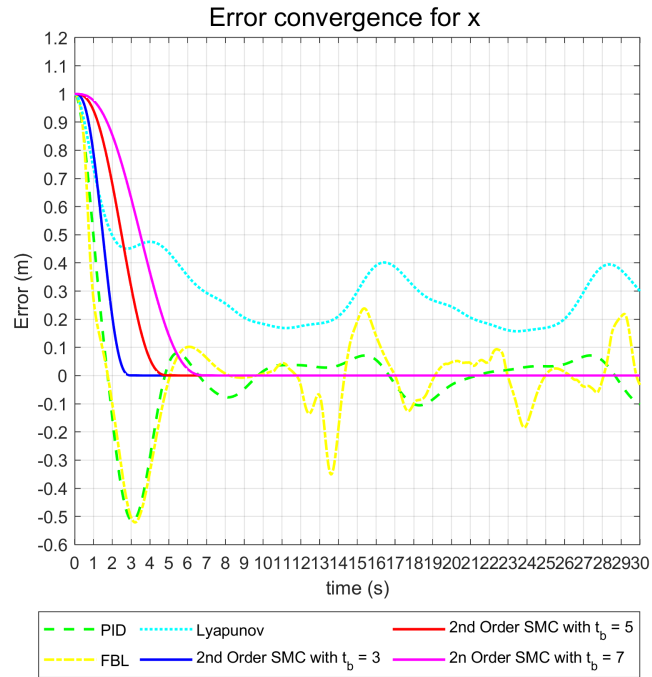

Figure 5.50: Comparison of the error convergence of all the controllers in the x DOF subject to marine currents.
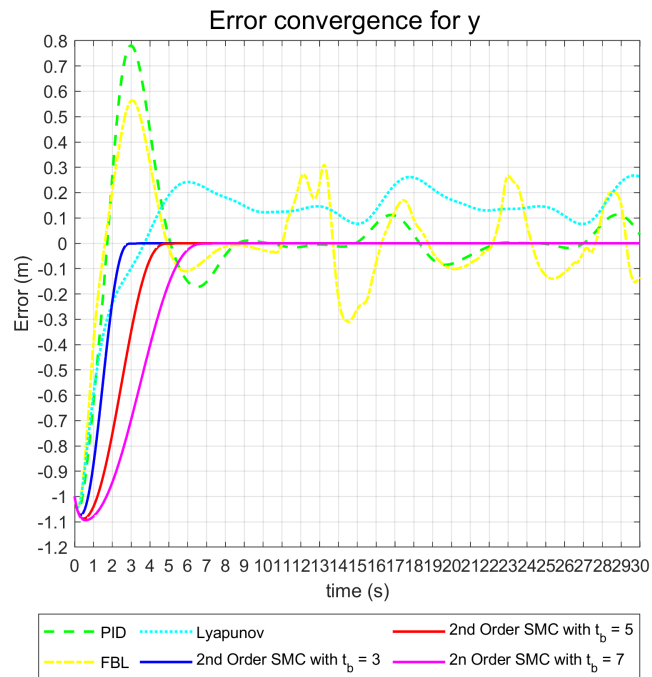
Figure 5.51: Comparison of the error convergence of all the controllers in the y DOF considering the effects of marine currents.
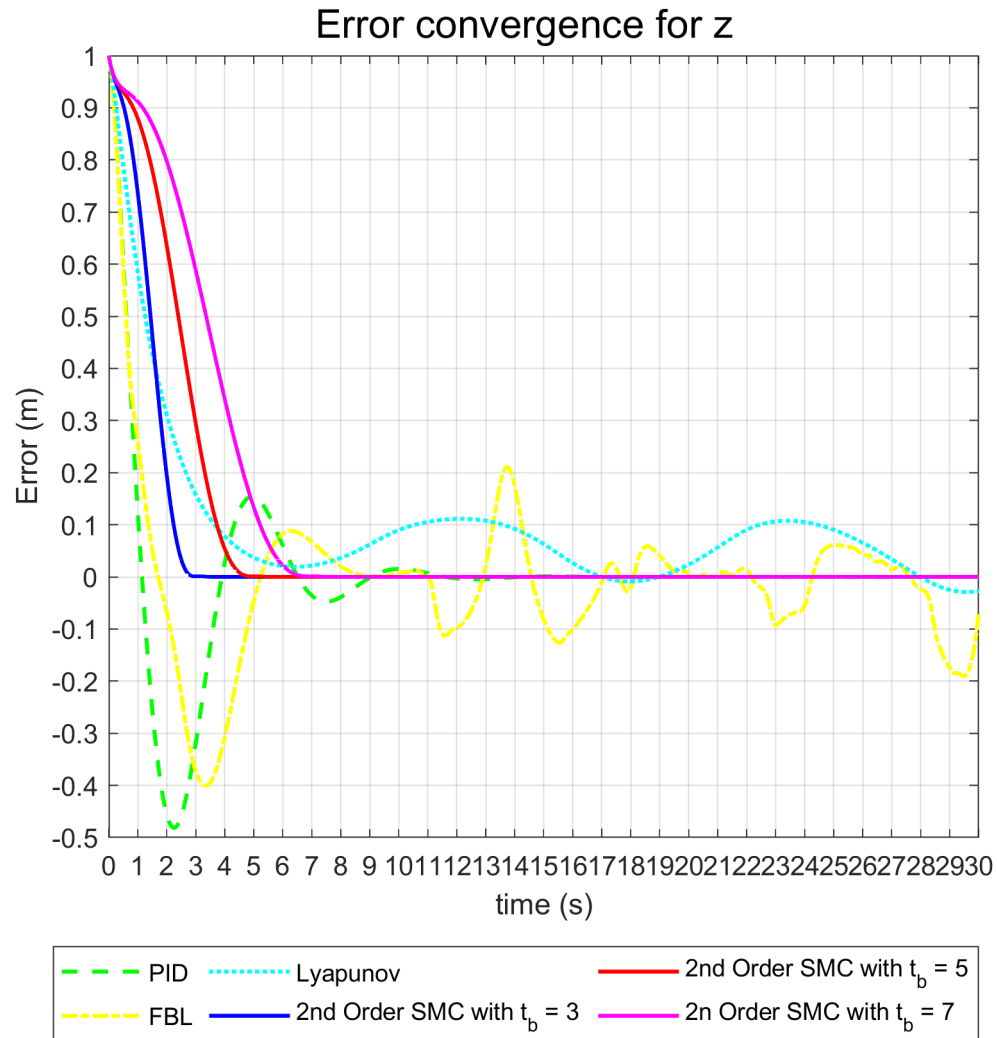
Figure 5.52: Comparison of the error convergence of all the controllers in the z DOF considering the effects of marine currents..

   In Fig.5.53, the error convergence of ϕ is shown. For the case of the Feedback Linearization Controller, the behavior of the ϕ DOF is one order of magnitude greater that the others controllers. Fig. 5.54 shows the comparison in this DOF on magnification. It can be seen that the Feedback Linearization Controller has the worst behavior, since the error reaches the $240°$. After, the Lyapunov based controller has the second greatest error, with values of approximately $6°$. The PID controller also generates an error. The only controller that is not affected is the 2nd Order SMC, mantaining the error in 0, along the whole trajectory.

Figure 5.53: Comparison of the error convergence of all the controllers in the ϕ DOF.

Figure 5.54: Magnification of the error convergence of all the controllers in the ϕ DOF (without Feedback Linearization Controller).

In Fig.5.55, the error convergence of ψ. For the case of the Feedback Linearization Controller, the behavior of the ψ is the worst, since the error reaches up to $400°$. Fig. 5.56 shows the comparison in this DOF on magnification and shows that the PID and the Lyapunov based Controller presented oscillations allong the whole trajectory. The 2nd Order SMC maintains its robustness, since the convergence times are not affected, and the error is kept in 0.

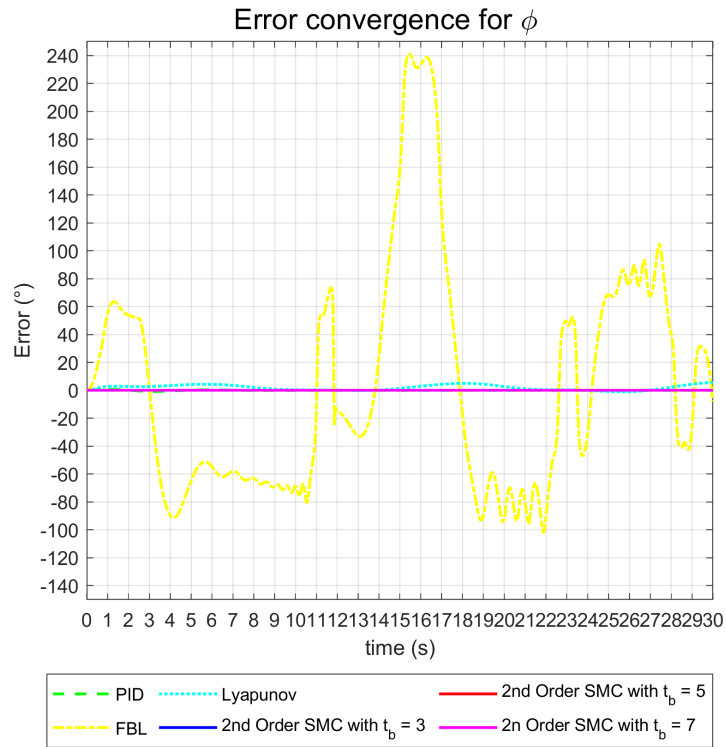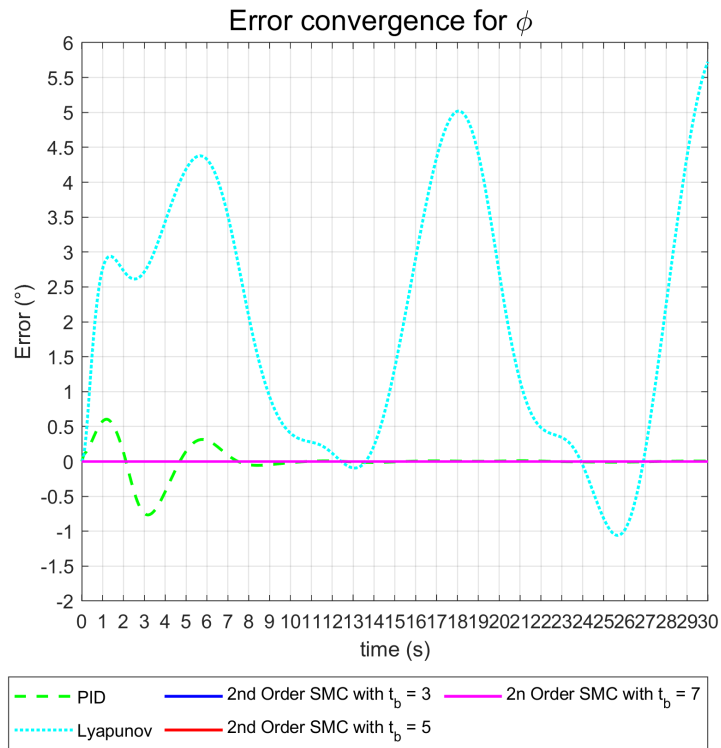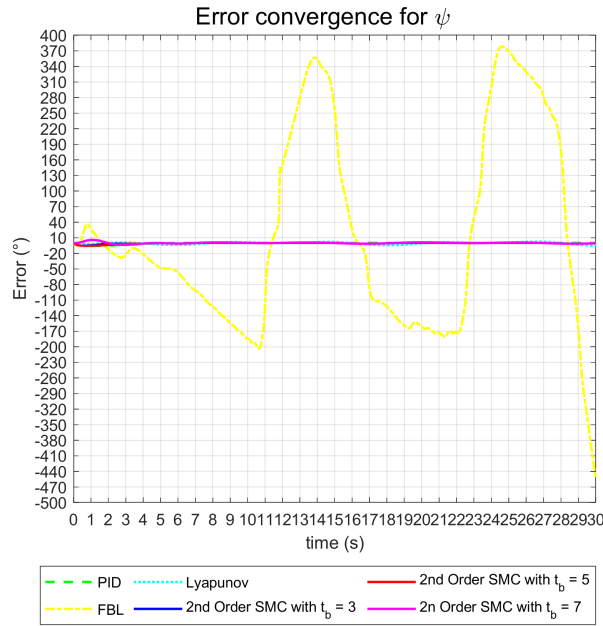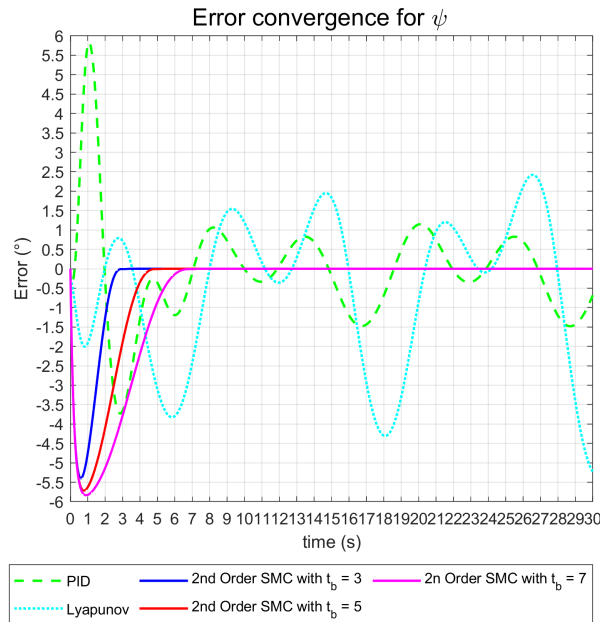Figure 5.55: Comparison of the error convergence of all the controllers in the ψ DOF.

Figure 5.56: Magnification of the error convergence of all the controllers in the ψ DOF (without Feedback Linearization Controller).

5.2.2 RMS values

A new calculus of the RMS values of the tracking errors and the control signals was performed in order to identify which the level of degradation in the performance of every controller subject to marine currents. The RMS values are calculated with Eq.4.51.

The summary of the results are reported in the tables 5.5, 5.6 and 5.7.

Linear positions

Table 5.5: RMS error for the linear positions x,y and z considering marine currents.

Controller	RMSE x (m)	RMSE y (m)	RMSE z (m)	Mean
PID	0.2009	0.2571	0.1630	0.2070
Feedback Linearization	0.2072	0.2374	0.1678	0.2041
Lyapunov-Based	0.3515	0.2473	0.1905	0.2619
2nd Order SMC with $t_b = 3\ s$	0.1989	0.2164	0.1878	0.2010
2nd Order SMC with $t_b = 5\ s$	0.2563	0.2805	0.2410	0.2593
2nd Order SMC with $t_b = 7\ s$	0.3032	0.3327	0.2845	0.3068

The RMS values of the tracking errors remain practically the same in the case of the 2nd Order SMC even with the introduction of the marine currents. For the case of the classical controllers, the mean of the RMS values of the errors increased up to 5% for the PID,18% for the Feedback Linearization Controller, and 42% for the Lyapunov Based Controller.

Angular positions

Table 5.6: RMS error for the angular positions ϕ,θ and ψ

Controller	RMSE ϕ (°)	RMSE θ (°)	RMSE ψ (°)	Mean (°)
PID	0.1995	0.3693	1.3934	0.6541
Feedback Linearization	83.5222	38.3770	190.7710	104.2234
Lyapunov-Based	2.6583	17.0146	1.9994	7.2241
2nd Order SMC with $t_b = 3\ s$	0	0.0705	1.0404	0.3703
2nd Order SMC with $t_b = 5\ s$	0	0.3498	1.4182	0.5893
2nd Order SMC with $t_b = 7\ s$	0	0.5358	1.7176	0.7511

In the case of the angular position, the controller that degrates the worst was the Feedback Linearization Controller. The mean of the RMS values had an increase of 600%. For the PID,

the increment of the mean of the RMS errors of the angular position was of 1700% and for the Lyapunov based controller, the increment was of 1500%. However, since the Feedback Linearization controller already had the worst performance managing the angular errors, it has the greatest mean of $17.2489°$. The RMS values of the error for all the cases of the 2nd Order SMC remains practically the same.

Control Signals

Considering the marine currents the lowest mean of the RMS values of the control signals was obtained by the 2nd Order SMC with $t_b = 7s$. All the controller incremented its energy consumption, the PID in a 39%, the Feedback Linearization Controller in a 147%, the Lyapunov based controller in a 56% and the 2nd Order SMC in a 58%, 67% and 82% respectively.

Table 5.7: RMS values of control signals for each thruster.

Controller	T_1	T_2	T_3	T_4	T_5	T_6	Mean
PID	0.3254	0.3131	0.3534	0.3163	0.1135	0.1761	0.2663
Feedback Linearization	0.3978	0.4008	0.4056	0.3892	0.7889	0.7749	0.5262
Lyapunov Based	0.2732	0.2479	0.2607	0.2306	0.0578	0.0843	0.1924
2nd Order SMC with $t_b = 3$ s	0.2790	0.2684	0.3093	0.2646	0.0578	0.0840	0.2105
2nd Order SMC with $t_b = 5$ s	0.2909	0.2670	0.2801	0.2535	0.0500	0.0556	0.1995
2nd Order SMC with $t_b = 7$ s	0.2897	0.2525	0.2625	0.2421	0.0479	0.0469	0.1903

5.3 Simultaneous Scheme

Simulations were conducted to test and measure the performance of the controllers presented in the section 4.4: state-of-the art controllers . First, without considering the effects of marine currents, and then including them as perturbations.The euclidean distance between UUVs must remain constant in order to assure the correct gripping, transporting and releasing of the object. It is considered that the object is gripped by the front faces of the UUVs, in such a way, that the resulting heading orientations of the UUVs must be $\psi_1 = -\frac{\pi}{2}$ and $\psi_2 = \frac{\pi}{2}$. The difference in the orientation of the vehicles must remain equal to $180°$ during the gripping, transporting and releasing of the object.

The gains used for every controller are shown in the Table 5.8.

Table 5.8: Control parameters for simulations

Control schemes	Control parameters
2nd Order SMC	$K_d = \mathrm{diag}\{800, 800, 800, 800, 0, 800\};\ K_i = \mathrm{diag}\{1, 1, 1, 1, 0, 1\};$ $\kappa = 1;\ \alpha_0 = 1.01;\ \alpha_c = 25\ \delta = 0.001;\ t_b = 6\quad s$
NSTSMC (Liu et al.,2020)[46]	$\beta = 0.5;\ \epsilon_0 = 2;\ \gamma = \frac{2}{3};\ \epsilon_1 = 0.01[1, 1, 1, 1, 1, 1]^T;$ $\lambda_m = \mathrm{diag}(0.5, 0.5, 0.5);\ \lambda_p = \mathrm{diag}(0.5, 0.5, 0.5);$ $\alpha_1 = \mathrm{diag}(5, 5, 5, 30, 30, 30);\ \alpha_2 = \mathrm{diag}(5, 5, 5, 30, 30, 30);$ $\hat{L}_m(0) = [2.5, 0.5, 0.5]^T;\ \hat{K}_m(0) = \mathrm{diag}(0.1, 0.1, 0.1)$
FTSOSMC (Liu et al., 2017) [44]	$\lambda = 0.8;\ b = 0.7;$ $k_1 = 30;\ k_2 = 20;$ $k_3 = 15;\ k_4 = 20$

5.3.1 Results without considering marine currents

A simulation without marine currents was performed with a initial position given by $\eta_1 = [1, 2, 1, 0, 0, 0]^T$ for UUV1 and $\eta_2 = [4, 1, 1.5, 0, 0, 0]^T$ for UUV2. In order to compare the controller properly, in this section the 2nd Order SMC, will be called Model-Free Second Order SMC (MFSOSMC). Since MFSOSMC sliding surface is parameterized with a TBG, a smooth convergence with a time-base $t_b = 6$ is achieved. The comparison between the desired and the real positions along all the trajectory are shown in Figures 5.57 and 5.58 for UUV1 and UUV2 respectively. The error of all the controllable degrees of freedom converge to 0 in the desired time, and remains on the desired trajectory.
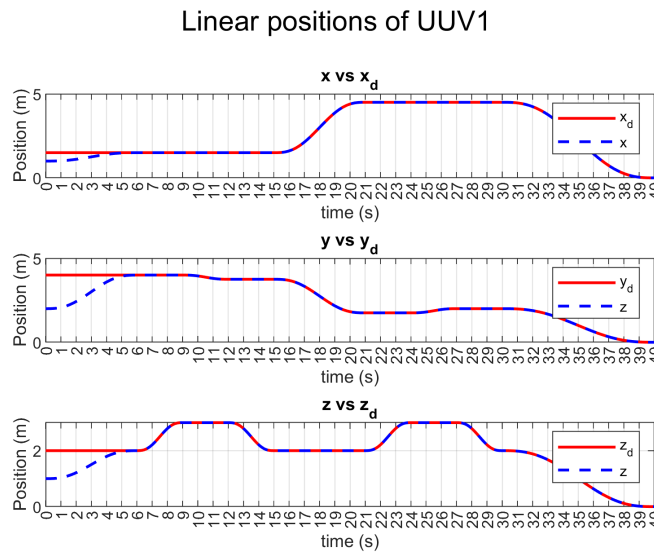

Figure 5.57: Comparison between the desired and the real positions for UUV1 with the MF-SOSMC.
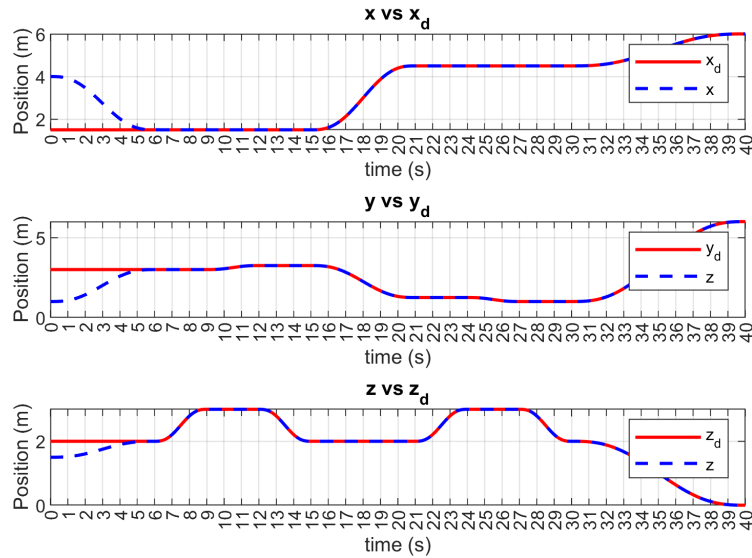
Linear positions of UUV2

Figure 5.58: Comparison between the desired and the real positions for UUV2 with the MF-SOSMC.

The comparison between the desired and real attitudes are shown in Figures 5.59 and 5.60 for UUV1 and UUV2 respectively. The error converges in the desired t_b except for θ, which, as stated before, is not controllable and generating a small error between the range $\pm 1°$ for UUV1 and $\pm 2°$ for UUV2, that it is caused by the movement of the vehicle.

Angular positions of UUV1
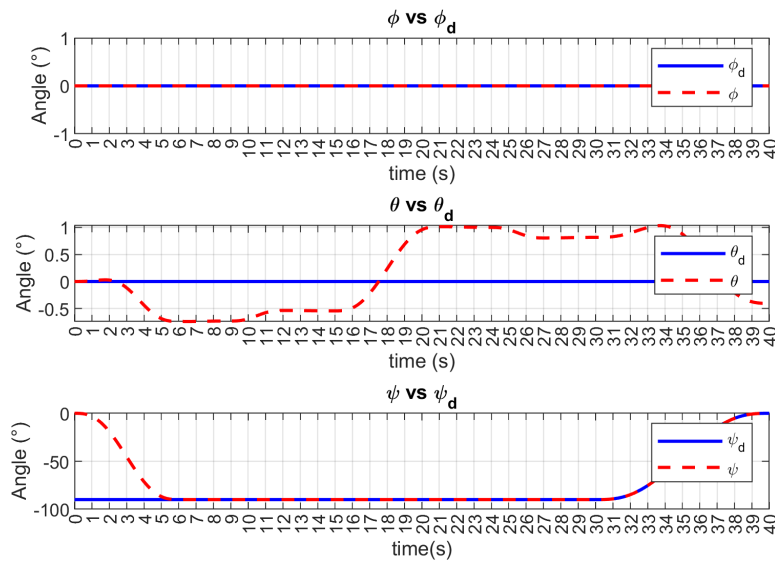
Figure 5.59: Angular positions for UUV1 with the MFSOSMC.

Angular positions of UUV2
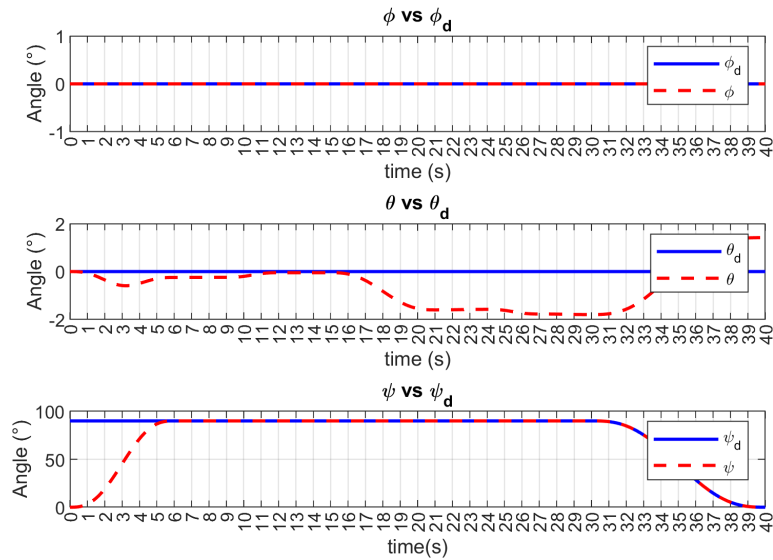
Figure 5.60: Angular positions for UUV2 with the MFSOSMC.

The comparison between the desired and the real velocities are shown in Figures 5.61, 5.62 5.63, 5.64. The velocities converge to their desired value in the same established time $t_b = 6s$. Since angular velocity q is not controllable, the effect generated in that DOF is consequence of the movement of the UUV.

Linear velocities of UUV1

Figure 5.61: Linear Velocities for UUV1 with MFSOSMC.

Linear velocities of UUV2
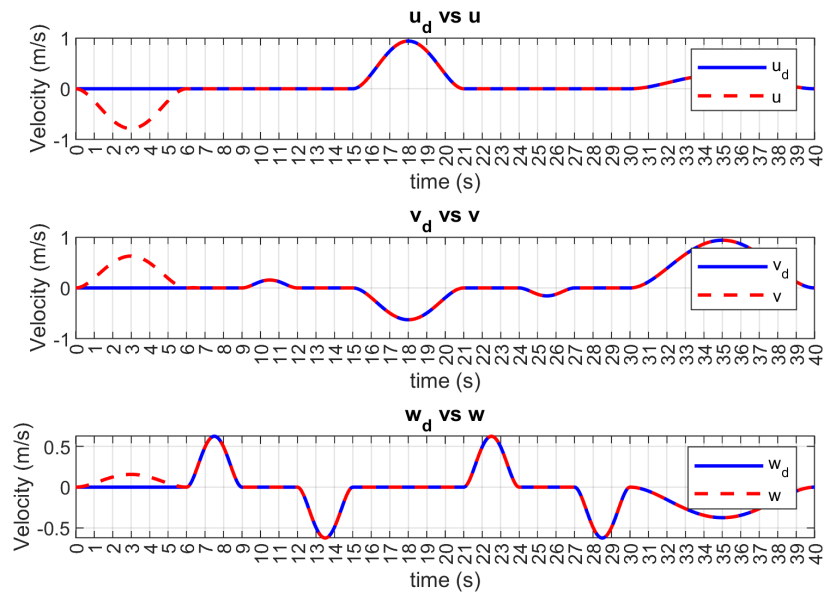
Figure 5.62: Linear Velocities for UUV2 with MFSOSMC.

Angular velocities of UUV1
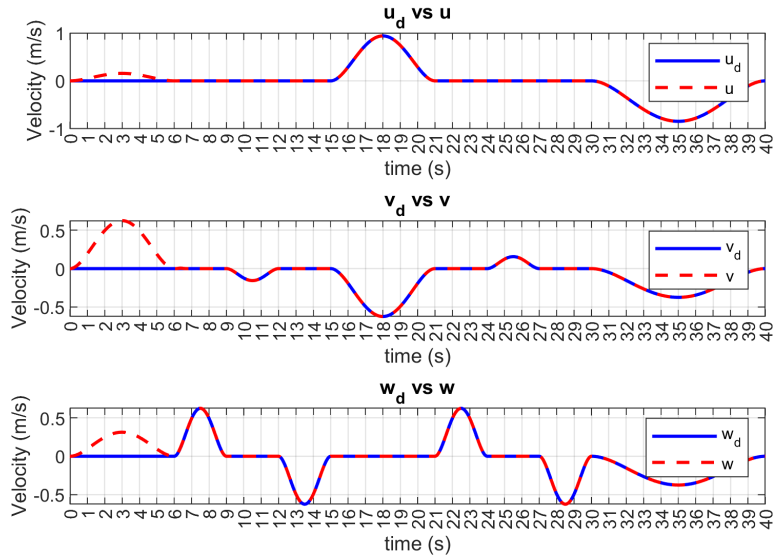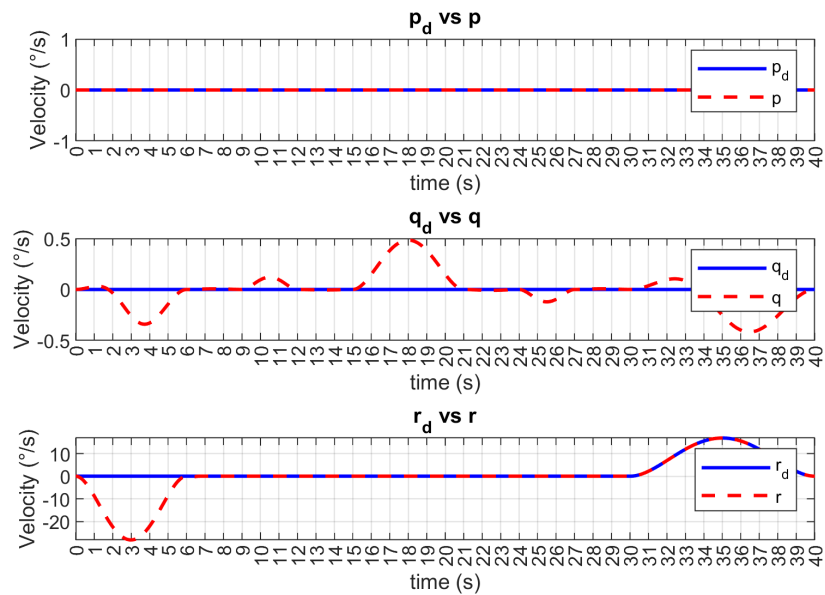

Figure 5.63: Angular Velocities for UUV1 with MFSOSMC.
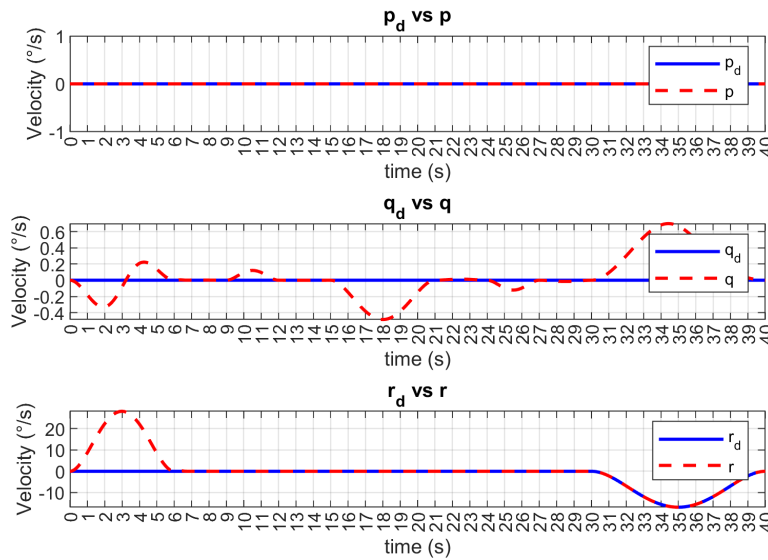
Figure 5.64: Angular Velocities for UUV2 with MFSOSMC.

The performance of the MFSOSMC within the desired trajectory is shown in Fig. 5.65 and 5.66. Coordinate systems of the body-fixed frame of both UUVs are added in order to identify their orientations. Since the vehicles must take the object with the front face, the x axis (shown in red) of both vehicles must be aligned and with opposite directions. Recall that the orientation for heading must be $\psi_1 = -\frac{\pi}{2}$ and $\psi_2 = \frac{\pi}{2}$ for UUV1 and UUV2 respectively.
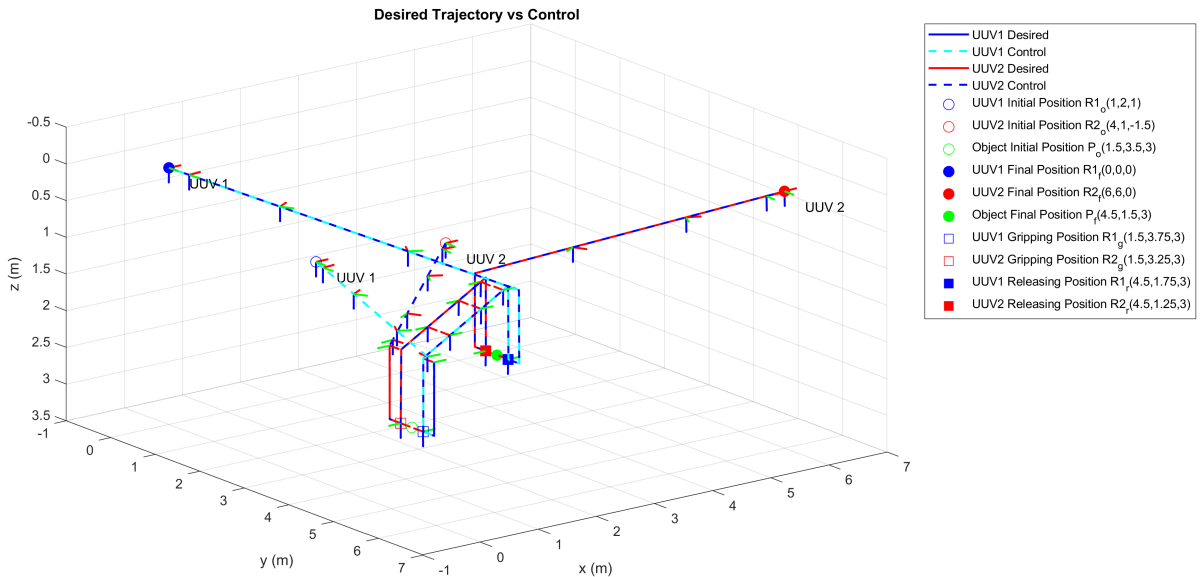
Figure 5.65: Comparison between the desired trajectory and the real trajectory with the MF-SOSMC in an Isometric perspective.
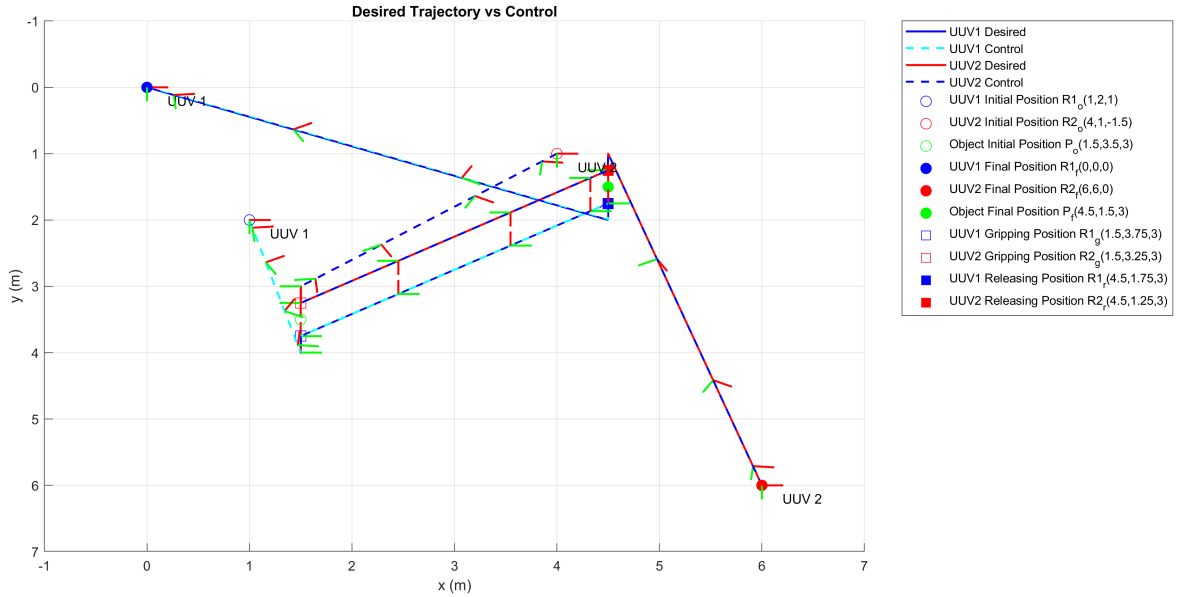
Figure 5.66: Comparison between the desired trajectory and the real trajectory with the MF-SOSMC seen from above.

5.3.2   Comparisons

The performance of the controllers are compared against each other in this section. For the proposed MFSOSMC, the finite-time convergence at $6s$ can be achieved just by setting $t_b = 6s$. However, for the other controllers, the convergence cannot be arbitrary set, since it depends of the initial positions η_0 and the proposed tuning gains. Recall that for the MF-SOSMC, all the tracking error converge in the same established time $t_b = 6s$, while the errors of the FTSOSMC and the NSTSMC schemes converge in different times. For the case of the FTSOSMC the convergence time is $t_r < 5s$ for both UUV1 and UUV2; and for the NSTSMC the time is $tc \leq 2.18s$ for UUV1 and $t_c \leq 2.37s$ for UUV2.

The comparisons among the behaviors of the errors are are shown in the Figure 5.67 for the x direction, in the Figure 5.68 for the y direction and in the Figure 5.69 for the z direction. The behaviors of the angular errors are shown in the Fig. 5.70 for the ϕ angle, and in the Fig. 5.71 for the ψ angle. The comparisons show that all the controllers converge to the desired trajectory and kept the error in a vicinity near to 0.

Figure 5.67: Behavior of the error convergence on the x axis without the presence of currents.

Figure 5.68: Behavior of the error convergence on the y axis without the presence of currents.

Figure 5.69: Behavior of the error convergence on the z axis without the presence of currents.

Figure 5.70: Behavior of the error convergence on the ϕ angle without the presence of currents.

Figure 5.71: Behavior of the error convergence on the ψ angle without the presence of currents.

Finally, the Euclidean Distance between both UUVs and the difference in orientations, for every control scheme, are shown. The euclidean distance is maintained constant during the gripping, the transport and the realising of the object, which has been established to be $0.5m$ in the z axis. The difference in orientation shows the desired value of $180°$ between the gripping and releasing points. The comparison of the euclidean distance and the difference in orientation is shown in Fig. 5.72 and 5.73, respectively.
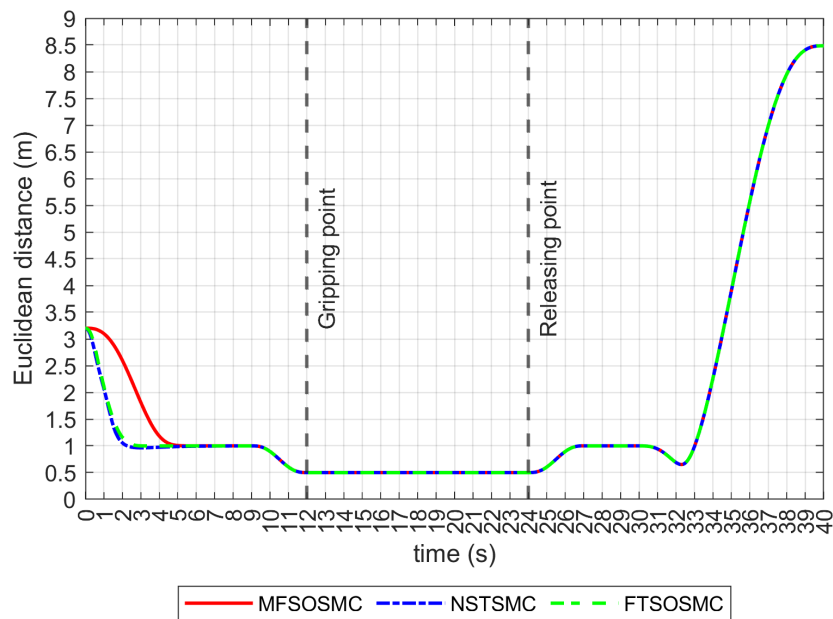
Figure 5.72: Comparison of the euclidean distance between the UUVs.
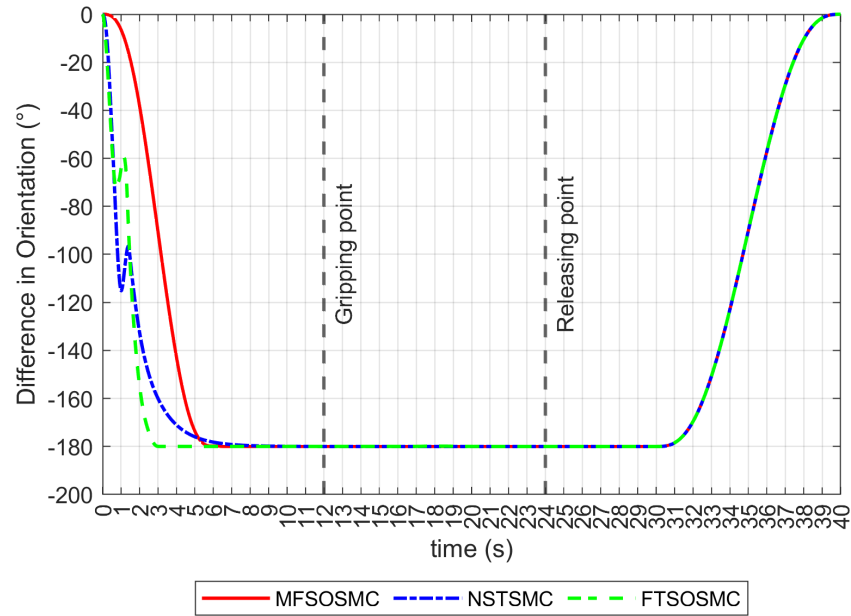
Figure 5.73: Comparison of the difference between the psi angles of the UUVs.

5.4 Simultaneous Scheme considering the fects of marine currents.

The marine currents velocities described by Zhang et al. [75] were applied to the simulation in order to evaluate the performance of the controllers, the applied currents velocity vector is $v_c = [0.75, 0.25, 0.3, 0, 0, 0]^T$. Figures from 5.74 to 5.76 shows that the MFSOSMC maintains its robustness even in the presence of the disturbance, and the error converges to 0 in the same $t_b = 6s$. The NSTSMC and the FTSOSMC keep also their robustness and the error is maintained in a vicinity near to 0 along all the trajectory. However, Fig 5.77 and 5.78 show that in the attitude control, only the MFSOSMC and the FTSOSMC are robust since the ϕ and ψ errors are maintained at 0 the whole trajectory after the convergence time, while for the NSTSMC the performance degrades at the end of the trajectory.
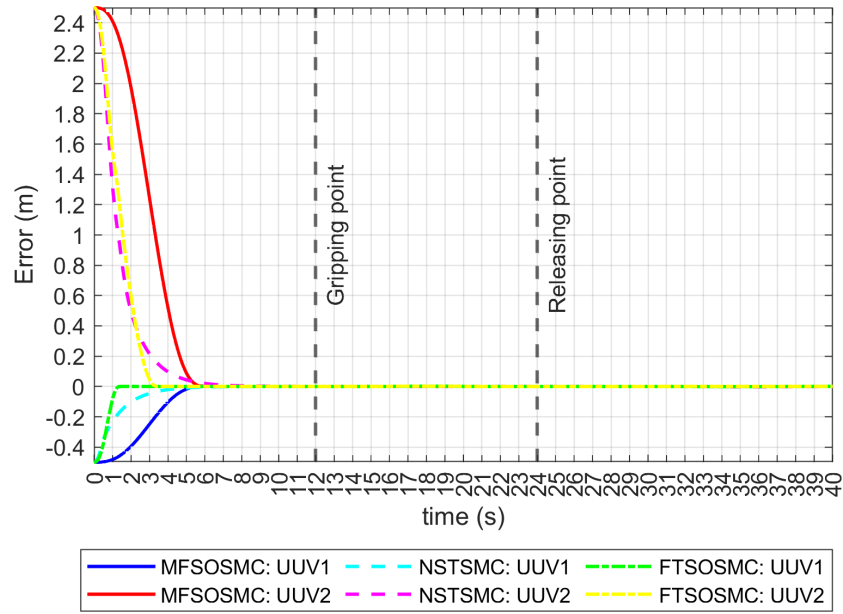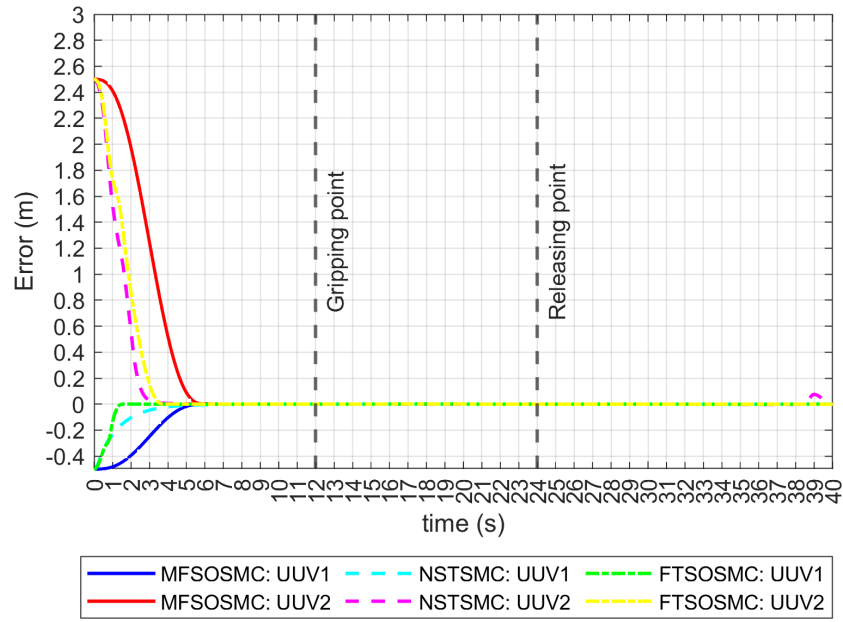
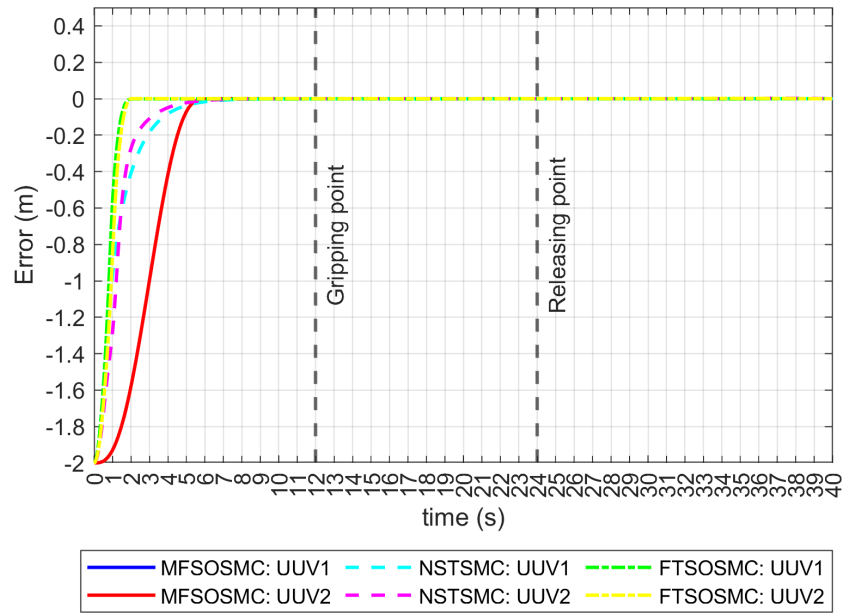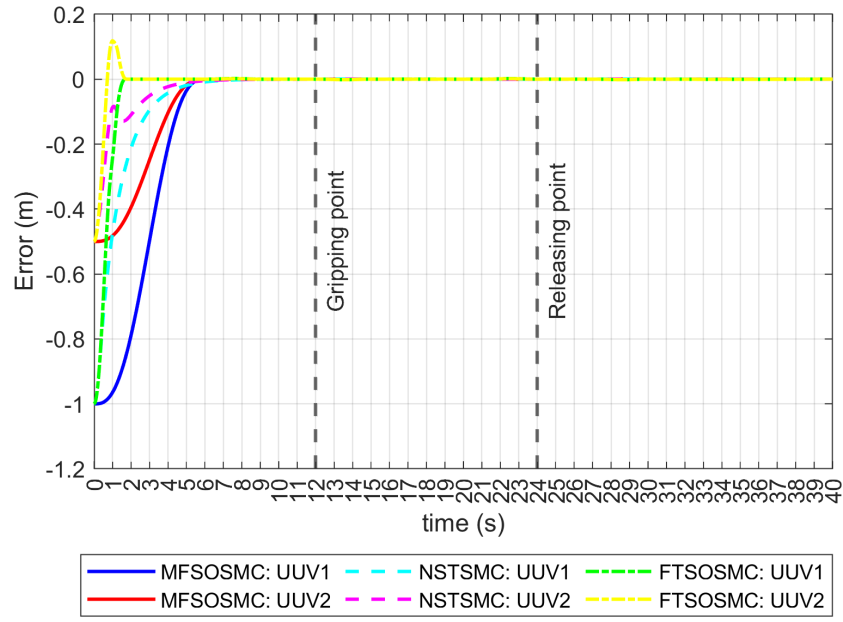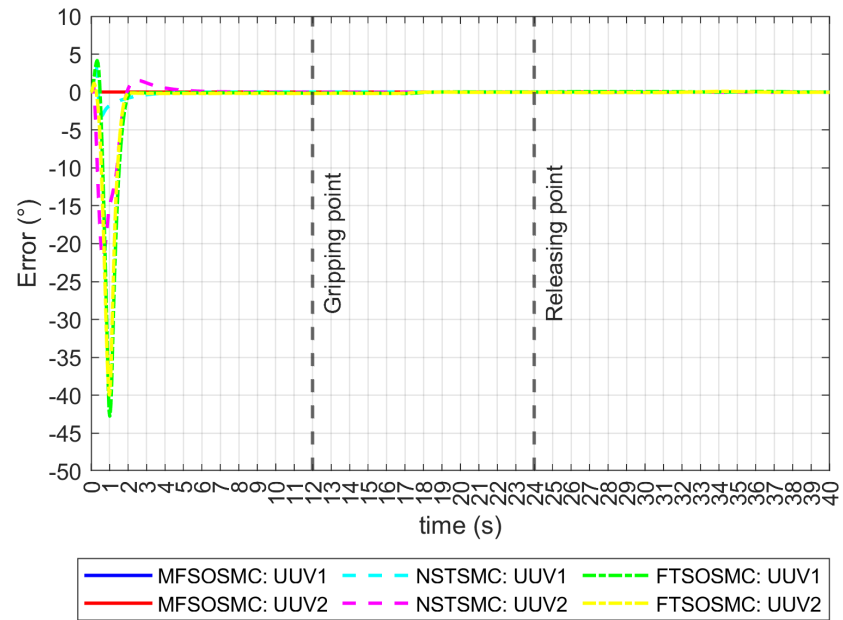Figure 5.74: Behavior of the error convergence on the x axis in the presence of marine currents.
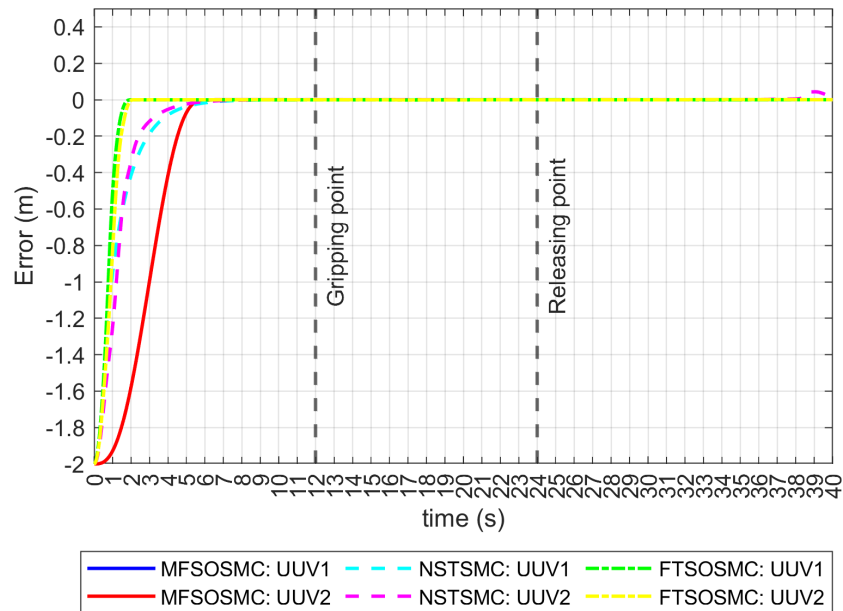
Figure 5.75: Behavior of the error convergence on the y axis in the presence of marine currents.
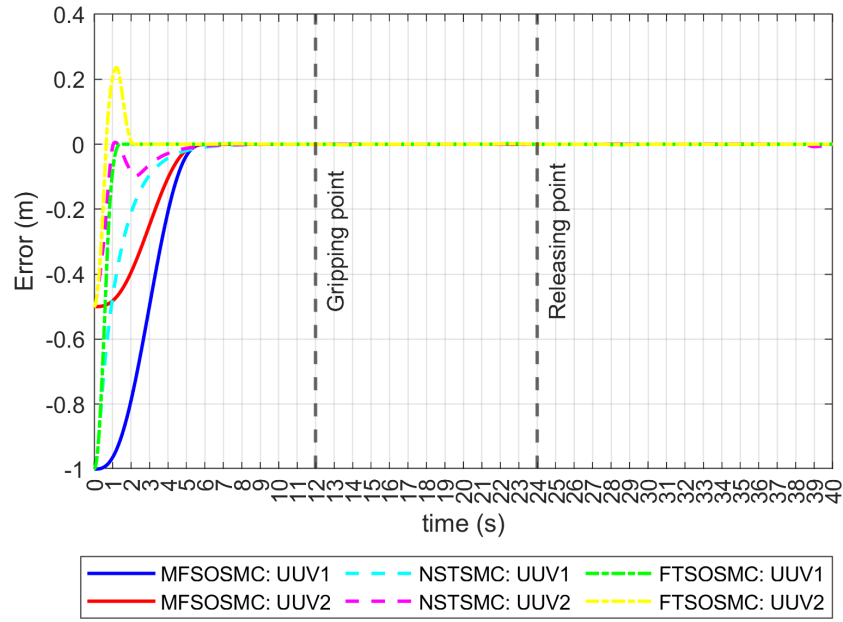
Figure 5.76: Behavior of the error convergence on the z axis in the presence of marine currents.
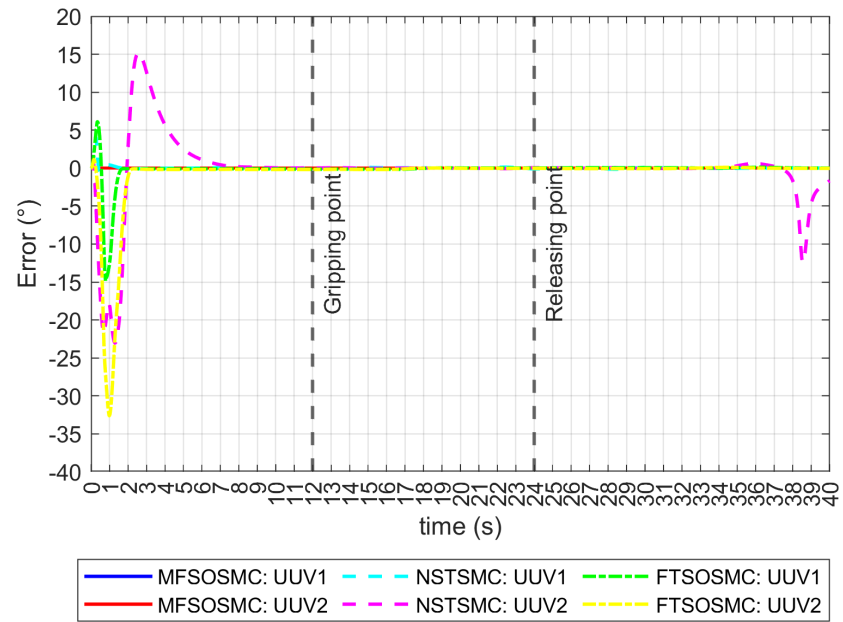
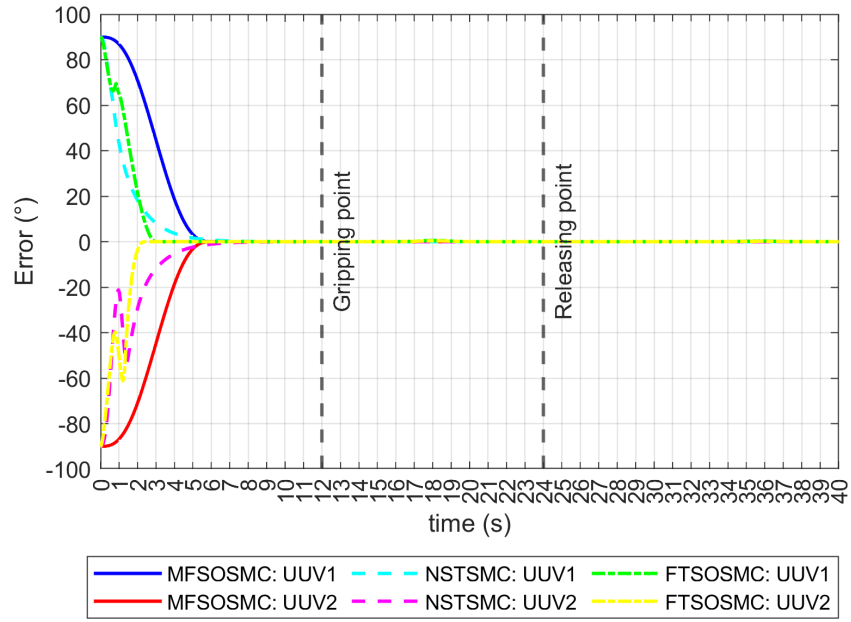Figure 5.77: Behavior of the error convergence on the ϕ angle in the presence of marine currents.
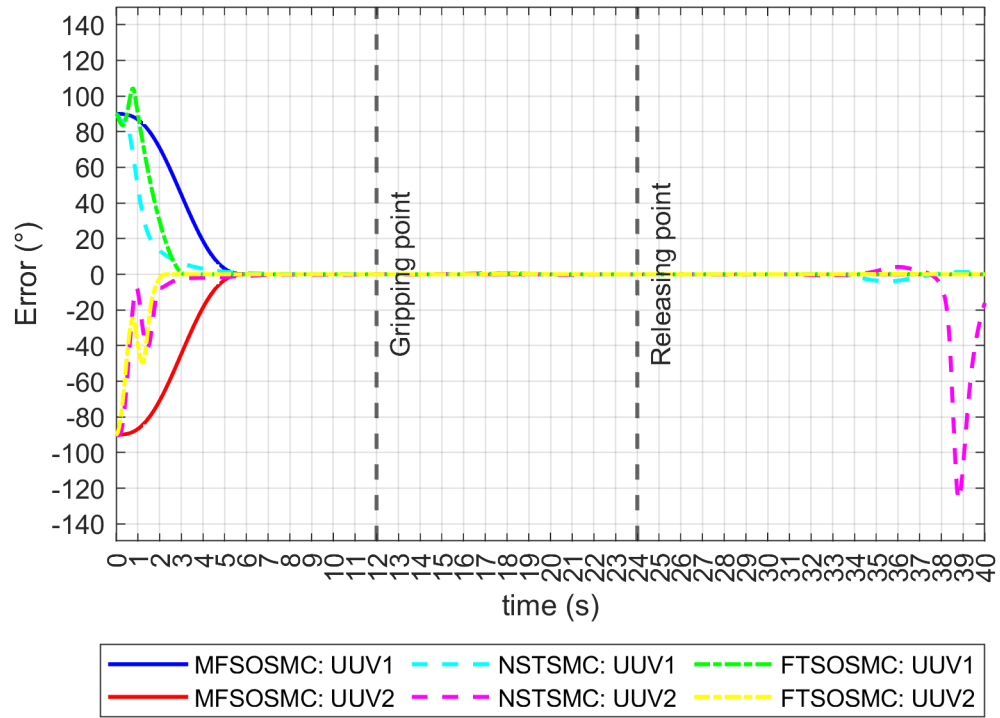
Figure 5.78: Behavior of the error convergence on the ψ angle in the presence of marine currents.

The euclidean distance and the difference in orientations are also shown in Fig. 5.79 and Fig. 5.80, respectively.

Figure 5.79: Behavior of the euclidean distance between UUVs in the presence of marine currents

Figure 5.80: Comparison of the difference between the ψ angles of the UUVs in the presence of marine currents.
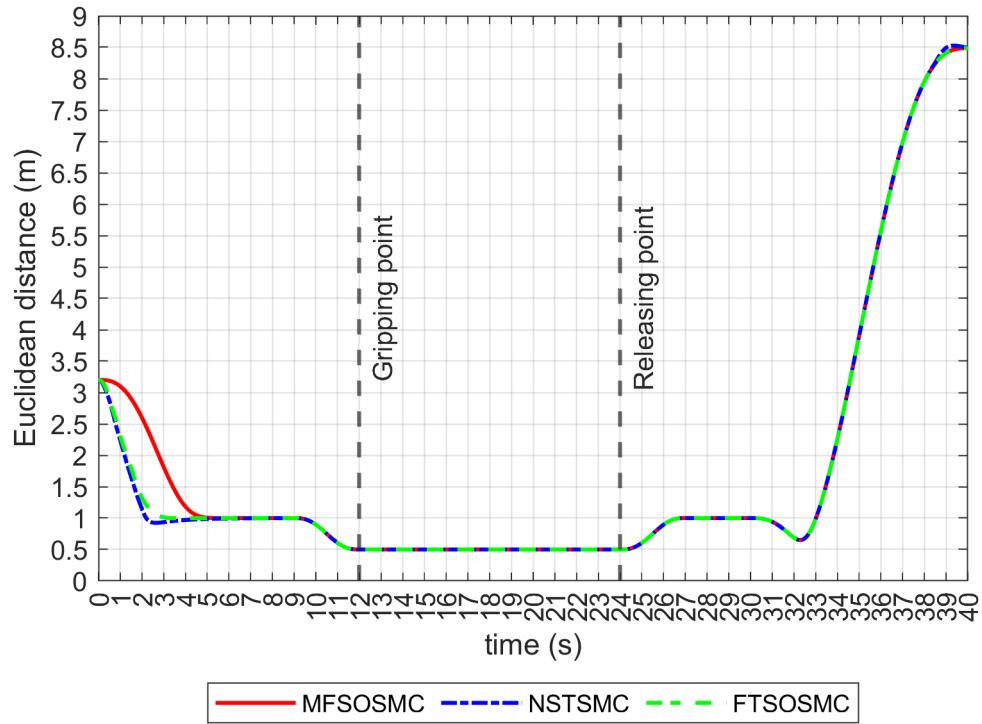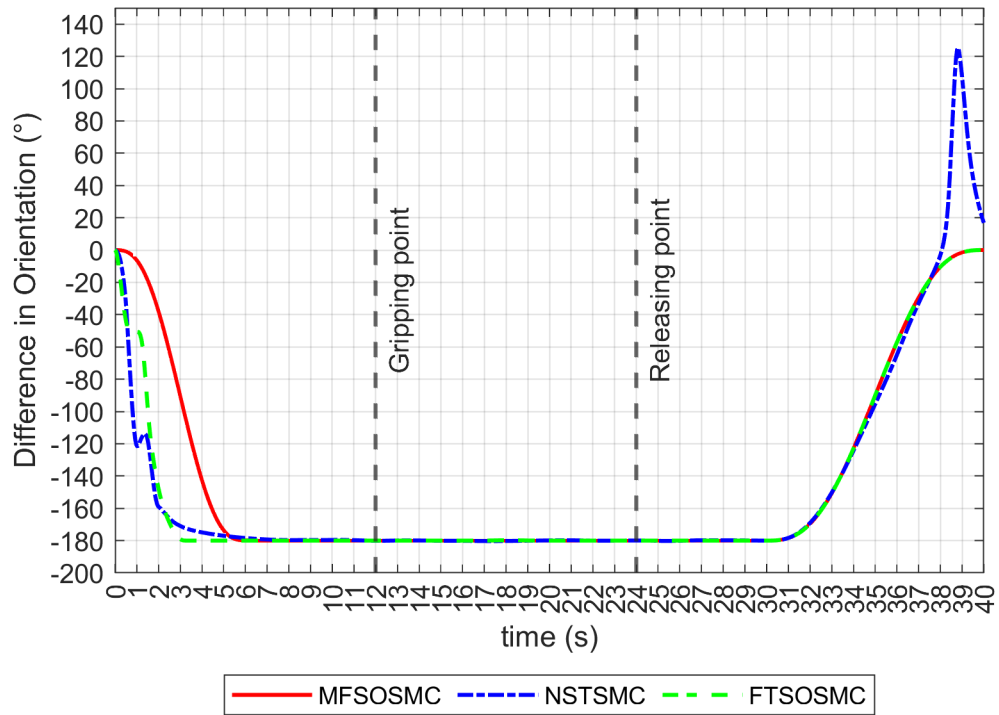
Chapter 6

Conclusions

Several control techniques have been applied to solve the trajectory tracking problem in underwater vehicles. However, the marine environment is complex and non-linear, making this task a matter of study. Model-based controller can have a good performance only when all the dynamics of the environment are precisely modeled and the parameters of the vehicle are completely and exactly known. In reality this is a complex time-consuming and it is impossible to completely model all the underwater environment, since some perturbations might be stochastic.

The purpose of this work is to synthesize and implement a sliding mode algorithm with finite-time convergence for trajectory tracking of a BlueROV2 underwater vehicle. The finite-time convergence is fundamental to allow vehicles to successfully perform tasks involving complex trajectories. The application of trajectory tracking in the space (x,y and z axes) will allow the system to deal to external disturbances and reduce the position error to a certain vicinity, normally near to zero, in a specific time.

The methodology of the project included a series of simulations performed on a Matlab/Simulink environment, and comparing the performance of four different type of controllers: a traditional PID, a Feedback Linearization controller, a Lyapunov-based controller and the proposed 2nd order Sliding Mode Controller with finite-time convergence. The simulations include parameters of the underwater vehicle BlueROV2, and considerations regarding to the position of the center of gravity. Conditions of movement with low velocities were also taken into account. This conditions simplified the model and made possible to simulate with less computational effort.

After this work, it was possible to synthesize of the 2nd Order Sliding Mode Controller by the integration of a variable gain α on the sliding surface. The gain α is parametrized by a Time Base Generator, which is a soft polynomial that smoothly goes from 0 to 1 in an specific time. Several times of convergence were selected, obtaining the expected results and avoiding the thrusters saturation. This indicates that the time t_b can only be established considering the physical limitations of the thrusters.

Also, it has been probed that the controller can manage external perturbations as marine currents, since the time RMS values of the controller remained in the exact same values that before considering the presence of the marine currents. However, this performance requires higher values of torques for all the thrusters and thus, a higher energy consumption.

As a second part, a novel application of the Model-free Second-order Sliding Mode

Control (MFSOSMC) is developed in this work. The finite-time convergence characteristic is taken in advantage to position two UUVs, on two different trajectories, to perform a simultaneous tracking, and to emulate a coordinated task of gripping, transporting and releasing an object.

Simulation results showed the robustness of the three proposed control schemes: a Model-Free Second-Order Sliding Mode Control (MFSOSMC), a Finite-Time Second-Order Sliding Mode Control(FTSOSMC) and a Non-Singular Terminal Sliding Mode Control(NSTSMC). The three controllers were capable of completing the task successfully, even in the presence of high marine currents. The three control schemes kept a constant Euclidian distance of 0.5 m between the two UUVs, and the difference in orientation was mantein in a value of $180°$ along all the time of the task.

However, the MFSOSMC presents superior characteristics, since its convergence time t_b can be set arbitrary and does not depend on any control parameter. Also, simulations showed the superiority of the MFSOSMC, since the tracking error of every DOF converge in the same established time, even in the presence of high marine currents.

Future work will consider the dynamic and physical properties of the object being transport, as well as the hydrodynamic effects of dragging forces acting on it.

The information presented in this paper will be a guide for the realization of future research work related with collaborative tasks of underwater vehicles.

Bibliography

[1] AGUIAR, A. P., AND HESPANHA, J. P. Trajectory-tracking and path-following of underactuated autonomous vehicles with parametric modeling uncertainty. *IEEE Transactions on Automatic Control 52*, 8 (2007), 1362–1379.

[2] AL MAKDAH, A. A. R., DAHER, N., ASMAR, D., AND SHAMMAS, E. Three-dimensional trajectory tracking of a hybrid autonomous underwater vehicle in the presence of underwater current. *Ocean Engineering 185*, April 2018 (2019), 115–132.

[3] ANDERLINI, E., PARKER, G. G., AND THOMAS, G. Control of a ROV carrying an object. *Ocean Engineering 165*, March (2018), 307–318.

[4] BAGHERI, A., AND MOGHADDAM, J. J. Simulation and tracking control based on neural-network strategy and sliding-mode control for underwater remotely operated vehicle. *Neurocomputing 72*, 7-9 (2009), 1934–1950.

[5] BALDINI, A., CIABATTONI, L., FELICETTI, R., FERRACUTI, F., FREDDI, A., AND MONTERIÙ, A. Dynamic surface fault tolerant control for underwater remotely operated vehicles. *ISA Transactions 78* (2018), 10–20.

[6] BESSA, W. M., DUTRA, M. S., AND KREUZER, E. Depth control of remotely operated underwater vehicles using an adaptive fuzzy sliding mode controller. *Robotics and Autonomous Systems 56*, 8 (2008), 670–677.

[7] BESSA, W. M., DUTRA, M. S., AND KREUZER, E. An adaptive fuzzy sliding mode controller for remotely operated underwater vehicles. *Robotics and Autonomous Systems 58*, 1 (2010), 16–26.

[8] BINUGROHO, E. H., DEWANTO, R. S., AND PRAMADIHANTO, D. Erov: Preliminary design of 5 dof rov using 6 thrusters configuration. In *2018 International Electronics Symposium on Engineering Technology and Applications (IES-ETA)* (2018), IEEE, pp. 281–287.

[9] CAMPOS, E., CHEMORI, A., CREUZE, V., TORRES, J., AND LOZANO, R. Saturation based nonlinear depth and yaw control of underwater vehicles with stability analysis and real-time experiments. *Mechatronics 45* (2017), 49–59.

[10] CHEN, H. H., CHUANG, W. N., AND WANG, C. C. Vision-based line detection for underwater inspection of breakwater construction using an ROV. *Ocean Engineering 109* (2015), 20–33.

[11] CHEN, Y., ZHANG, R., ZHAO, X., AND GAO, J. Adaptive fuzzy inverse trajectory tracking control of underactuated underwater vehicle with uncertainties. *Ocean Engineering 121* (2016), 123–133.

[12] CHIN, C. S., AND LIN, W. P. Robust Genetic Algorithm and Fuzzy Inference Mechanism Embedded in a Sliding-Mode Controller for an Uncertain Underwater Robot. *IEEE/ASME Transactions on Mechatronics 23*, 2 (2018), 655–666.

[13] CHU, Z., XIANG, X., ZHU, D., LUO, C., AND XIE, D. Adaptive trajectory tracking control for remotely operated vehicles considering thruster dynamics and saturation constraints. *ISA Transactions*, xxxx (2019).

[14] CHU, Z., ZHU, D., AND YANG, S. X. Observer-based adaptive neural network trajectory tracking control for remotely operated vehicle. *IEEE Transactions on Neural Networks and Learning Systems 28*, 7 (2017), 1633–1645.

[15] CUI, R., CHEN, L., YANG, C., AND CHEN, M. Extended State Observer-Based Integral Sliding Mode Control for an Underwater Robot With Unknown Disturbances and Uncertain Nonlinearities. *IEEE Transactions on Industrial Electronics 64*, 8 (2017), 6785–6795.

[16] CUI, R., YANG, C., LI, Y., AND SHARMA, S. Adaptive Neural Network Control of AUVs With Control Input Nonlinearities Using Reinforcement Learning. *IEEE Transactions on Systems, Man, and Cybernetics: Systems 47*, 6 (2017), 1019–1029.

[17] CUI, R., ZHANG, X., AND CUI, D. Adaptive sliding-mode attitude control for autonomous underwater vehicles with input nonlinearities. *Ocean Engineering 123* (2016), 45–54.

[18] DE AMORIM ALVES, R. P. Localização e controlo de proximidade em veículos aquáticos autónomos.

[19] DO, K. D. Robust adaptive tracking control of underactuated ODINs under stochastic sea loads. *Robotics and Autonomous Systems 72* (2015), 152–163.

[20] ELLENRIEDER, K. D. V. Dynamic surface control of trajectory tracking marine vehicles with actuator magnitude and rate limits. *Automatica 105* (2019), 433–442.

[21] ELMOKADEM, T., ZRIBI, M., AND YOUCEF-TOUMI, K. Terminal sliding mode control for the trajectory tracking of underactuated Autonomous Underwater Vehicles. *Ocean Engineering 129*, August 2016 (2017), 613–625.

[22] FERREIRA, C. Z., CARDOSO, R., MEZA, M. E. M., AND ÁVILA, J. P. J. Controlling tracking trajectory of a robotic vehicle for inspection of underwater structures. *Ocean Engineering 149*, July 2017 (2018), 373–382.

[23] FOSSEN, T. I. Marine control systems–guidance. navigation, and control of ships, rigs and underwater vehicles. *Marine Cybernetics, Trondheim, Norway, Org. Number NO 985 195 005 MVA, www. marinecybernetics. com, ISBN: 82 92356 00 2* (2002).

[24] FOSSEN, T. I. *Handbook of marine craft hydrodynamics and motion control.* John Wiley & Sons, 2011.

[25] GAN, W., ZHU, D., AND JI, D. QPSO-model predictive control-based approach to dynamic trajectory tracking control for unmanned underwater vehicles. *Ocean Engineering 158*, March (2018), 208–220.

[26] GAO, J., AN, X., PROCTOR, A., AND BRADLEY, C. Sliding mode adaptive neural network control for hybrid visual servoing of underwater vehicles. *Ocean Engineering 142*, January (2017), 666–675.

[27] GAO, J., PROCTOR, A., AND BRADLEY, C. Adaptive neural network visual servo control for dynamic positioning of underwater vehicles. *Neurocomputing 167* (2015), 604–613.

[28] GAO, J., PROCTOR, A. A., SHI, Y., AND BRADLEY, C. Hierarchical Model Predictive Image-Based Visual Servoing of Underwater Vehicles with Adaptive Neural Network Dynamic Control. *IEEE Transactions on Cybernetics 46*, 10 (2016), 2323–2334.

[29] GARCIA-VALDOVINOS, L. *Seguimiento Perfecto en Tiempo Finito de Robots Manipuladores Sujetos a Fricción Dinámica.* PhD thesis, Master Thesis, Dept of EE, Mechatronics Division, CINVESTAV-IPN, México, DF, 2003.

[30] GARCÍA-VALDOVINOS, L. G., FONSECA-NAVARRO, F., AIZPURU-ZINKUNEGI, J., SALGADO-JIMÉNEZ, T., GÓMEZ-ESPINOSA, A., AND CRUZ-LEDESMA, J. A. Neurosliding control for underwater rov's subject to unknown disturbances. *Sensors 19*, 13 (2019), 2943.

[31] GARCÍA-VALDOVINOS, L. G., SALGADO-JIMÉNEZ, T., BANDALA-SÁNCHEZ, M., NAVA-BALANZAR, L., HERNÁNDEZ-ALVARADO, R., AND CRUZ-LEDESMA, J. A. Modelling , Design and Robust Control of a Remotely Operated Underwater Vehicle. *International Journal of Advanced Robotic Systems 11*, 1 (2014).

[32] GONZÁLEZ-GARCÍA, J., GÓMEZ-ESPINOSA, A., CUAN-URQUIZO, E., GARCÍA-VALDOVINOS, L. G., SALGADO-JIMÉNEZ, T., AND CABELLO, J. A. E. Autonomous underwater vehicles: localization, navigation, and communication for collaborative missions. *Applied Sciences 10*, 4 (2020), 1256.

[33] GUERRERO, J., TORRES, J., CREUZE, V., AND CHEMORI, A. Trajectory tracking for autonomous underwater vehicle: An adaptive approach. *Ocean Engineering 172*, August 2018 (2019), 511–522.

[34] GUERRERO, J., TORRES, J., CREUZE, V., CHEMORI, A., AND CAMPOS, E. Saturation based nonlinear PID control for underwater vehicles : Design , stability analysis and experiments. *Mechatronics 61*, June (2019), 96–105.

[35] HERNÁNDEZ-ALVARADO, R., GARCÍA-VALDOVINOS, L. G., SALGADO-JIMÉNEZ, T., GÓMEZ-ESPINOSA, A., AND FONSECA-NAVARRO, F. Neural network-based self-tuning PID control for underwater vehicles. *Sensors (Switzerland) 16*, 9 (2016), 1–18.

[36] HOSSEINI, M., AND SEYEDTABAII, S. Robust ROV path following considering disturbance and measurement error using data fusion. *Applied Ocean Research 54* (2016), 67–72.

[37] HUANG, B., AND YANG, Q. Double-loop sliding mode controller with a novel switching term for the trajectory tracking of work-class ROVs. *Ocean Engineering 178*, March (2019), 80–94.

[38] HUO, X., GE, T., AND WANG, X. Horizontal path-following control for deep-sea work-class ROVs based on a fuzzy logic system. *Ships and Offshore Structures 13*, 6 (2018), 637–648.

[39] KARKOUB, M., WU, H. M., AND HWANG, C. L. Nonlinear trajectory-tracking control of an autonomous underwater vehicle. *Ocean Engineering 145*, May (2017), 188–198.

[40] KHOJASTEH, D., AND KAMALI, R. Design and dynamic study of a ROV with application to oil and gas industries of Persian Gulf. *Ocean Engineering 136*, June 2016 (2017), 18–30.

[41] KIM, M., JOE, H., KIM, J., AND YU, S. C. Integral sliding mode controller for precise manoeuvring of autonomous underwater vehicle in the presence of unknown environmental disturbances. *International Journal of Control 88*, 10 (2015), 2055–2065.

[42] KUMAR, N., AND RANI, M. An efficient hybrid approach for trajectory tracking control of autonomous underwater vehicles. *Applied Ocean Research 95*, October 2019 (2020), 102053.

[43] LI, J., GUO, H., ZHANG, H., AND YAN, Z. Double-Loop Structure Integral Sliding Mode Control for UUV Trajectory Tracking. *IEEE Access 7* (2019), 101620–101632.

[44] LIU, S., LIU, Y., CHEN, Z., AND LIANG, X. Finite-time tracking control of underwater vehicles with system uncertainties and unknown disturbances. In *2017 36th Chinese Control Conference (CCC)* (2017), IEEE, pp. 6581–6585.

[45] LIU, X., ZHANG, M., AND ROGERS, E. Trajectory tracking control for autonomous underwater vehicles based on fuzzy re-planning of a local desired trajectory. *IEEE Transactions on Vehicular Technology 68*, 12 (2019), 1–1.

[46] LIU, X., ZHANG, M., YANG, C., AND YIN, B. Finite-time tracking control for autonomous underwater vehicle based on an improved non-singular terminal sliding mode manifold. *International Journal of Control* (2020), 1–10.

[47] LONDHE, P. S., MOHAN, S., PATRE, B. M., AND WAGHMARE, L. M. Robust task-space control of an autonomous underwater vehicle-manipulator system by PID-like fuzzy control scheme with disturbance estimator. *Ocean Engineering 139*, April (2017), 1–13.

[48] MARTIN, S. C., AND WHITCOMB, L. L. Nonlinear Model-Based Tracking Control of Underwater Vehicles with Three Degree-of-Freedom Fully Coupled Dynamical Plant Models: Theory and Experimental Evaluation. *IEEE Transactions on Control Systems Technology 26*, 2 (2018), 404–414.

[49] MIAO, B., LI, T., AND LUO, W. A DSC and MLP based robust adaptive NN tracking control for underwater vehicle. *Neurocomputing 111* (2013), 184–189.

[50] MORASSO, P., SANGUINETI, V., AND SPADA, G. A computational theory of targeting movements based on force fields and topology representing networks. *Neurocomputing 15*, 3-4 (1997), 411–434.

[51] MOREIRA, M. L. *Visual Servoing on Deformable Objects*. PhD thesis, Université De Toulon, 2019.

[52] NEJATBAKHSH ESFAHANI, H., AZIMIRAD, V., AND DANESH, M. A Time Delay Controller included terminal sliding mode and fuzzy gain tuning for Underwater Vehicle-Manipulator Systems. *Ocean Engineering 107* (2015), 97–107.

[53] OGATA, K. Modern control engineering 5th edition. lugar: Upper saddle river, new jersey 07458. *ed: Prentice Hall* (2009), 55.

[54] PARRA-VEGA, V. Second order sliding mode control for robot arms with time base generators for finite-time tracking. *Dynamics and Control 11*, 2 (2001), 175–186.

[55] PARRA-VEGA, V., GARCÍA-VALDOVINOS, L., CASTILLO-TAPIA, A., AND DOMÍNGUEZ-RAMÍREZ, O. A. Sliding pid control for tracking in finite time for robot arms. In *Proceedings of the 11th International Conference on Advanced Robotics, ICAR* (2003), pp. 1526–1531.

[56] QIAO, L., YI, B., WU, D., AND ZHANG, W. Design of three exponentially convergent robust controllers for the trajectory tracking of autonomous underwater vehicles. *Ocean Engineering 134*, March (2017), 157–172.

[57] QIAO, L., AND ZHANG, W. Adaptive Second-Order Fast Nonsingular Terminal Sliding Mode Tracking Control for Fully Actuated. *IEEE Journal of Oceanic Engineering 44*, 2 (2019), 363–385.

[58] QIAO, L., AND ZHANG, W. Double-Loop Integral Terminal Sliding Mode Tracking Control for UUVs with Adaptive Dynamic Compensation of Uncertainties and Disturbances. *IEEE Journal of Oceanic Engineering 44*, 1 (2019), 29–53.

[59] SHEN, C., BUCKHAM, B., AND SHI, Y. Modified C/GMRES Algorithm for Fast Nonlinear Model Predictive Tracking Control of AUVs. *IEEE Transactions on Control Systems Technology 25*, 5 (2017), 1896–1904.

[60] SHEN, C., SHI, Y., AND BUCKHAM, B. Trajectory Tracking Control of an Autonomous Underwater Vehicle Using Lyapunov-Based Model Predictive Control. *IEEE Transactions on Industrial Electronics 65*, 7 (2018), 5796–5805.

[61] SLOTINE, J.-J. E., LI, W., ET AL. *Applied nonlinear control*, vol. 199. Prentice hall Englewood Cliffs, NJ, 1991.

[62] SNAME, T. Nomenclature for treating the motion of a submerged body through a fluid. *The Society of Naval Architects and Marine Engineers, Technical and Research Bulletin No* (1950), 1–5.

[63] SOYLU, S., PROCTOR, A. A., PODHORODESKI, R. P., BRADLEY, C., AND BUCK-HAM, B. J. Precise trajectory control for an inspection class ROV. *Ocean Engineering 111* (2016), 508–523.

[64] WADI, A., MUKHOPADHYAY, S., AND LEE, J.-H. A novel disturbance-robust adaptive trajectory tracking controller for a class of underactuated autonomous underwater vehicles. *Ocean Engineering 189*, July (2019), 106377.

[65] WANG, J., WANG, C., WEI, Y., AND ZHANG, C. Command filter based adaptive neural trajectory tracking control of an underactuated underwater vehicle in three-dimensional space. *Ocean Engineering 180*, November 2018 (2019), 175–186.

[66] WANG, Y., ZHANG, M., WILSON, P. A., AND LIU, X. Adaptive neural network-based backstepping fault tolerant control for underwater vehicles with thruster fault. *Ocean Engineering 110* (2015), 15–24.

[67] WU, C.-J., AND DISCIPLINE, E. *6-DoF Modelling and Control of a Remotely Operated Vehicle*. PhD thesis, 2018.

[68] YAN, J., GAO, J., YANG, X., LUO, X., AND GUAN, X. Tracking control of a remotely operated underwater vehicle with time delay and actuator saturation. *Ocean Engineering 184*, June (2019), 299–310.

[69] YAN, Y., AND YU, S. Sliding mode tracking control of autonomous underwater vehicles with the effect of quantization. *Ocean Engineering 151*, January (2018), 322–328.

[70] YAN, Z., YANG, Z., ZHANG, J., ZHOU, J., JIANG, A., AND DU, X. Trajectory Tracking Control of UUV Based on Backstepping Sliding Mode With Fuzzy Switching Gain in Diving Plane. *IEEE Access 7* (2019), 166788–166795.

[71] YU, H., GUO, C., AND YAN, Z. Globally finite-time stable three-dimensional trajectory-tracking control of underactuated UUVs. *Ocean Engineering 189*, March (2019), 106329.

[72] ZEREIK, E., BIBULI, M., MIŠKOVIĆ, N., RIDAO, P., AND PASCOAL, A. Challenges and future trends in marine robotics. *Annual Reviews in Control 46* (2018), 350–368.

[73] ZHANG, M.-J., AND CHU, Z.-Z. Adaptive sliding mode control based on local recurrent neural networks for underwater robot. *Ocean Engineering 45* (2012), 56–62.

[74] ZHANG, S., YU, J., ZHANG, A., AND ZHANG, F. Spiraling motion of underwater gliders: Modeling, analysis, and experimental results. *Ocean Engineering 60* (2013), 1–13.

[75] ZHANG, Y., LIU, X., LUO, M., AND YANG, C. MPC-based 3-D trajectory tracking for an autonomous underwater vehicle with constraints in complex ocean environments. *Ocean Engineering 189*, March (2019), 106309.

[76] ZHOU, J., ZHAO, X., CHEN, T., YAN, Z., AND YANG, Z. Trajectory Tracking Control of an Underactuated AUV Based on Backstepping Sliding Mode with State Prediction. *IEEE Access 7* (2019), 181983–181993.

Curriculum Vitae

Néstor Alejandro Narcizo Nuci was born in Zamora, Michoacán, México on September 18th, 1995. He got the B.Sc. in Mechatronics Engineering from Tecnológico de Monterrey (ITESM) in 2018. He graduated with Honors and with the EGAL Excellence Price. He collaborated within a PEI CONACYT project related with mechanical design and instrumentation. He worked as professor during one year at PrepaTec Morelia and couched the robotics FRC team Monarch-e 4731. He is currently pursuing the degree of Master of Science in Engineering.

This document was typed in using LaTeX 2_ε by Néstor Alejandro Narcizo-Nuci.